MITNE-189

MULTIDIMENSIONAL MODELING OF THE ROD DROP ACCIDENT

John U. G. Valente

April, 1976

DEPARTMENT OF NUCLEAR ENGINEERING
MASSACHUSETTS INSTITUTE OF TECHNOLOGY
Cambridge, Massachusetts 02139

Work Sponsored by
Commonwealth Edison Company
Chicago, Illinois

MULTIDIMENSIONAL MODELING OF THE ROD DROP ACCIDENT

by

John Umberto George Valente

B.A., Queens College/CUNY
1973

B.S., Columbia University
1973

M.S., Columbia University
1974

Submitted in Partial Fulfillment
of the Requirements for the Degrees of

Nuclear Engineer

and

Master of Science in Nuclear Engineering

at the

MASSACHUSETTS INSTITUTE OF TECHNOLOGY

April , 1976

Signature of Author _____
Department of Nuclear Engineering
April , 1976

Certified by _____
Thesis Advisor

Accepted by _____
Chairman, Department Committee on Graduate Students

MULTIDIMENSIONAL MODELING OF THE ROD DROP ACCIDENT

by

John Umberto George Valente

Submitted to the Department of Nuclear Engineering on April 8, 1976
in partial fulfillment of the requirements for the degrees of
"Nuclear Engineer" and Master of Science in Nuclear Engineering.

ABSTRACT

This work investigates, using a newly developed neutronic kinetics code, MEKIN, a Rod Drop Accident (RDA) for a BWR in 3-D.

A completely independent investigation is carried out. This involved generating two-group diffusion theory parameters for BWR subassemblies. The homogenization model for doing this, Model III, uses the spectrum code, LEOPARD, and spatial code, CITATION. Model III gives good agreement with supplied subassembly criticalities and pin power distribution provided both the control blade and curtains are either both in or out.

Using analytic means of analysis, resistor-capacitor circuit analog of fuel pin and point kinetics with some feedback, a physical intuition for some aspects of the accident was attained. In particular, the "RC" constant is shown to be a function of fuel pin radial temperature distribution. As such, it was found that this constant may indeed be smaller than 7 seconds. A rough estimate of accident timetable and peak power were able to be determined by analytic means.

The thermal-hydraulic conditions affect the neutronic parameters. Hence, an investigation into just how the non-uniform distribution of void fraction and pin temperature within a subassembly affect these parameters is made with aid of the thermal-hydraulic code, COBRA 3C. It was found that when significant non-uniform void fractions occur, subassembly average void fractions should not be used to obtain homogenized neutronic parameters for the subassembly.

A good part of this work was to model the RDA in MEKIN by judicious choice of input parameters. This involved a method for handling the gap water, and how to determine the void fraction in gap water if the void fraction in lattice water is known.

Finally, the results of the accident as modelled by MEKIN are studied and some conclusions drawn from this preliminary investigation. It is pointed out by means of form factors that there are delay times in reactor response between different parts of a large BWR core.

Thesis Supervisor: K. F. Hansen
Title: Professor of Nuclear Engineering

IN MEMORY OF

JOSEPH C. POGGIOLI

"FRIENDSHIP IS THE MOST IMPORTANT

ELEMENT ONE CAN ATTAIN OR BE REMEMBERED FOR"

ACKNOWLEDGEMENTS

To Professor Hansen, my thesis advisor, I would like to express my thanks for choosing me to work under him on this contract and thereby introducing me to the field of safety analysis. Further, his willingness to give me a good deal of responsibility during this work helped build self-confidence and is very much appreciated.

I wish to acknowledge the generous assistance of Commonwealth Edison in financing this study. Her employees Herb Massin, Rick Pinnock and Bruce Momsen were of help. In particular the friendliness and assistance of Terry Rieck will be remembered by this author.

Professor Henry aided me in some of the neutronic aspects of this thesis. His instruction and humor are gratefully acknowledged.

I also wish to thank Professor Lanning for his interest and willingness to serve as my thesis reader.

In the area of computers the author would like to thank the following for their aid: Rachel Morton, Ed Fujita, Randall Sims and Tony Shober.

The discussions with George Solan, Pablo Moreno and Chong Chiu, Andy Cook, Steve Shultz and Mike Krammen were stimulating. Thanks, also to Lynda DuVall for her patience in typing this work.

In somewhat of a different nature I would like to thank Susan Liptak for her friendship and letters received during my graduate education.

Finally, this author would like to acknowledge the encouragement and understanding of his entire family during the course of this work.

TABLE OF CONTENTS

LIST OF FIGURES

LIST OF TABLES

Chapter I

INTRODUCTION

Nuclear power is presently going through a critical evaluation by many citizens. The safety of reactors appears to be paramount in their minds. It is just such a safety issue which this thesis attempts to address.

Of the four design basis accidents in a Boiling Water Reactor (BWR), the "Loss of Coolant Accident" (LOCA), "Steamline Break Accident", "Fuel Bundle Drop Accident", and "Control Rod Drop Accident" (RDA), it is the last which will be considered here. For a BWR a rod drop is a control rod expulsion. This will result in a large reactivity insertion.

It is the LOCA which has received most of the attention, however, the RDA is considered by some to be the more serious accident. This accident involves a far more interesting neutronic problem than the others. Primarily because of the neutronics, the utilities and almost all the reactor vendors lacked an accident code which would handle the three dimensional problem associated with a non-symmetric rod drop. The BWR vendor has in the past used the adiabatic approximation for analysis[1].

This method (which utilizes point reactor kinetics) does not allow one to observe how parts of the reactor may go prompt critical while others have not. Further, it is

expected that the subassemblies which have lost their control blade will suffer the greatest fuel temperature increase. They will reach their peak temperature sooner, and so contribute their Doppler feedback sooner. Hence, these subassemblies which have lost their control blade will lead the others in power ascension and decline. If the control blade has fallen out from an off center position, flux tilting should occur. Only a three dimensional analysis will explicitly represent all these results. The newly developed MEKIN^2 code now presents the possibility of just such an analysis.

If the fuel pins reach certain enthalpies (see Chapter 5), fission gas will be released from the clad. Then, depending on the operating condition of the plant, this radioactive gas may be released to the environment. It is possible to tie the severity of the accident to the peak fuel temperature of the pins. It is this parameter which will be closely examined.

This can be correlated into the main purpose of the work; to examine by multidimensional modeling, using MEKIN, the Rod Drop Accident in a BWR.

In order to do an independent study, it was important to generate homogenized two group parameters. MEKIN allows either one or two energy group parameters as input. Three models of homogenization were investigated. The necessary preliminaries to these models are outlined in Chapter 2.

The models and their results are then described in the following chapter. For the final model, model III, a step by step evolution from Model II is explained. Chapter 4 then investigates the accuracy and limitations of the chosen Model III.

Chapter 5 outlines the accident which will be investigated in this thesis. In particular, 2 reactor vendors' means of analysis and conclusions are considered.

In an analysis as complicated as this accident, it is good to get some type of physical understanding of what to expect and a feel for the individual tools of investigation. This accident can be broken into its neutronic, thermal-hydraulic, and coupling parts. In chapter 6, some important ideas on the time scale of the accident, and how to model the accident in MEKIN^2 (the 3-D Nodal kinetics code used to analyze the accident are developed.

The actual modeling of the accident in MEKIN is then carried out in Chapter 7. The choice of the basic neutronic and thermal-hydraulic nodes is the main topic of this chapter.

Due to the particular low power and coolant flow conditions of the accident, modifications had to be made in the original version of MEKIN. Also, due to the very size of the problem, some data management optimization

had to be made. The theory behind the optimization is also covered in Appendix II, but the actual modifications and corrections to the original version of MEKIN are discussed in Appendix III.

The results of the analysis are given in Chapter 8. Finally, some conclusions are drawn in the final chapter, Chapter 9.

Before starting it is believed advisable to give some basic descriptions. The reactor to be analyzed is Dresden III[3]. It is a 2527 MWt rated BWR with 724 subassemblies. Each subassembly is composed of 49 pins in a 7 x 7 array. Also included for neutronic homogenication are parts of curtain, control blade, gap water, and zircaloy can that surrounds the 49 pins. A list of the reactor's characteristics, and figures which should help describe the important terms that will be used throughout the work can be found in Appendix I.

Chapter 2

HOMOGENIZATION PRELIMINARIES (SOLUTION TO THE ENERGY EQUATION)

Before we can obtain homogenized cross sections for a subassembly we must get the individual region (control rod, curtain, etc.) cross sections. Since we will be dealing with just 2 energy groups, this requires solving the energy equation so that we may correctly reduce our fine groups by spectrum weighting. Hence, this chapter deals with the solution to the energy equation. We utilize the LEOPARD[4] code for this purpose. LEOPARD will be discussed further in section 2 of this chapter.

While LEOPARD will give us the diffusion theory two-group parameters, diffusion theory will not hold for a strong absorber like the control blades. A number of methods to obtain effective diffusion theory parameters for these blades are examined in section 4.

Effective diffusion theory constants must also be created for the curtains. The problem with the curtains will be reserved for section 3.

We begin with obtaining a number of parameters that are important input for the flux spectrum solution.

2.1 Determination of Buckling, UO_2 Density and Fuel Pin Physical Constants

The difference in the two energy group parameters when the buckling of base or reflected cores was used is trivial. For example, for a given simple cell LEOPARD run, varying only the bucklin we obtained:

	Bare Core	Reflected Core
Σ_1	.9146E-02	.9146E-0
Σ_2	.7752E-01	.7751E-01

This small dependence on choice of buckling seems to hold for all other parameters of interest, as well as the absorption cross section. The input of LEOPARD requires a buckling in order to determine the diffusion coefficient, D.

$$DB^2 \int \phi du = B \int J du$$

Here the flux, ϕ , and the current, J, which are calculated by LEOPARD, are integrated over lethargy.

To get a bare buckling of 1.736E-04, we used a core diameter of 189.4" and height of 144". The reflected buckling was determined as a first approximation to be 1.539E-04. This reflector savings was found using[5]:

$$\delta(\text{cm}) = 7.2 + .1(M^2 - 40.0)$$

where M^2 is migration area

$$M^2 = L^2 + \tau$$

$$\tau = (3\Sigma_{tr}\Sigma_s)^{-1}$$

$$L^2 = L_m^2\,(1-f)(V/V_m)$$

where:

L = thermal diffusion length

τ = Fermi age

Σ_{tr} = macroscopic transport cross section

Σ_s = macroscopic scattering cross section

V_m = volume of moderator

V = core volume

f = thermal utilization factor

The microscopic cross sections used to get Σ_{tr} and Σ_s were from a LEOPARD run using zero buckling. The reflected buckling is hence only a first approximation, but since its value changes the parameters of interest so little, we did not determine a better approximation.

The undished fuel pin density was found by knowing the fuel loading was 4566 gm and the volume of the fuel

$$\text{Vol} = \pi r^2 \times \text{height}$$

$$\text{Vol} = \pi(.244)^2\,(144) = 26.93\ \text{in}^3$$

$$\text{Vol} = 441.4\ \text{cc}$$

Thus the density = 10.345 gm/cc. Since 100% T.D. (theoretical density) = 10.96 gm/cc we have 94.39% T.D.

The density of the dished fuel will also be represented by 94.3% and the extra volume associated with the dishing will be represented as void in the LEOPARD fuel region.

Finally, the LEOPARD input requires the horizontal cross-sectional areas of the clad and fuel pellet-clad gap. These were determined to be for cold (room temperature) conditions.

$$\text{Area of clad} = .05338 \text{ in}^2$$

$$\text{Area of gap} = .0085269 \text{ in}^2$$

2.2 The LEOPARD Code

This standard spectrum code uses the MUFT and SOFOCATE routines. MUFT is used to obtain the fast group parameters starting with a 54 fine group library. SOFOCATE solves for the thermal spectrum utilizing a 172 fine group library. The energy value separating the fast and thermal spectrums if 0.625 ev.

2.2.1 The LEOPARD Regions

In all the calculations made in this work, LEOPARD was set up as either a supercell or simple cell.

A LEOPARD cell allows the following regions of concentric cylinders. They are:

1) cylindrical fuel region
2) annular clad and void region
3) moderator
4) extra region

The simple cell is composed of the first three regions. The supercell is made up of all four regions. This will be the terminology used throughout this work.

2.2.2 Effective Resonance Temperature

The resonance integral is a function of the temperature of the fuel. LEOPARD allows for the input of an effective resonance temperature. Throughout, the volume average fuel temperature will be used. This is in agreement with both Van Binneck[10] and Dresner[11].

2.2.3 Effect of Dishing

Simple LEOPARD cells were run to observe the effect of dishing at hot standby conditions (no coolant voids, all regions at 547 °F - see Chapter 5) for the three different enrichments present in our subassemblies. The thermal parameter results follow:

Table 2.1

The Effect of Dishing on Thermal Parameters

	$\underline{D}$	$\underline{\Sigma_a}$	$\underline{\nu\Sigma_f}$
Dished	.3884	.75118E-01	.1222
High Enrichment			
Undished	.3855	.77519E-01	.1264
Dished	.389	.5977E-01	.8916E-01
Medium Enrichment			
Undished	.386	.6172E-01	.9239E-01
Dished	.389	.4890E-01	.6573E-01
Low Enrichment			
Undished	.386	.5050E-01	.6819E-01

The results indicate the dishing has a significant effect on our thermal parameters. When we homogenize the subassemblies this will require separate calculations for dished and undished cases.

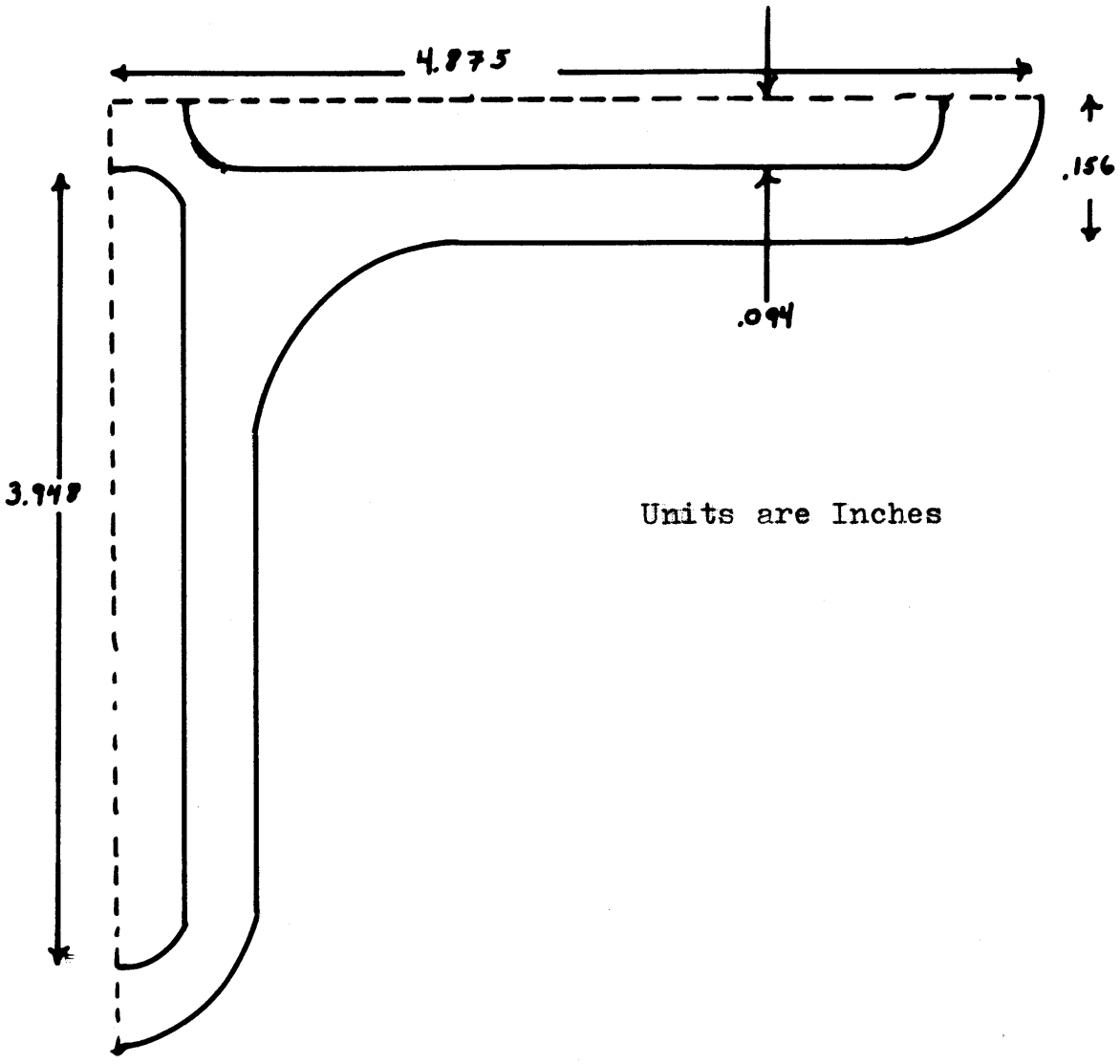

CONTROL BLADE GEOMETRY

FIG. 2.1

2.3 Determination of Two-Group Parameters for Control Blades

The control blade is composed of a stainless steel sheath, and four cavities. In the cavities are rods of stainless steel clad B_4C. These rods are only one row deep and are close packed. The remaining volume of the cavities is filled with water. Figure 2.1 gives some idea of the scheme.

In obtaining two group parameters for the blade, diffusion theory will not hold due to the strong absorption qualities of the B_4C. One must then go to some higher-order transport theory approximation or Monte Carlo. Blackness theory was employed. This deals with using Transport theory to solve for the flux in the interior of the blade. The basic assumptions of Blackness theory are[12, 13]:

1) the directional flux, $\psi(x,\mu,E)$, has the P_1 form at the surfaces of the slab for neutrons directed into the slab,

2) there is no source of neutrons inside the slab due either to fission or to scattering from other energies,

3) the net current density $J(x,E)$ is continuous at the boundaries.

The second assumption doesn't prohibit scattering into and out of directions.

If scattering is much less than absorption, one may derive the following method of obtaining equivalent cross sections:

$$\alpha = \frac{1 - 2E_3(z)}{2[1 + 3\,E_4(z)]} \tag{2.1}$$

$$\beta = \frac{1 + 2E_3(z)}{2[1-3E_4(z)]} \tag{2.2}$$

$$\langle\alpha\rangle = \frac{\sum_{i=1}^{j} \frac{\alpha_i \psi_i \Delta U_i}{1 + \sqrt{3}\,\alpha_i}}{\sum_{i=1}^{j} \frac{\psi_i \Delta U_i}{1 + \sqrt{3}\,\alpha_i}} \tag{2.3}$$

$$\Sigma_a = \frac{\sqrt{\langle\alpha\rangle\,\langle\beta\rangle}}{2t}\ \ell n\ \frac{1 + \sqrt{\frac{\langle\alpha\rangle}{\langle\beta\rangle}}}{1 - \sqrt{\frac{\langle\alpha\rangle}{\langle\beta\rangle}}} \tag{2.4}$$

$$D\Sigma_a = \langle\alpha\rangle\,\langle\beta\rangle \tag{2.5}$$

where α & β = blackness coefficients. Once α is determined it is usually adequate to obtain β from:

$$\alpha\beta = \frac{1}{4} \tag{2.6}$$

$\langle\alpha\rangle \equiv$ is the averaged α over letharge.

E_4 & E_3 are exponetial integral functions

t = half thickness of slab

$z = 2\Sigma_a t$ where Σ_a is the diffusion cross section.

The above then represents the basic theory and equations of Blackness theory. Since, at the boundaries where the current is matched we assume diffusion theory holds outside the control material, it is important that the outside material be such that this assumption isn't too far from the truth. Hence, water would probably be a better material to fulfill this assumption than stainless steel. We now look at three different ways in which the control blade was handled.

2.3.1 B_4C Volume Conservation.

The control blade must be put in the form of a one dimensional slab if the above equations are to hold. Three slabs, of B_4C, H_2O and stainless steel respectively were constructed (see fig. 2.2). The stainless steel contained that steel which made up the B_4C clad as well as the cruciform sheath. The volume of the elements was conserved during reconstruction. Looking at a horizontal cross-section we have

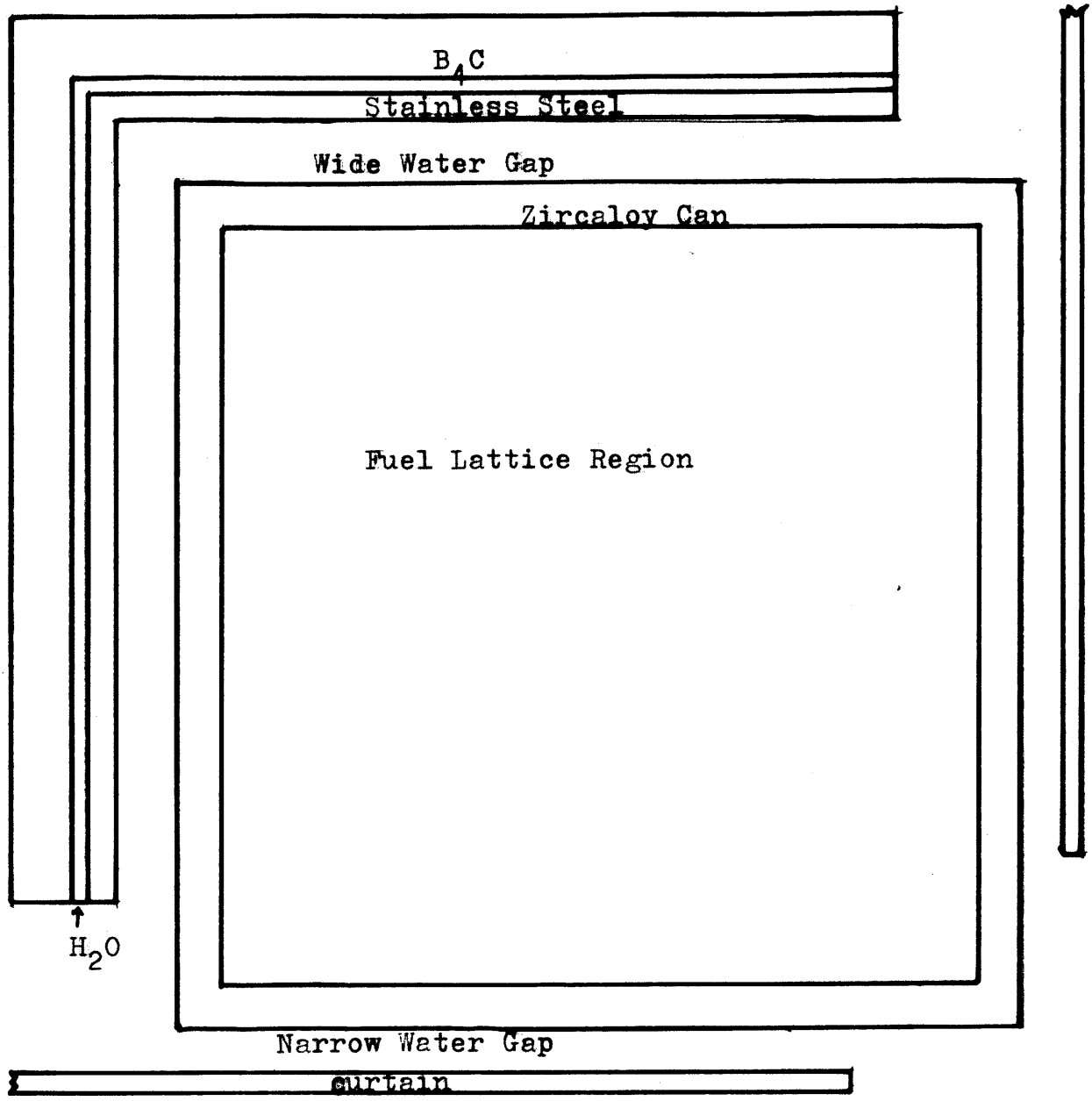

Model I Subassembly Layout

FIG. 2.2

$$\text{Area}_{\text{Control blade}} = 1.5910 \text{ in}^2$$

$$A_{\text{Boron rods}} = .5829 \text{ in}^2$$

i) $A_{\text{rod clad}} = .1550 \text{ in}^2$

ii) $A_{B_4C} = .4279 \text{ in}^2$

$$A_{H_2O} = .1795 \text{ in}^2$$

$$A_{ss} = .8286 \text{ in}^2$$

Using this we get a B_4C thickness, t , of

$$t = .0438845 \text{ in} = .1114666\text{cm}$$

Neglecting absorption of C and B-11, and with a number density of $N_{B-10} = .015296 \times 10^{24}$ atm/cc; we can find Σ_a

The microscopic absorption cross section of Boron-10 depends on the spectrum to which it is exposed. For thermal group considerations we took a pin type one enrichment (2.44 wt % U^{235}), and put Zr subassembly can material and water in the extra region of the cell making it a supercell. The non-lattice fraction was that of the actual physical situation. The spectrum found is different from actual conditions since we have type 2 (1.69 wt % U^{235})

and type 3 (1.20 wt % U-235) enrichments bordering the control rod (Fig 2.3). However, the total effect on the parameter of importance, microscopic absorption cross-section of B-10, is minimal. For a comparison, a LEOPARD run which used type 2 pin, and included the H_2O and stainless steel of the control rod gave:

Cross section including H_2O + SS + type 2 pin = 2237.967b

Cross section used in obtaining αth = 2235.045b

Therefore, we get for the thermal group

$$Z_{th} = 2\Sigma_{th}t = 7.62147$$

One then uses the equations given in section 2.3.

In this method we only consider the B_4C as the material in which the blackness theory is to apply, not the entire control blade.

In calculating the thermal parameters only one Z was used and the resulting α was the average thermal value $\langle\alpha\rangle$th. This was necessary since only one thermal group is supplied by LEOPARD.

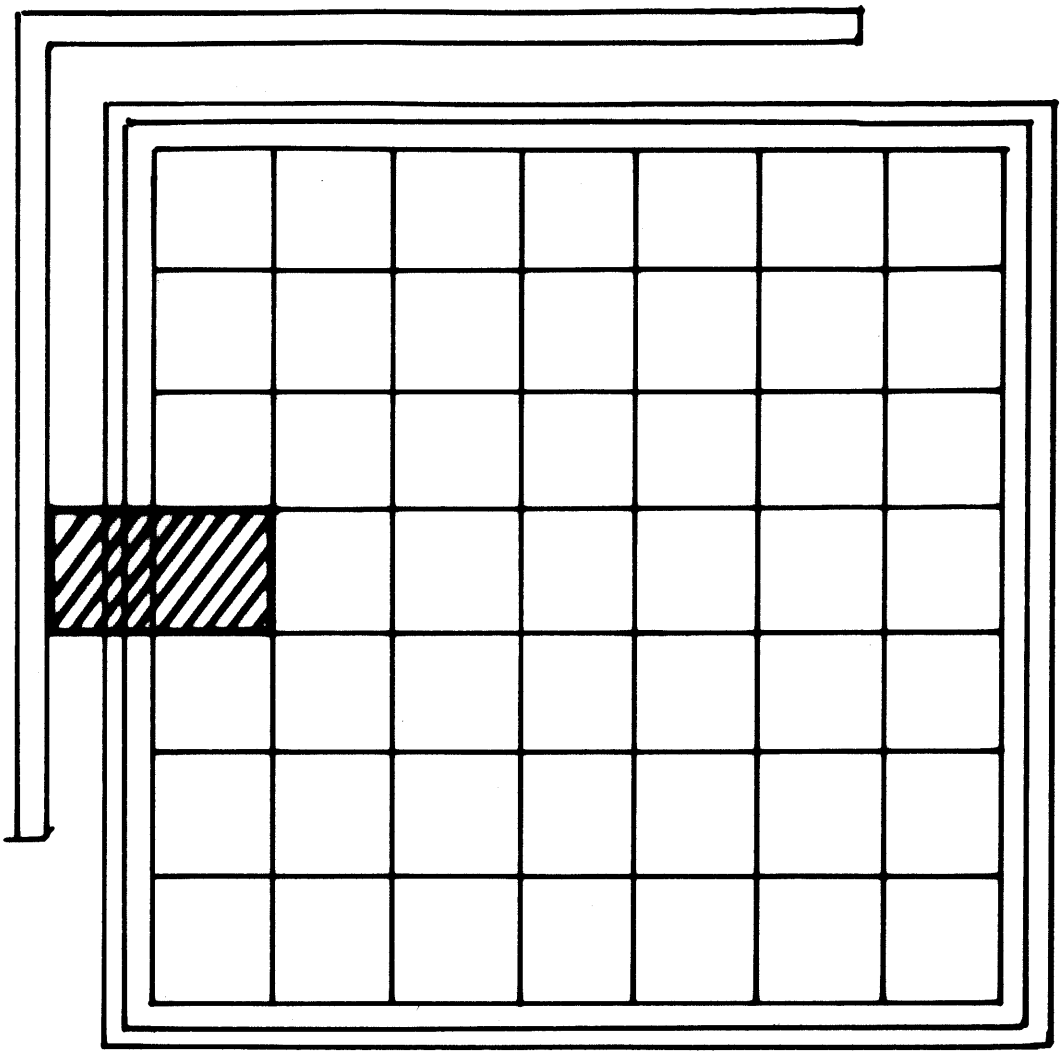

LEOPARD SUPERCELL TO GET
SPECTRUM FOR CONTROL BLADE

Fig. 2.3

In the fast region we have 3 groups supplied by LEOPARD which allows us to average the 3 fast α_i to get an effective $\langle\alpha\rangle_f$. This method is considered more accurate than using only one fast group cross section to obtain one Z. Thus, when possible, one would like to average over the α_i's rather than over the input cross sections. Carrying this out we get Z_1, Z_2, Z_3 and their corresponding α_1, α_2, & α_3. Then we use Eq. (2.3), the ψ_i's supplied by the LEOPARD edit, and the lethergy widths of each fast group in MUFT.

$$\Delta U_1 = 2.50$$

$$\Delta U_2 = 5.00$$

$$\Delta U_3 = 7.2111$$

The spectrum used was one based on a fast supercell which had the average enrichment of the subassembly (2.13%), and an extra region containing the water gap water and Zr from the subassembly can. The actual physical geometry was used in determining the extra region volume and composition. Stainless steel and control rod water were not included in the calculation, but later results with these materials included again showed little variance in the microscopic absorption cross section of B-10.

Carrying out the above calculations one obtains:

	Σ_a (cm^{-1})	D (cm)
Thermal	20.4231	.012241
Fast	1.2515	.1997595

2.3.2 Surface Area Conservation[14]

If we have a strong absorber it is possible that the conservation of surface area is more important than volume conservation. This may be caused by self shielding. Therefore if we consider a single tube and want to know the equivalent slab thickness such that

1) surface area is conserved
2) the width (not thickness) of the slab is set equal to the diameter (d) of the tube

t' = thickness

the equation then is

surface area of tube = surface area of slab

$\pi d = 2(t' + d)$

$$t' = d(\frac{\pi}{2} - 1) \qquad (2.7)$$

Duffy[6] in his article states that experimentally it was found that if the spacing between the tubes is very small, then a slab whose thickness is determined from Eq. (2.7) will have close to the same worth of the array of tubes.

Under these assumptions it was found that for the control blade under investigation, the half-thickness, t, was found to be:

$$2t = t' = .138\ (\frac{3.14159}{2} - 1)\ \text{inches}$$

$$t = .1000\ \text{cm}$$

Because this value was so close to the value for half-thickness calculated in the previous section, it wasn't investigated in any of the subassembly homogenization models which will be presented in Chapter 3.

2.3.3 Michelini's Method[15]

Michelini defines the blackness coefficients, α & β in terms of transmission, T_{ij}, and reflection, R_{ij}, coefficients.

$$\alpha = \frac{1}{2}\,\frac{1 - 2R_{10} - 2T_{10}}{1 + 3R_{11} + 3T_{11}}$$

$$\beta = \frac{1}{2}\,\frac{1 - 2R_{10} + 2T_{10}}{1 + 3R_{11} - 3T_{11}}$$

He then deals only with the transmission coefficients. Doing this one obtains:

$$\alpha = \frac{1}{2}\,\frac{1 - p_1}{1 + p_2} \tag{2.8}$$

$$\beta = \frac{1}{2}\,\frac{1 + p_1}{1 - p_2} \tag{2.9}$$

where

$$\left.\begin{aligned} p_1 &= 2T_{10} \\ p_2 &= 3T_{11} \end{aligned}\right\} \text{ called transmission probabilities}$$

Then, he shows that

$$\bar{p}_i = K_i \left[\, 1 - \frac{a}{2(R+a)} \,\right] \frac{a[a(2R-a)]^{1/2}}{R(R-a)} \left(\frac{1}{2} + \frac{0.167}{1 + w_i a/R}\right) \tag{2.10}$$

where: a = thickness of B_4C tube clad

R = outside radius of tube

$K_1 = 1$

$K_2 = 4/\pi$

$w_1 = 2.33$

$w_2 = 3.70$

These values for $\bar{p}_1$ & $\bar{p}_2$ would be used in Eqs. (2.8, 2.9). A correction is used if the control blade sheath enclosing the B_4C tubes is to be considered. The probability of transmission through the sheath (p_s) is used to multiply each of the round tube transmission probabilities calculated in Eq. (2.10)

$$p_s = 2E_3 (\Sigma_a t) \qquad (2.11)$$

where t is thickness of sheath.

The derivation above was for the case of perfectly absorbing control tubes. This is a good approximation for the thermal group but not so for the fast group where we must use the grey material approximation. The blackness coefficients now are defined as:

$$\alpha = \frac{1}{2}\frac{1 - p}{1 + p}$$

$$\beta = \frac{1}{2}\frac{1 + p}{1 - p} \qquad (2.12)$$

where:

$$p = p_{black} + (1 - p_{black})p_o \qquad (2.13)$$

$$p_{black} = (\bar{p}_1 + \bar{p}_2) / 2$$

$$p_o \tilde{-} \exp(-\Sigma_a d)[0.84 + 0.16 \exp(-0.6\ \Sigma_a d)]$$

$$d = 2(R - a)$$

The $\bar{p}_1$ and $\bar{p}_2$ are calculated as was done in Eq. (2.10)

With this method one obtains equivalent diffusion theory parameters for the entire blade, not just the B_4C material. The equations suggested for determining these diffusion parameters are as follows:

$$D = \frac{\tau}{2}(\beta - \alpha)$$

$$\Sigma_a = \frac{2\alpha}{\tau} \qquad (2.14)$$

τ = thickness of blade

These equations appear to be the reduced form of the equations in section 2.3, when $\frac{<\alpha>}{<\beta>} << 1$.

Using Michelini's method the following parameters were obtained for the control blade:

$D_1 = 1.2418$

$\Sigma_1 = .166$

$D_2 = .11451$

$\Sigma_2 = .953967$

These parameters are used in the Model III for homogenization in the next chapter.

2.4 Two Group Parameters for Curtains

From the table in Appendix I it can be observed that the curtains consist of 5400 ppm natural boron in stainless steel. The following number densities were then used.

$N_B = .4583 * 10^{21}$ atoms/cc

$N_{SS} = .08441 * 10^{24}$ atoms/cc

$N_{B-10} = .09065 \text{ X } 10^{21}$ atoms/cc.

Two sets of curtain cross sections were determined. One using Blackness theory and the other diffusion theory.

2.4.1 Use of Blackness Theory for Curtains

As was pointed out in section 2.3, the blackness theory parameters derived at by Eqs. (2.1, 2.2) assume no scattering. The effective diffusion theory absorption so derived will then be less than the straight diffusion theory parameters.[12] Still, Blackness theory, as outlined in Eqs. (2.1, 2.2) was tried and used in some of the homogenizing schemes. As it turned out, the worth of the curtains was under-estimated by this scheme. The scattering of the stainless steel is probably sufficient to make the use of the aforementioned equations non-valid.

The blackness theory parameters so derived are given below.

$D_1 = 15.836$

$\Sigma_1 = .015787$

$D_2 = .7750$

$\Sigma_2 = .32257$

In their calculation the stainless steel and boron cross-sections were summed before utilizing Blackness theory. Hence, the effect of stainless steel was included, as it must be.

2.4.2 Use of Diffusion Theory for Curtain.

As mentioned above the worth of the curtains could be increased by using their straight diffusion theory parameters. This was done in the Model III of the homogenization schemes. The diffusion parameters used were:

$D_1 = 1.06467$

$\Sigma_1 = .762439E-02$

$D_2 = .2955$

$\Sigma_2 = .353$

Chapter 3

SUBASSEMBLY HOMOGENIZATION (SOLUTION OF THE SPATIAL EQUATION)

The smallest unit of the core which contains all the elements of the core is the subassembly. This, then will be the subject of our homogenization.

The pins in the subassembly have different enrichments. There are three types of enrichments which can be discerned from figure I.1. In this discussion a cell or pin cell is taken to mean a fuel pin, its clad and surrounding moderator, a LEOPARD simple cell.

If we determine the group parameters for a cell using LEOPARD without considering the effect on this cell's spectrum due to the surrounding cells and subassembly environment, we have a non-interacting model. We will, of course, have some interaction between a cell and its environment. This could be taken into account by the following method, the interaction model.

Break up the subassembly into a number of different cells. In the pin region of the subassembly, each pin would act as a center for a cell. For each of these cells one would use a spectrum code which would both energy and volume average the nuclear parameters over the cell in a non-interacting manner. The width of

the energy groups of the analysis and resulting cross sections would be as small as one could make them. The smaller the width, the less accurate need be the spectrum used for group averaging in this interacting method[16]. Using these obtained fine group parameters for different zones (a zone being an area which can be represented by the same nuclear parameters), one would then use a spatial code to determine how each of the energy group fluxes varies over the volume of the subassembly.

Having obtained the fine-mesh energy group fluxes for the subassembly, including the initial cell regions, one would then contract the fine groups into broader groups. This by carrying out the necessary spectrum averaging over each of our cells. Since the energy fluxes used for this averaging included the interaction of the cells with their environment, so too will the newly created broader group cell cross sections.

These broader group cross sections one uses as feed into a spatial code to again generate energy group spatial dependent fluxes, which could then be contracted to get even broader group nuclear parameters. This procedure could be carried out until one obtains the sought after two-group diffusion parameters for the cells. One could then have these spatially averaged to get equivalent two-group parameters for the entire subassembly (desired input for MEKIN).

As one can see this method would be time consuming and expensive. One would also need a spectrum code that would print out the fine group parameters. MIT's version of LEOPARD has no such option. Its edit supplies one thermal group, and three fast groups or one fast group.

Having come to this realization, the following three homogenization models deal with LEOPARD in its present form. Interaction between zones is modelled using the supercell option of LEOPARD.

For spatial averaging the diffusion equation is solved using CITATION[17]. A CITATION zone is a region which contains the same nuclear parameters. The subassembly is broken up into a number of these zones whose two-group parameters were obtained using LEOPARD. LEOPARD essentially spectrum averages to give

$$\Sigma_{cell} = \frac{\int \Sigma(E)\phi(E)dE}{\int \phi(E)dE} \qquad (3.1)$$

Some cell spatial flux dependence, in the form of disadvantage factors, is also carried out by LEOPARD, but is not represented in equation 3.1. CITATION then homogenizes the subassembly to give:

$$\Sigma_{subassembly} = \frac{\int \Sigma(r)\phi(r)dr}{\int \phi(r)dr} \qquad (3.2)$$

Those LEOPARD cells or supercells which have parameters differing by less than a percent are usually grouped together to form a CITATION zone.

The zones are further divided up into geometric regions within each region one specifies the number of mesh points wanted for solution of the finite difference diffusion equations. If only one mesh point is specified for a region, CITATION places it in the center of that region.

With this background on how homogenization will be attempted, and the limitations of the codes in use, we now present the three models that were investigated. Models I and II were developed before any Dresden III subassembly power distribution or multiplication constant data was supplied.

3.1 Model I

This model takes its basic features from Harris of Northeast Utilities[18]. Each of the interior 36 pins is considered a LEOPARD cell and homogenized thermal group cross sections are found for them. (see fig. 3.1). The corner pins, those bordering on the zircaloy can, are each made into supercells by including in the extra region that part of the can, H_2O and stainless steel that might fall into its boundaries.

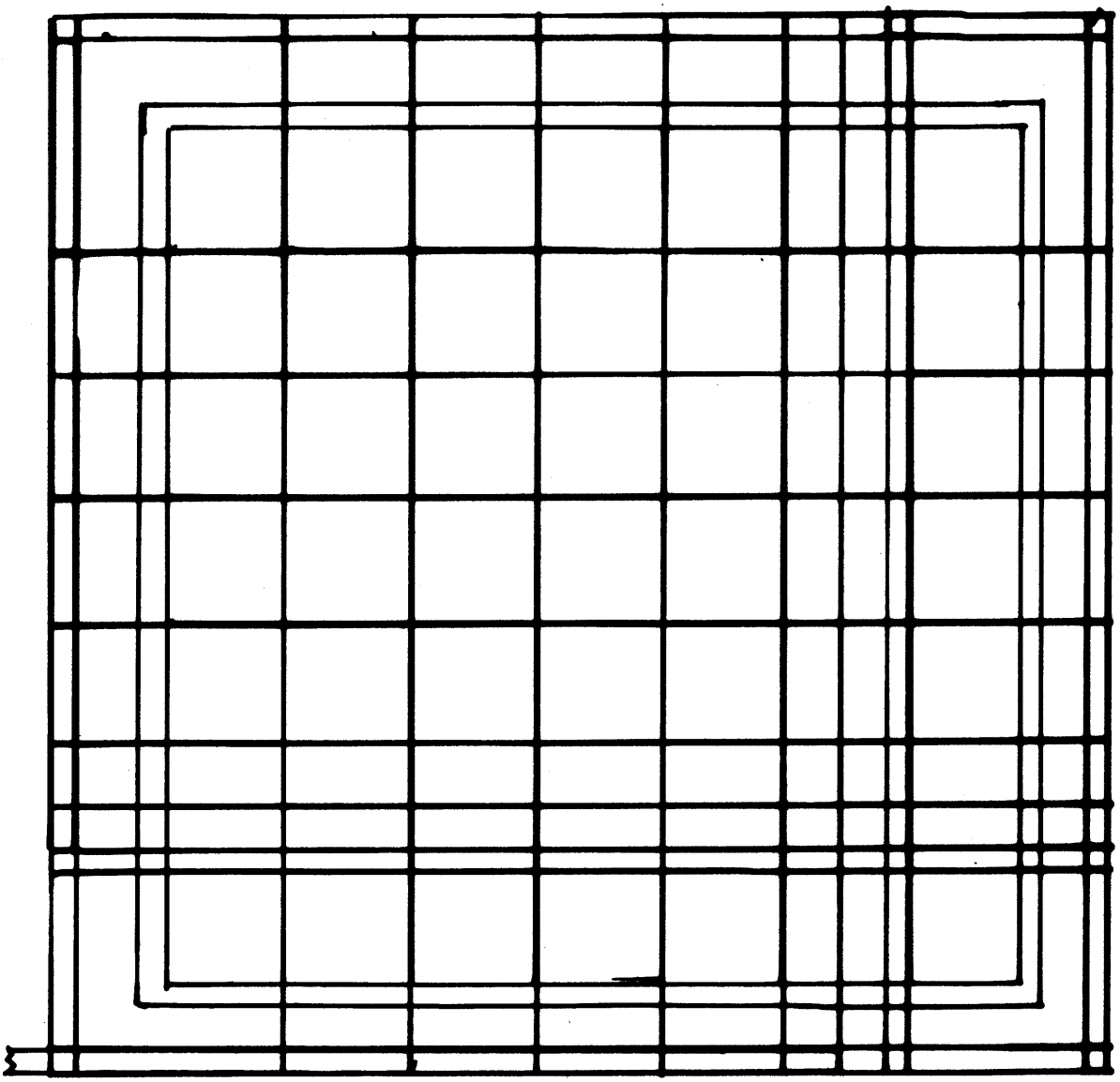

Model I CITATION
Region Arrangement

Fig. 3.1

The amount of extra region and its material volume fractions are dictated by the physical situation. By doing this we make an approximation that is embedded in the LEOPARD code, the Wigner-Seitz approximation[19]. This method models the volume of the supercell into an equivalent volume but of cylindrical shape. Therefore, though the corner pins might be located to one side of the actual geometry of their region; the code in effect center adjusts the fuel pin in the region of consideration and surrounds it equally on all sides by the extra region. Not only is this not reality, but as will be seen in the comparison results with Commonwealth data, k_∞ of this model is lower due to the closness of the pin source to the control material. However, this model seems to work well in determining power distributions within the subassembly. The only configuration tested with this Model I was that of control rod in and full curtains.

The can facing pins bordering on a control blade do not have the boron of the control blade included in their LEOPARD region calculation for their thermal spectrum. However, both the stainless steel and H_2O of the control blade are included in their extra region. Those pins bordering on the curtains never have any curtain material included in their extra region LEOPARD thermal spectrum calculation.

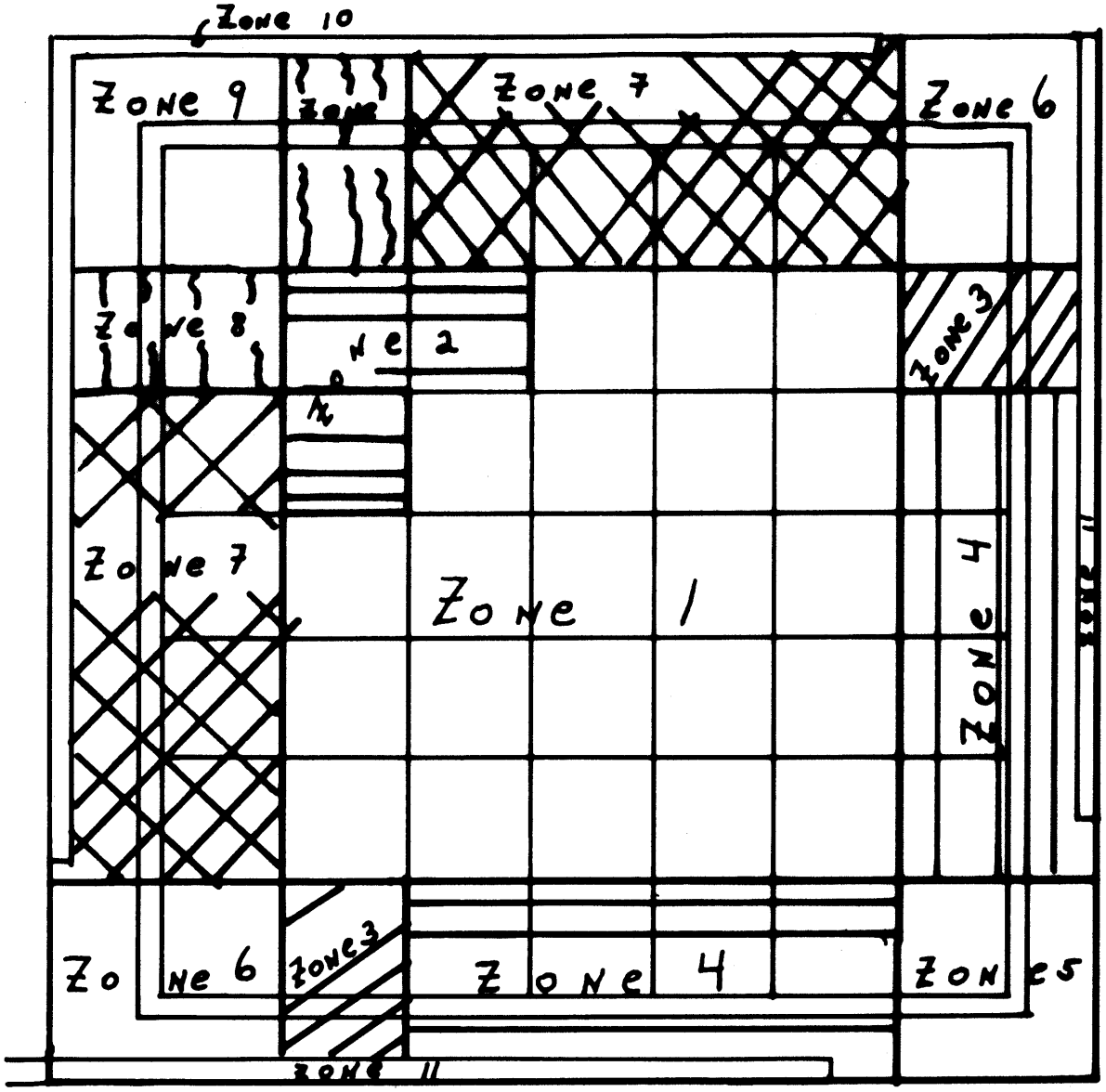

Model I CITATION
Zone Arrangement

Fig. 3.2

.32 .39	.39 .45	.56 .65	.62 .67	.68 .71	.80 .81	.90 .92
	.60 .65	.69 .67	.93 .95	1.00 .98	1.12 1.07	.92 .92
		.95 .98	1.03 1.01	1.10 1.04	1.18 1.06	1.23 1.25
			1.11 1.05	1.18 1.09	1.25 1.11	1.30 1.30
				1.25 1.12	1.33 1.16	1.38 1.39
					1.44 1.32	1.53 1.62
M I C E						1.27 1.45

Model I Results

k = .791

CONTROL ROD * IN
CURTAIN FULL
UNDISHED
NODE HOT STANDBY

FIG. 3.3

Blackness theory with volume conservation, as outlined in section 2.3.1, is used for the control rod's B_4C. For the curtain blackness theory is again used in accordance with section 2.4.1.

The Model I cell and supercell arrangements are shown in Fig. 3.1, while the zone arrangements are sketched in fig. 3.2.

The fast group parameters for all regions except those containing the B_4C of the control rod and the curtain are found by using a supercell whose extra region includes all the materials from the Zr can outward in their volume fraction of the entire subassembly. Neither the B_4C of control rod nor the curtain material was included in the fast group supercell. The enrichment was taken to be that of the average cell enrichment.

Fig. 3.3 shows the comparison of results using Model I and Commonwealth's supplied data. The k_∞ for Model I was .791 while Commonwealth's supplied data gave k_∞= .881 for this case. The Model I parameters are given below:

	D	Σ_a	$\nu\Sigma_f$	Σ_r
Fast	1.52345	1.5972E-02	4.5380E-03	1.7777E-02
Thermal	3.7289E-01	6.9586E-02	8.6718E-02	

No cross section data is supplied by Commonwealth. Verification exists in the form of checking the power distributions and criticality.

From the power distribution, it appears that the flux is depressed too much in the area of the control rod. This results in a tilting of the flux so that the pins along the narrow water gap region are over rated. This could be attributed to the same condition that caused the criticality to be so low, the Wigner-Seitz effective adjustment of the pins closer to the control rod. This effect was partially alleviated in Model II.

3.2 Model II

This model is more heterogeneous in nature than Model I, and does not include any supercells as zones for CITATION input (figure 3.4). All 49 pins including their surrounding water moderator only are used in LEOPARD cell calculations to get homogenized thermal group cross sections. The can-facing cells do not include anything outside the can or the Zr can itself. Instead, from the microscopic cross section edit of the LEOPARD code, the discrete regions of the zircaloy can, water and stainless steel have their nuclear parameters determined for hot standby condition. The formula $D = (3\Sigma_{tr})^{-1}$ where Σ_{tr} is the transport macroscopic cross section was used to obtain the diffusion coefficient, D.

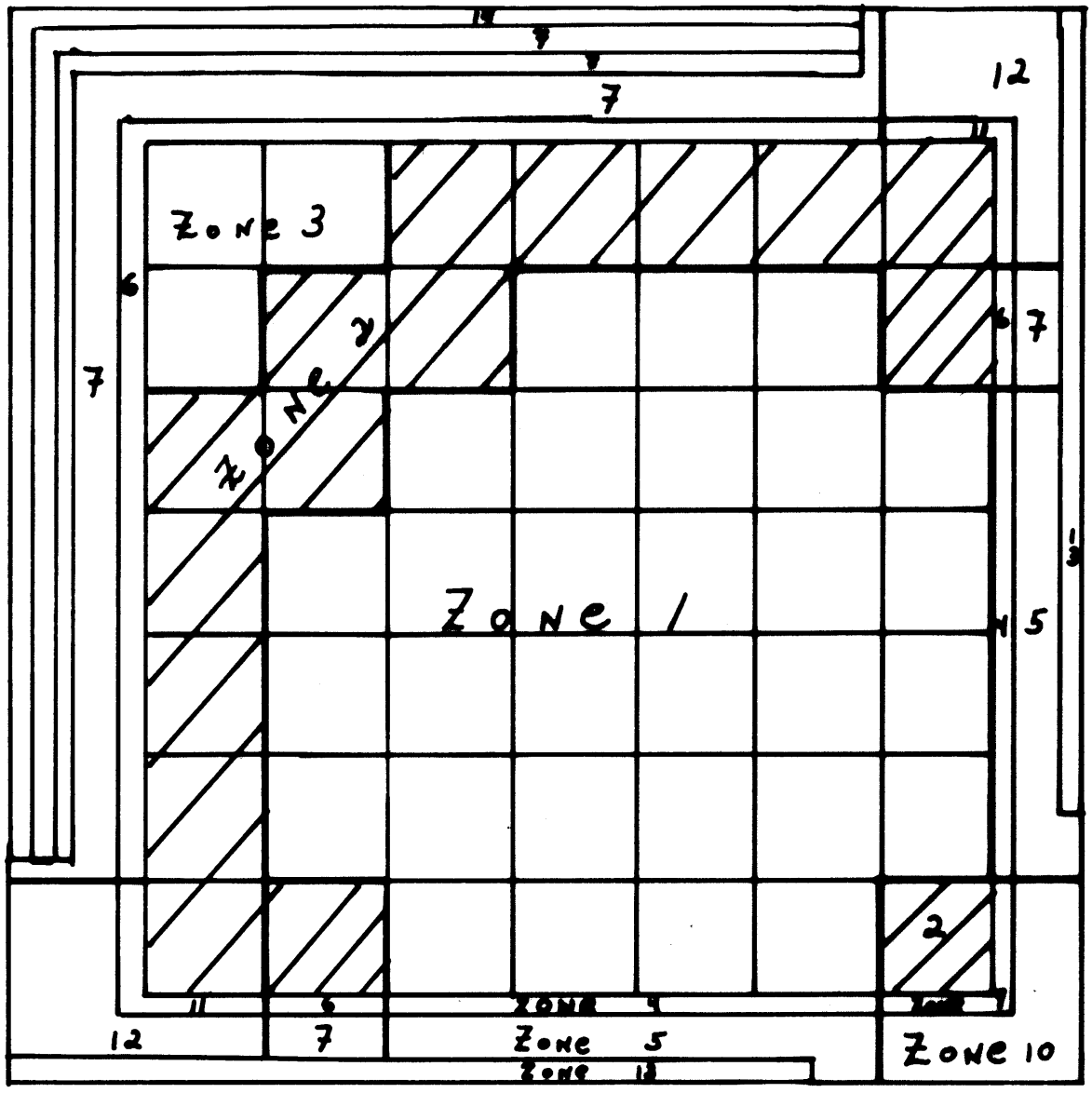

Model II
CITATION Zone Arrangement

Fig. 3.4

In determining a thermal spectrum for these discrete regions the Model I can-facing supercell spectrums were used (figure 3.1). This gave the spectrum averaged microscopic cross sections for the materials of interest. The average fast spectrum obtained as described in Model I, was used to obtain the microscopic cross sections for the materials.

In considering the thermal spectrum, those supercells which gave microscopic parameters for their materials close to others were combined for use in the CITATION zone and region arrangements (figures 3.2 and 3.4).

As in Model I, CITATION was used to obtain the subassembly effective parameters. Reflective boundary conditions for the 2-D CITATION runs were used in all sides.

The B_4C of the control rod and the curtains were handled as in Model I.

Results of Model II applied to the eight different subassembly cases are presented in the following table, Table 3.1.

Table 3.1

Hot Standby Subassembly 2-Group Parameters Using Model II

			UNDISHED	DISHED		
				CURTAIN		
			FULL	FULL	1/2	NO
IN	FAST	D_1	1.52062	1.53123	1.46575	1.40172
		Σ_1	1.58528E-02	1.57544E-02	1.57540E-02	1.55451E-02
		$\nu\Sigma_{f1}$	3.70785E-03	3.63266E-03	3.63508E-03	3.63517E-03
		Σ_R	1.77823E-02	1.78307E-01	1.79123E-02	1.79954E-02
	THERMAL	D_2	3.97962E-01	3.99023E-01	3.96751E-01	3.94549E-01
		Σ_2	6.96214E-02	6.87181E-02	6.66847E-02	6.43665E-02
		$\nu\Sigma_{f2}$	8.73469E-02	8.57959E-01	8.53427E-02	8.46443E-02
C.R.	K		.773	.771	.789	.814
	FAST	D_1	1.54646	1.55735	1.50033	1.44390
		Σ_1	7.48812E-03	7.36891E-03	7.33528E-03	7.30202E-03
		$\nu\Sigma_{f1}$	3.56536E-03	3.49395E-03	3.49479E-03	3.49571E-03
		Σ_E	1.88320E-02	1.88761E-02	1.89515E-02	1.90261E-02
OUT	THERMAL	D_2	3.91265E-01	3.92266E-01	3.90659E-01	3.89145E-01
		Σ_2	5.35239E-02	5.26981E-02	5.13721E-02	5.01141E-02
		$\nu\Sigma_{f2}$	7.60617E-02	7.46577E-02	7.44417E-02	7.42323E-02
	K		1.152	1.152	1.178	1.203

.31 20.5 .39	.38 15.6 .45	.54 16.9 .65	.59 11.9 .67	.66 7.0 .71	.76 6.2 .81	.86 6.5 .92
	.60 7.7 .65	.67 0.0 .67	.93 2.1 .95	1.01 3.0 .98	1.08 .93 1.07	.90 2.2 .92
		.95 3.1 .98	1.02 1.0 1.01	1.09 4.6 1.04	1.17 9.4 1.06	1.20 4.0 1.25
			1.10 4.5 1.05	1.17 6.8 1.09	1.24 10.5 1.11	1.27 2.3 1.30
				1.25 10.4 1.12	1.32 12.1 1.16	1.34 3.6 1.39
					1.41 6.4 1.32	1.46 9.9 1.62
M II %Diff C E						1.22 15.9 1.45

Model II Results

k = .771

$\overline{\text{ABS(\%Diff)}}$ = 6.97%

CONTROL ROD * IN
CURTAIN FULL
DISHED
NODE HOT STANDBY

Fig. 3.5

.92 23. 1.20	.83 19. 1.02	1.02 17. 1.23	.97 14. 1.13	.96 10. 1.07	.95 8.0 1.03	.96 1.0 .97
	.98 4.9 1.03	.91 3.3 .88	1.12 0.9 1.11	1.10 5.6 1.04	1.08 3.7 1.04	.86 3.5 .83
		1.09 2.8 1.06	1.03 4.9 .98	1.02 8.8 .93	1.03 12.6 .90	1.05 2.9 1.02
			1.00 9.0 .91	.99 11. .88	1.00 14. .86	1.02 3.9 .98
				.98 12. .86	1.00 14. .86	1.04 2.9 1.01
					1.04 9.6 .94	1.10 3.5 1.14
M II %Diff C E						.93 7.9 1.01

Model II Results

k = 1.152

$\overline{ABS(\%Diff)}$ = 8.3%

Fig. 3.6

CONTROL ROD * OUT
CURTAIN FULL
DISHED
NODE HOT STANDBY

.33	.40	.57	.63	.70	.82	.94
	.59	.66	.92	1.00	1.07	.94
		.94	1.01	1.08	1.14	1.26
			1.09	1.16	1.21	1.32
				1.23	1.28	1.40
					1.39	1.56
M II						1.33

Model II Results

k = .7735

CONTROL ROD * IN
CURTAIN FULL
UNDISHED
NODE HOT STANDBY

Fig. 3.7

The four criticalities that were compared with the Commonwealth data show poor agreement. However, the case of dished pellets, control rod out, and full curtain was better than the Model III results to be presented shortly. The reasons why Model II give lower k_∞ than Model III will yield is due to the deliberate deletion from the CITATION input of the fast group production cross section from all the zones which lie outside the fuel pin lattice region. Figure 3.6 is the power distribution for this case. Figure 3.7 shows the power plot for the undished pellet case with full curtain and control rod in.

3.3 Development of Model III

Both Model I and Model II compared poorly with the Commonwealth supplied criticalities. Therefore, starting with Model II, a step by step development was made which concentrated on bringing the subassembly power distribution of the developing model and supplied data into better agreement. This was carried out for the curtain full, no control rod case (refer to figure 3.8).

Among the more important innovations made to Model II to arrive at Model III were the following: A new version of LEOPARD, Farrar's version was employed. It allowed one to make use of the supercell option and yet maintain the simple cell atomic number densities to obtain macroscopic parameters.

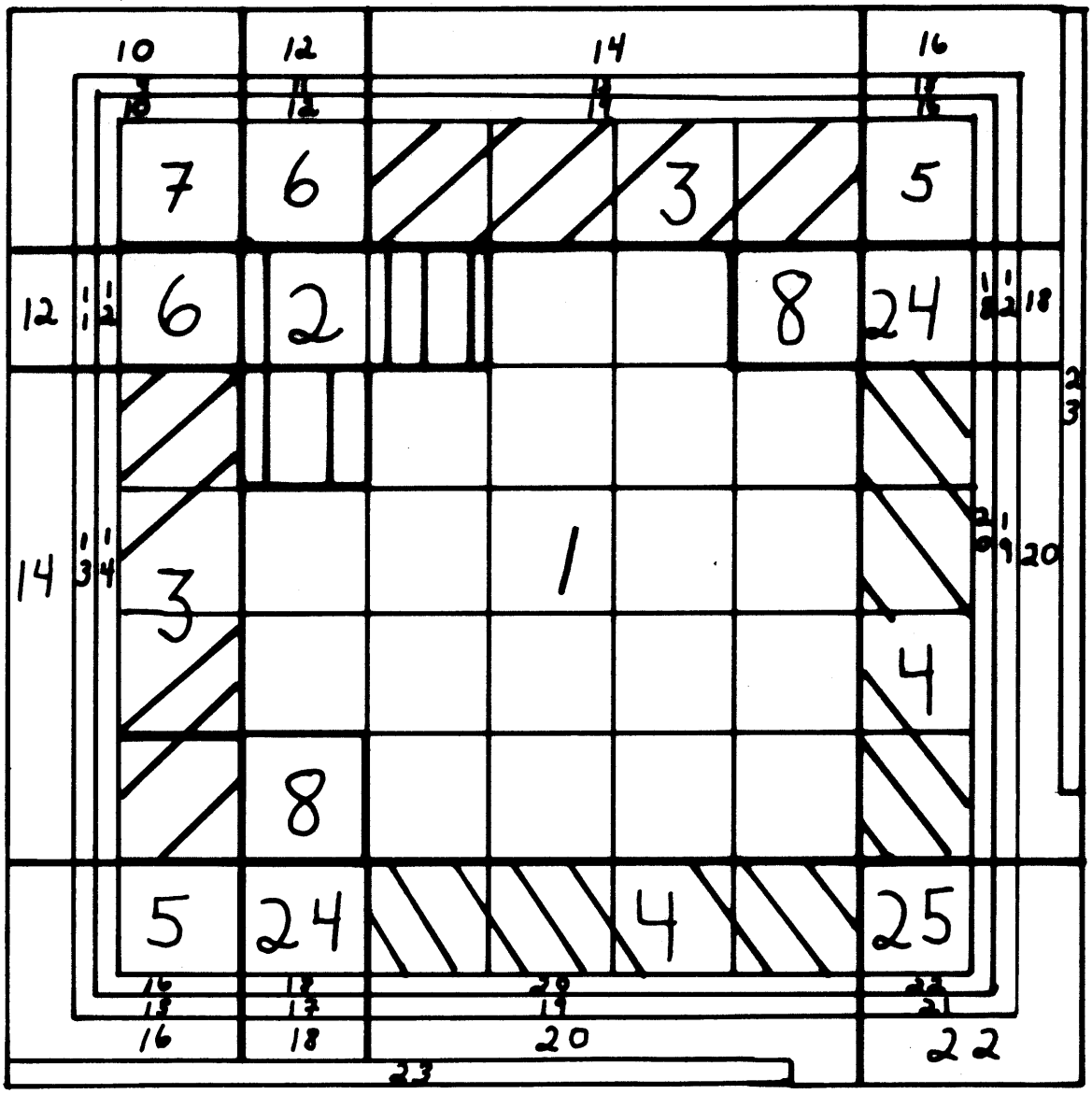

Model III
CITATION Zone Arrangement

Fig. 3.8

Both the fuel cell and water gap material regions (discrete regions) were no longer given one set of fast parameters, but fast parameters more representative of their atomic number densities.

Because the pin power of the curtain facing pins was too high the curtain cross sections were represented now by diffusion theory parameters instead of Blackness theory derived equivalent diffusion parameters. This increased the curtains' worth and shifted the flux to the wide gap region.

Breen[21] has shown that cores with large water gaps are better represented by using the smaller Maxwellian diffusion coefficients for the thermal group than the Wigner-Wilkens diffusion coefficient. One noticed greater water gap-facing pin power when this switch was made because less of the thermal neutrons from the water gaps, which are the major source of thermal neutrons, diffused into the interior.

To further shift the flux to the wide gap corner, where the rod existed, the narrow gap water and zircaloy can were excluded from the narrow gap-facing pin spectrum averaging. Justification could be found in the belief that if one neglects the curtain from the spectrum calculation for these pins, one should also neglect the water gap water. The curtains tend to harden the flux, while the water would soften it.

.43 9.3 .39	.45 0.0 .45	.61 6.2 .65	.63 6.0 .67	.69 2.8 .71	.81 0.0 .81	.98 6.1 .92
	.67 3.0 .65	.70 4.3 .67	.95 0.0 .95	1.01 3.0 .98	1.09 1.8 1.07	.94 2.1 .92
		.96 2.0 .98	1.00 1.0 1.01	1.06 1.9 1.04	1.15 7.8 1.06	1.23 1.6 1.25
			1.05 0.0 1.05	1.11 1.8 1.09	1.20 7.5 1.11	1.27 2.3 1.30
				1.17 4.3 1.12	1.27 8.7 1.16	1.36 2.2 1.39
					1.38 4.3 1.32	1.52 6.2 1.62
M III %Diff C E						1.38 4.8 1.45

Model III Results

k = .882

$\overline{\text{ABS(\%Diff)}}$ = 3.6%

Fig. 3.9

CONTROL ROD * IN
CURTAIN FULL
DISHED
NODE HOT STANDBY

1.04 13.3 1.20	.91 8.8 1.02	1.10 10.6 1.23	1.04 8.0 1.13	1.02 4.7 1.07	1.02 .97 1.03	.99 2.0 .97
	1.02 .97 1.03	.91 3.3 .88	1.12 .89 1.11	1.09 4.6 1.04	1.08 3.7 1.04	.85 2.4 .83
		1.07 .93 1.06	1.00 2.0 .98	.98 5.1 .93	1.00 10. .90	1.03 .97 1.02
			.95 4.2 .91	.93 5.4 .88	.96 10.4 .86	.99 1.0 .98
				.93 7.5 .86	.96 10.4 .86	1.00 1.0 1.01
					1.02 7.8 .94	1.08 5.3 1.14
M III %Diff C E						.96 5.0 1.01

Model III Results

k = 1.184

$\overline{ABS(\%Diff)}$ = 4.81%

Fig. 3.10

CONTROL ROD * OUT
CURTAINS FULL
DISHED
NODE HOT STANDBY

Interior to the zircaloy can is a small water gap which will be called an interior water gap. It was represented discretely and no longer becomes part of the thermal spectrum calculation for the narrow gap-facing pins.

The inclusion of the curtain material in the bundle average fast spectrum calculation was made. This fast spectrum is used to obtain the fast parameters for the non-fueled regions.

Finally, for the case where the control rod was present, it was represented by Michelini's method. See figures 3.9 and 3.10 for power plots obtained using Model III.

3.3.1 Model III Defined

This then represents the final MIII used in the homogenization of subassemblies.

Using figure 3.8:

T h e r m a l

1.→ Calculate interior zones 1, 2 and if present 8, with LEOPARD simple cells,

2.→ For pins facing water gap without any control blade or curtain in its supercell geometry use Farrar's LEOPARD with supercell option to include effect of gap water on spectrum. When curtain or control blade is present, do not include any material outside the simple fuel cell itself.

→ For zone 5 when a curtain is present, use only that material that lies on the wide gap side in the extra region.

3.→ For H_2O, stainless steel, Zr-4, and B-10, use spectrum of can-facing zones, as calculated above to get micro's.

4. Use $D_{Maxwellian} = (\frac{1}{v})_{max} D_{MND}$ for all fuel cells, Zr-4 can, and water in water gap.

F A S T

1. Use an average fast bundle cell to get micro's for discrete regions of H_2O, stainless steel, Zr-4, and B-10 not in fuel containing cells. This involves adding <u>all</u> of the materials in the average fast supercell.
2. Use macro edits from LEOPARD for fuel cells and in can facing cells use only the simple cell spectrum (no supercells).

C U R T A I N S

Use diffusion theory parameters

C O N T R O L B L A D E

Use Michelini's method.

Chapter 4

APPROXIMATIONS AND LIMITATIONS OF MODEL III

Model III was used to generate the homogenized diffusion theory parameters for the eight types of subassemblies. The results are presented in Table 4.1.

The objective of the present chapter is to conduct a criticality comparison of the four subassembly cases we have supplied data on. Having done that in Section 4.1, a reconcilliation of the discrepancies will be attempted in the second section of this Chapter. That is, theoritically plausible arguments are made for the difference in criticality Model III yields. An attempt to substantiate these arguments is made in Sections 4.3 and 4.4.

The purpose of this Chapter is not to further develop Model III. In truth, the present form of Model III is adopted for use in the remainder of this work. Rather, it is hoped to shed some light on the limitations of the model.

Table 4.1

Hot Standby Subassembly 2-Group Parameters Using Model III

		Undished		Dished	
		Full	Full	$\frac{1}{2}$	No
	D_1	1.36400E-00	1.37379	1.37686	1.37998
	Σ_1	1.14038E-02	1.12987E-02	1.12428E-02	1.1189E-02
	$\nu\Sigma_{f1}$	4.56898E-03	4.48533E-03	4.48554E-03	4.48558E-03
	Σ_r	1.75298E-02	1.76204E-02	1.77644E-02	1.79087E-02
IN	D_2	3.59099E-01	3.60686E-01	3.60913E-01	3.61260E-01
	Σ_2	6.94146E-02	6.85316E-02	6.62760E-02	6.42189E-02
	$\nu\Sigma_{f2}$	8.3376E-02	8.17748E-02	8.17508E-02	8.18471E-02
↑ CR ↓	K	.88505	.88215	.9101	.939
	D_1	1.40806	1.41393	1.42143	1.42400
	Σ_1	6.97241E-03	6.86399E-03	6.83143E-03	6.80745E-03
	$\nu\Sigma_{f1}$	4.45534E-03	4.37317E-03	4.37176E-03	4.37592E-03
	Σ_r	1.80100E-02	1.80632E-02	1.81663E-02	1.82665E-02
OUT	D_2	3.56765E-01	3.55324E-01	3.58724E-01	3.58735E-01
	Σ_2	5.1728E-02	5.08966E-02	4.99564E-02	4.85943E-02
	$\nu\Sigma_{f2}$	7.22440E-02	7.08294E-02	7.15367E-02	7.13526E-02
	K	1.185	1.184	1.2155	1.244

4.1 Comparison of Model III with Commonwealth Data

Table 4.2 gives us a look at the differences in criticality for four subassembly cases.

Table 4.2

Criticality Comparison

Method	Curtain Only	Control Rod and Curtain	Control Rod Only	No Control
	ΔK_1=.302	ΔK_2=.057	ΔK_3=.305	
MIII	1.1844	.8882	.939	1.244
|% diff|	4.4	.11	6.0	1.4
Common Ed.	1.134	.8811	.999	1.262
	ΔK_1=.253	ΔK_2=.118	ΔK_3=.263	

From the ΔK's it appears that MIII overestimates the strength of the control rod both for when the curtains are present, ΔK_1; and when no curtains are present, ΔK_3.

On the other hand, MIII underestimates the strength of the curtains, ΔK_2. These discrepancies are partially cancelled when we compare MIII to Commonwealth Edison's data for the cases of no control, and control rod plus curtain.

For the analysis of the accident to be described in Chapter 5, nearly three quarters of our core at initiation of accident is of the well-predicted subassembly type control rod and curtain. At the accident's conclusion, nearly all subassemblies will be of this case. The rather poorly predicted case of curtain only will represent nearly all of the remaining one quarter of the core at accident initiation. In this case, MIII overpredicts the criticality and this will be seen to be a conservative condition in our accident.

It was largely due to the good agreement of MIII for the control rod and curtain case that this homogenization model was accepted at its development stage.

4.2 Major Approximations of Model III

Among the more major approximations of Model III are the following.

4.2.1 Use of Just Two Energy Groups

The parameters generated for our accident permit a maximum of only two energy groups. The use of such a small number of energy groups puts a very large demand on how accurate the flux spectrum was which was used to spectrum average our broad group parameters. Intrinsic

to this, of course, is the accuracy of the theory used in the codes to solve the spectrum equation, and the number of fine groups we start out with. The accuracy of our fine group cross section library also comes into play.

For the most part, this approximation was noted but no sensitivity analysis was carried out.

4.2.2 Insufficient Account Taken of Overlapping Spectrum Effects.

As pointed out in the beginning of Chapter 3, this approximation goes hand in hand with the one above in obtaining accurate two group parameters.

The BWR subassembly by its very nature of varying enrichments, dished and undished pellets, water gaps, control and structural material, makes one wonder if an asymtotic spectrum is attained anywhere in the bundle; except maybe in the center of the high enrichment pins. The use of the LEOPARD extra region can only partially allow us to consider overlapping spectrum effects. However, LEOPARD'S calculation of disadvantage factors for each of its cell regions at each thermal energy group should help take into account some spatial effects, at least within a pin cell. These disadvantage factors are then used to get homogenized LEOPARD cell fine-group parameters before the energy equation for the cell is solved.

The use of the LASER code composed of MUFT (fast spectrum) and THERMOS (solution of thermal spectrum) may have resulted in better cross sections. Though the LASER version at MIT does not allow for slab geometry or an option for an extra region, it is more accurate in handling the spatial effects of the spectrum due to its use of the integral transport equation, rather than a computed regionwise disadvantage factor. Its scattering kernal model, the Nelkin scattering kernal, has been accepted as a more exact model for LWR's than the heavy gas model used by LEOPARD.

On the subassembly scale the interaction model discussed in the beginning of Chapter 3 would be a more correct way of obtaining two group subassembly homogenized parameters (then MIII). An approximation to this would be to use flux synthesis. Here one could solve the spectrum equation for each of the LEOPARD cells; and then take account of overlapping spectrum effects by mixing the (non-interacted cell) spectrums to arrive at an interacted spectrum for each of the cells before a final spectrum weighting to obtain the two group parameters for each of the cells was obtained. This would involve a good before-hand knowledge of what weighting factors each of the surrounding non-interacting spectrum should have to arrive at the correct final interacting spectrum for each of our cells.

It should be noted that the fine group disadvantage technique used by LEOPARD differs from the flux synthesis just defined. In the disadvantage technique we divide the interested region up into zones and find disadvantage factors for these zones for all energy levels. We then find total region average fine group parameters before solving the spectrum equation for the entire region over all energy groups.

In the flux synthesis scheme we solve the fine group energy equation for all the zones in the region first. Then, using weighting factors, obtain a blend of spectrums to arrive at an adjusted blended spectrum for each zone. The two group parameters for each zone would thus be found which could then be used in a spatial code to solve for the region two group parameters.

This flux synthesis scheme would be an improvement in Model III. It could have been used to obtain better spectrums for each of our pin cells. The derivation of correct weighting functions would make this all too time consuming for the purpose of this work however.

LASER was also not used. It is more expensive to run and its added accuracy for simple pin cells did not justify the additional cost.

4.2.3 Use of Diffusion Theory

Diffusion theory lacks exactness in the presence of high absorbers. It is a well-known fact that it tends to underpredict the dip in the flux within absorbers.

4.2.4 Use of Blackness Theory For Control Rods.

As described in Section 2.3, Blackness Theory attempts to equate the current of our absorber. That is, it uses transport theory for within the absorber and diffusion theory outside the absorber. Then it sets the current derived from the transport theory to that from diffusion theory at the boundary of the absorber. Hence, blackness theory is basically a current conserving device. However, its use of the diffusion theory equation for the region just outside the absorber is incorrect.

In MIII, where we have used Michelini's method, we again make the approximation that the reflecting terms are neglected and we deal only with transmission probabilities. We do include the stainless steel sheath as part of the absorber since not to do so would increase the error in assuming the diffusion theory equations hold up to the surface of our absorbers.

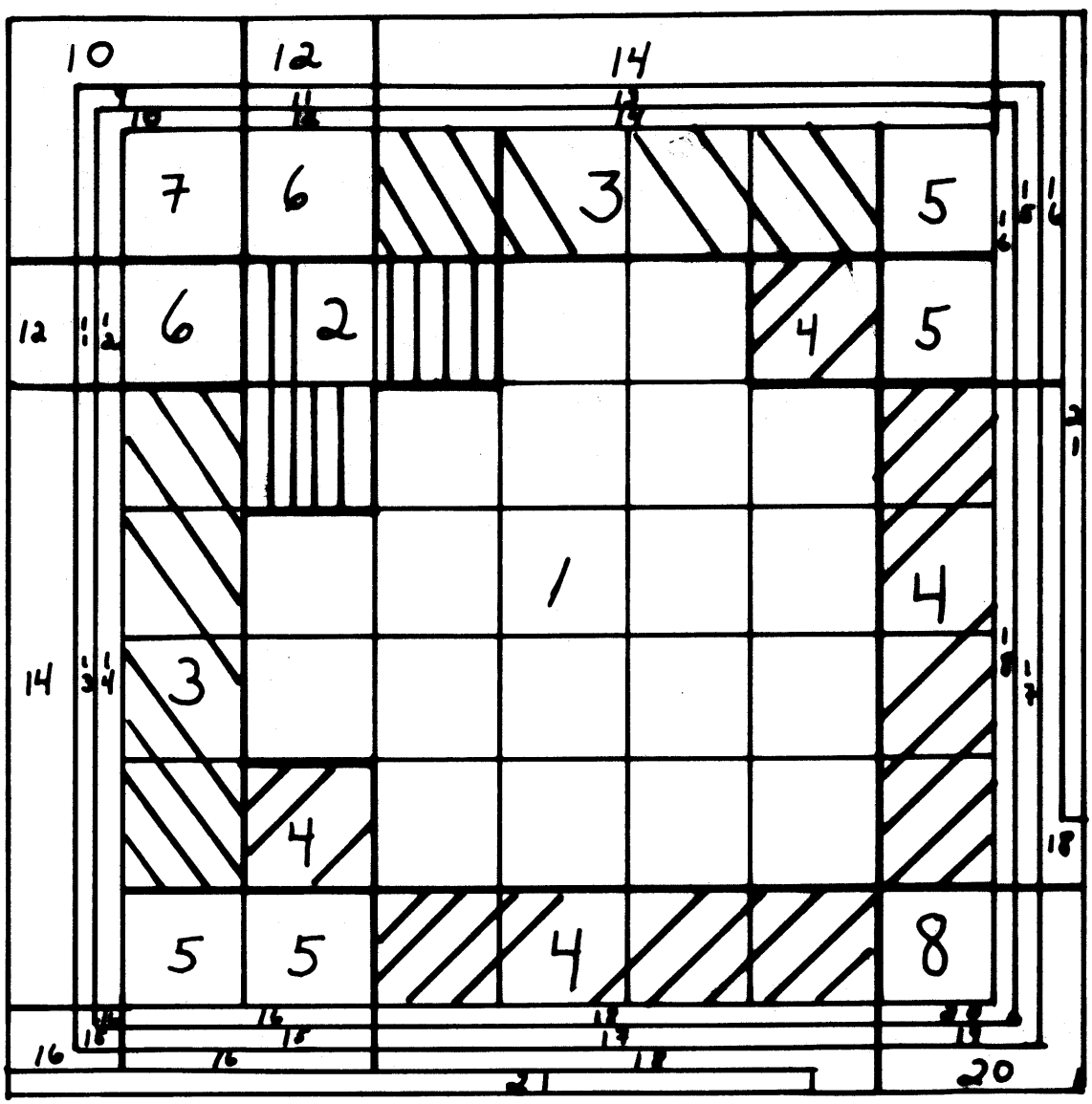

Variations'
CITATION Zone Arrangement

Fig. 4.1

4.3 Variations on MIII For Control Rod Out-Curtain In Case

For this case approximations 4.2.1, 4.2.2, and 4.2.3 come into play. A series of runs were made to see the effects of changing the spectrum weighting, and to find the effect of including some of the curtain's boron in the narrow gap water to offset approximation 4.2.3.

It should be recalled that Model III uses a single pin LEOPARD to get fast and thermal parameters for the narrow gap-facing pins when the curtain is present. Also, we will be concerned only with those zones facing or in the narrow gap whose supercell boundaries would include the curtain. That is, fuel cell zones 4 and 5, and discrete zones 17, 18, and curtain zone 21 on figure 4.1. This figure will be the one used in naming zones unless otherwise mentioned.

4.3.1 Spectrum-Non-Spatial Effect Analysis

Model III doesn't include the spectrum effects of the discrete region material on the spectrum used for averaging our group parameters in zones 4, 5, 17, 18, and 21. An analysis was carried out to see the effect of including some or all of the discrete zone material in the LEOPARD runs.

The following five LEOPARD runs were carried out.

Run	Condition
L1	Interior Simple Cell - High enrichment interior cell used in MIII.
L2	Supercell - Includes Zr, H_2O and stainless steel in extra region in actual volume fraction amounts except that boron of curtain is replaced by stainless steel.
L3	Supercell - Includes Zr, H_2O and stainless steel in extra region and spreads the Boron-10 of the curtain into the moderator.
L4	Supercell - No curtain (stainless steel or B-10) material present, just gap water and Zr in extra region.
L5	Supercell - The average fast supercell containing the B-10 of curtain spread throughout subassembly. Used in MIII to get fast parameters for discrete zones.

The results of these runs for H_2O, B-10 and stainless steel are presented in Table 4.3.

Table 4.3

Spectrum Analysis Effects

Leopard Run	H_2O			B-10		S.S.	
	σ_1	σ_2	$\sigma_{removal}$	σ_1	σ_2	σ_1	σ_2
L1	.1785E-01	.3727	1.153	44.72	2154	.3733E-01	1.677
L2	.1848E-01	.3847	1.246	47.58	2224	.3975E-01	1.731
L3	.1855E-01	.3827	1.258	47.99	2212	.4010E-01	1.722
L4	.1882E-01	.3888	1.226	46.90	2247	.3921E-01	1.749
L5	.1882E-01	.3884	1.245	47.52	2245	.3973E-01	1.744

Then, comparing MIII and L3 we get Table 4.4:

Table 4.4

Model III vs. L3 For Some Discrete Materials

	H_2O			B-10		S.S.	
	σ_1	σ_2	σ_r	σ_1	σ_2	σ_1	σ_2
MIII	.1882E-01	.3727	1.245	47.52	2154	.3973E-01	1.677
|% Diff|	1.4	2.6	1.1	1.0	2.6	.92	2.6
L3	.1855E-01	.3827	1.258	47.99	2212	.4010E-01	1.722

From Table 4.4 we see that by using L3 instead of MIII we could raise absorption in thermal group by 2.6%, and increase removal by about 1% (this for the narrow gap water). In addition from the results for boron and stainless steel, the use of L3 parameters could raise absorption of curtain by about 2.0%.

This shows that the inclusion of stainless steel and boron, or the use of L3, would help shift thermal flux to the control rod absent wide water gap; thereby improving the power distribution. Also, the increase in the absorption of material will lower k_∞ to a better agreement with Commonwealth supplied data.

Examining Table 4.3 the following conclusions seem plausible:

a) Effect of stainless steel (L2 vs. L4)

The addition of S.S.

1) raises σ_r of H_2O
2) on the whole, shifts more of the flux into the epithermal fast group thus raising σ_1 (the fast absorption) and lowering σ_2 (the thermal absorption).

b) Effect of stainless steel and boron (L2 vs. L3)

The replacement of some stainless steel with B-10

1) raises σ_r of H_2O
2) shifts flux from thermal to epithermal group thus raising σ_1 and lowering σ_2

c) Simple interior cell vs. all other cases

The interior cell

1) gives low σ_r for H_2O

2) gives lower σ_1 and σ_2 for H_2O, S.S. and B-10

The results of (C) above may be due to the fact that its spectrum is very hard as compared to any of the supercell cases. In the fast group the neutrons populate the higher energy groups more so than in the other cases. Hence, the fast group is harder. THis is probably due to the presence of little water and greater volume proportion of fuel.

This same reasoning may be applied to the case of no curtain - no control rod. There the difference in criticality between Commonwealth and MIII could be partly due to the Wigner-Seitz approximation which puts the fuel pin in the center of a cell. The pin is then surrounded evenly by water and zircaloy. Based on (C) above this hardens the fast and thermal spectrums, and lowers σ_r. A lower σ_r would help explain MIII's lower criticality for this no curtain - no control rod case as compared to Commonwealth's.

Based on this spectrum analysis it was thought that using L3 thermal parameters in place of those used in MIII would improve results for the homogenized subassembly parameters. This was done and labeled Variation A. Except for zones 4, 5, 17, 18, and 21, we stick to MIII exactly. Then if we label zones 4 and 5 fuel regions, and zones 17, 18, and 21 discrete regions we can say

1.04 13.3 1.20	.91 10.8 1.02	1.11 9.8 1.23	1.04 8.0 1.13	1.02 4.7 1.07	1.02 1.0 1.03	.99 2.0 .97
	1.02 1.0 1.03	.91 3.3 .88	1.12 0.9 1.11	1.09 4.6 1.04	1.08 3.7 1.04	.85 2.4 .83
		1.06 0.0 1.06	.99 1.0 .98	.97 4.1 .93	1.00 10.0 .90	1.02 0.0 1.02
			.94 3.2 .91	.93 5.4 .88	.96 10.4 .86	.99 1.0 .98
				.92 6.5 .86	.96 10.4 .86	1.00 1.0 1.01
					1.02 7.8 .94	1.08 5.3 1.14
V. A %Diff C E						.96 5.0 1.01

Variation A

k = 1.181

$\overline{ABS(\%Diff)}$ = 4.82%

Fig. 4.2

CONTROL ROD * OUT
CURTAIN FULL
DISHED
NODE HOT STANDBY

Variation A - Figure 4.2

Fuel Region

a) Fast parameters - MIII used

b) Thermal - MIII used

Discrete Region

a) Fast - MIII

b) Thermal - uses spectrum weighting supercell containing actual volume percentages of S.S., H_2O, Zr and 323 ppm B-10.

The results can be seen in Table 4.5, even with the extra 145 ppm of B-10 present above actual material content. Only a small step in the right direction resulted. The effect of change in such a small volume percentage of our subassembly is indeed small. Better results are hoped for if we include the effects of the approximation detailed in Section 4.2.3.

4.3.2 Space and Spectrum Effects

It is clear from figure 4.1 that one way to lower k_∞ would be to shift the flux away from the high enrichment section of the subassembly near the narrow water gap to the lower enrichment wide water gap region. This could be accomplished by strengthening our curtain. In section 4.3.1 we noted that pure spectrum effects don't accomplish this to the degree needed. We then call on approximation 4.2.3 and claim that the gist of what we shall do in this section is

based on this failing of MIII. That is, that diffusion theory, and diffusion theory parameters used for the curtains don't sufficiently attenuate the flux in this narrow gap region.

Through what follows, keep in mind that if we spread out the boron and other absorbers they will be placed in a higher flux zone for the greater part, and absorb more. THis should increase their effective strength.

4.3.2.1 Effect of Placing Boron in the Narrow Gap Adjacent Fuel Pin Cell's Water

In this case, Variation B, 323 ppm of B-10 were placed in the water of zones 4 and 5. No boron was placed in the narrow gap water, and the concentration of boron in the curtain was not decreased. The discrete regions were, however, spectrum averaged with a spectrum generated having 323 ppm of boron-10 in all the water of its supercell, as in Variation A.

We therefore have:

Variation B - Figure 4.3

Fuel Region

a) Fast - MIII

b) Thermal - Thermal supercell included 323 ppm boron-10 in water of moderator and extra region.

1.05 12.5 1.20	.92 9.8 1.02	1.11 9.8 1.23	1.05 7.1 1.13	1.02 4.7 1.07	1.01 1.9 1.03	.99 2.0 .97
	1.03 0.0 1.03	.92 4.3 .88	1.12 0.9 1.11	1.08 3.7 1.04	1.08 3.7 1.04	.85 2.4 .83
		1.07 0.9 1.06	1.00 2.0 .98	.97 4.1 .93	.98 8.2 .90	1.02 0.0 1.02
			.94 3.2 .91	.93 5.4 .88	.94 8.5 .86	.99 1.0 .98
				.92 6.5 .86	.95 9.5 .86	1.00 1.0 1.01
					1.00 6.0 .94	1.09 4.4 1.14
V. B %Diff C E						.95 5.9 1.01

Variation B

k = 1.171

$\overline{ABS(\%Diff)}$ = 4.57%

Fig. 4.3

CONTROL ROD * OUT
CURTAIN FULL
DISHED
NODE HOT STANDBY

Discrete Region - Same as Variation A

a) Fast - MIII

b) Thermal - Uses spectrum weighting of the fuel region thermal supercell above.

The result was a decrease in k_∞ of about 1.2% over MIII (see Table 4.5), a move in the right direction. We have not included B-10 in the fuel region for fast parameter calculations yet. This will be done in the following section dealing with Variation C.

The pin cell is several discrete regions removed from the curtain, and so one is less justified in placing B-10 here as opposed to in the water gap region.

The idea behind this Variation B was to carry the curtain effects into the parameter generation for the curtain adjacent fuel cells. However, to place boron in LEOPARD one must place it in all the supercell's water (moderator and extra region) or in none at all. Hence, the edit for the thermal parameters from LEOPARD for the pin cell area necessarily included the boron content as well as the spectrum effects of the presence of boron. One could obtain just the spectrum effects if the macroscopic parameters of the boron to the LEOPARD edit were subtracted out. This was not done

because even with no subtractions the effect of the presence of boron wasn't strong enough to get us really close to the Commonwealth supplied criticality for the case of k_∞ = 1.13.

4.3.2.2 Effect of Using a Single Set of Fast Homogenized Parameters for Narrow Gap Supercell Regions.

It was hoped that by weighting the fast parameters with a fast spectrum that takes into account the closeness of the neighboring regions to the curtain, one could increase the strength of the curtain. This is justified under approximation 4.2.2. In addition, the entire supercell region was given the same fast parameters in the CITATION run. This could be justified under approximation 4.2.3. Then in the general format we have

Variation C

Fuel Region

a) Fast - Supercell with 323 ppm B-10 in water regions plus actual amounts of other materials

b) Thermal - MIII

Discrete Regions

a) Fast - Same supercell as used in fast fuel region

b) Thermal - MIII

The results were again favorable in lowering k_∞ (Table 4.5), but again by only a small amount. It is true that we put 323 ppm of B-10 into the water regions when in reality only 178 ppm of B-10 should have been put in if the actual volumes of materials in the supercell area were to be placed in the LEOPARD supercell compositions. Even with this added amount of B-10, the effects were small.

4.3.2.3 Effect of Using Single Fast and Thermal Homogenized Parameters for Narrow Gap Supercell Regions

Encouraged by the results of Section 4.3.2.2, and the belief that by using a smeared zone we got more of the boron into a high flux area and hence increased its strength. We now did the same thing with the thermal group parameters as we had just done with the Fast.

Variation D

Fuel Region

a) Fast - Same as Variation C

b) Thermal - Used supercell edit of LEOPARD run used in Variation C which contained 323 ppm of B-10 in water regions.

Discrete Region

a) Fast - Same as Variation C

Table 4.5

Variations on Model III

Case	D_1	Σ_1	$\nu\Sigma_{f1}$	Σ_r	D_2	Σ_2	$\nu\Sigma_{f2}$	K_∞
Variation A	1.40705	6.86937E-03	4.37620E-03	1.83032E-02	3.60033E-01	5.10766E-02	7.07468E-02	1.181
B	1.40726	6.86875E-03	4.37558E-03	1.83045E-02	3.59914E-01	5.19523E-02	7.12342E-02	1.171
C	1.42113	7.06170E-03	4.38772E-03	1.83664E-02	3.63913E-01	5.11676E-02	7.13548E-02	1.180
D	1.42074	7.06806E-03	4.38487E-03	1.83704E-02	3.47181E-01	5.08977E-02	7.17087E-02	1.190
E	1.41927	7.13358E-03	4.36724E-03	1.80773E-02	3.61453E-01	5.88523E-02	7.15626E-02	1.045
MIII	1.41898	6.86179E-03	4.37317E-03	1.80632E-02	3.55324E-01	5.08968E-02	7.08296E-02	1.184

b) Thermal - Same smeared parameters as used in fuel region above

This variation worsened our k_∞ by increasing it to 1.19.

This was caused by the fact that the fuel was smeared into the water gap, which was the source of thermal neutrons. This effect raised k_∞ more than the presence of B-10 lowered it (Table 4.5).

4.3.2.4 Effect of Placing 100 ppm of B-10 in the Narrow Gap Water.

Finally, again claiming approximation 4.2.3 as justificiation, 100 ppm of B-10 was included in zones 16 and 18 (the narrow water gap regions). No decrease in the boron content of the curtain was carried out so in effect we have placed added material in our subassembly. The resulting changes were larger than at first expected.

Variation E

Fuel Region

a) Fast - MIII

b) Thermal - MIII

Decrete Region

a) Fast - MIII except for 100 ppm of B-10 placed in water zones

1.20 0.0 1.20	1.05 2.9 1.02	1.26 2.4 1.23	1.16 2.6 1.13	1.08 .9 1.07	.98 4.9 1.03	.81 16.5 .97
	1.17 12.0 1.03	1.04 15.4 .88	1.24 10.5 1.11	1.16 12.9 1.04	1.04 0.0 1.04	.71 14.5 .83
		1.20 11.7 1.06	1.10 10.9 .98	1.04 10.6 .93	.97 7.2 .90	.86 15.7 1.02
			1.03 11.7 .91	.98 10.2 .88	.93 7.5 .86	.83 15.3 .98
				.95 9.5 .86	.91 5.5 .86	.83 17.8 1.01
					.92 2.1 .94	.90 21.1 1.14
V. E %Diff C E						.82 18.8 1.01

Variation E

k = 1.045

$\overline{\text{ABS(\%Diff)}}$ = 9.7%

Fig. 4.3A

CONTROL ROD * OUT
CURTAIN FULL
DISHED
NODE HOT STANDBY

b) Thermal - MIII except for 100 ppm of B-10 placed in water zones.

As a result of the variation E, one observed a decrease of k_∞ for our subassembly of about 13%.

In a PWR the uniform addition of 100 ppm of boron to all the water will decrease the reactor's reactivity by only about 1.0%. The important word is uniform. In Variation E we added B-10 to the narrow gap water only. This has reshaped the flux, and weighted the lower enrichment fuel pins much more heavily than in the past. With this we get our large drop in k_∞.

Clearly this seems the way to go to get MIII and the Commonwealth supplied data to agree. It can also be justified by the approximations of section 4.2.

Truly, since it is the flux shaping that plays the major role in our situation we now see why for the control rod in-curtain in case we get good results. This is due to the fact that both the control blade and curtains are effected by assumption 4.2.3, and we get cancellation of errors.

It also explains why we get poor results for the unbalanced control cases of just the control blade in or just the curtains in. It again appears to be related to assumption 4.2.3 and 4.2.4 for the control blade only case.

Let us now look more closely at assumption 4.2.4 as exemplified by the control rod in-curtain out case.

4.4 Approximation 4 and The Control Rod In-Curtain Out Case

There is a large difference in the criticality between MIII and Commonwealth supplied data for this case (Table 4.2). Michelini's method has a number of assumptions as outlined in section 2.3.3. Also, our power distribution, figure 4.4, is shifted too much to the control blade. One would think, therefore, that from the power distribution results alone, our control blade is not strong enough. On the other hand the low criticality leads one to believe that it is already too strong.

To help clear this apparent discrepancy up, three cases were compared. Let us first label the following expressions which have been previously defined:

$$\Sigma_a = \frac{\sqrt{\langle\alpha\rangle \langle\beta\rangle}}{2t} \ln \left[\frac{1 + \sqrt{\frac{\alpha}{\beta}}}{1 - \sqrt{\frac{\alpha}{\beta}}} \right] \tag{4.1}$$

$$\Sigma_a = \frac{2\alpha}{\tau} \tag{4.2}$$

where α and β are blackness parameters.

Equation (4.1) is Henry's method to calculate the macroscopic absorption of the blade, and Eq. (4.2) is Michelini's method.

Case	Description
1	It uses the boron containing average fast supercell to obtain spectrum averaged micros to obtain Σ_1. Uses equation 4.2 to get Σ_2.
2	It was used in MIII Uses non-boron containing supercell for spectrum to get Σ_1. Uses equation 4.2 to obtain Σ_2.
3	Uses non-boron containing supercell for spectrum to get Σ_1. Uses equation 4.1 to obtain Σ_2.

Henry's equation 4.1 yields larger Σ_2's than the reduced form, equation 4.2, for the control blade. The spectrum averaging when boron is contained in the spectrum calculation gives larger Σ_1's than non-boron spectrum.

The homogenized two group parameters for our subassembly using the above cases for control rod parameter input results in Table 4.6 and Figures 4.4, 4.5 and 4.6.

.34 12.8 .39	.39 2.5 .40	.57 3.5 .55	.60 1.7 .59	.67 3.0 .65	.84 3.6 .81	1.12 1.8 1.10
	.56 8.2 .61	.59 7.8 .64	.85 4.5 .89	.92 5.2 .97	1.08 0.9 1.09	1.08 2.8 1.05
		.87 2.2 .89	.91 3.2 .94	.98 3.0 1.01	1.07 6.1 1.14	1.44 6.3 1.35
			.96 4.0 1.00	1.02 4.7 1.07	1.11 6.7 1.19	1.47 5.4 1.39
				1.08 5.3 1.14	1.16 7.9 1.26	1.54 5.2 1.46
					1.33 3.6 1.38	1.71 6.4 1.60
C E %Diff C. 1						1.49 7.4 1.38

Case 1

k = .925

$\overline{\text{ABS(\%Diff)}}$ = 4.65%

Fig. 4.4

CONTROL ROD * IN
CURTAIN OUT
DISHED
NODE HOT STANDBY

.34 12.8 .39	.39 4.9 .41	.57 1.8 .56	.60 1.7 .59	.67 1.5 .66	.84 3.6 .81	1.12 1.8 1.10
	.56 9.7 .62	.59 9.2 .65	.85 4.5 .89	.92 5.2 .97	1.08 0.9 1.09	1.08 2.8 1.05
		.87 2.2 .89	.91 3.2 .94	.98 3.0 1.01	1.07 6.1 1.14	1.44 6.9 1.34
			.96 3.0 .99	1.02 3.8 1.06	1.11 5.9 1.18	1.47 6.1 1.38
				1.08 4.4 1.13	1.16 7.2 1.25	1.54 5.8 1.45
					1.33 2.9 1.37	1.71 7.0 1.59
C E %Diff C. 2						1.49 8.7 1.36

Case 2

k = .939

$\overline{ABS(\%Diff)}$ = 4.68%

Fig. 4.5

CONTROL ROD * IN
CURTAIN OUT
DISHED
NODE HOT STANDBY

.34 5.6 .36	.39 0.0 .39	.57 8.8 .52	.60 6.7 .56	.67 6.0 .63	.84 7.1 .78	1.12 2.7 1.09
	.56 6.7 .60	.59 7.8 .64	.85 3.4 .88	.92 4.2 .96	1.08 0.0 1.08	1.08 2.8 1.05
		.87 2.2 .89	.91 3.2 .94	.98 3.9 1.02	1.07 7.0 1.15	1.44 5.6 1.36
			.96 4.0 1.00	1.02 5.6 1.08	1.11 7.5 1.20	1.47 4.8 1.40
				1.08 6.1 1.15	1.16 8.7 1.27	1.54 3.9 1.48
					1.33 5.0 1.40	1.71 5.3 1.62
C E %Diff C. 3						1.49 6.7 1.39

Case 3

k = .925

$\overline{ABS(\%Diff)}$ = 5.03%

Fig. 4.6

CONTROL ROD * IN
CURTAIN OUT
DISHED
NODE HOT STANDBY

Table 4.6

Control Blade Effect Comparison

Case	1	2	3
D_1	1.381	1.380	1.380
Σ_1	1.170E-02	1.119E-02	1.116E-02
$\nu\Sigma_{f1}$	4.496E-03	4.486E-03	4.489E-03
Σ_r	1.791E-02	1.791E-02	1.791E-02
D_2	3.613E-01	3.613E-01	3.622E-01
Σ_2	6.413E-02	6.422E-02	6.612E-02
$\nu\Sigma_{f2}$	8.194E-02	8.185E-02	8.273E-03
K	.9247	.9389	.9252

The best results were for Case 2. This was the reason it was made part of MIII. Its smaller fast absorption cross section improved the results over Case 1.

Because the change from Case 1 to Case 2 was in the fast group, not much change was observed in the power distribution which is primarily thermal group dependent.

When we increased the thermal absorption of the control blade in Case 3, we got a worsening of k_∞ over Case 2, as well as a worsening of the power distribution. The latter results being less severe than the former.

Yet, k_∞ is still too low. The pins bordering the control blade aren't underrated. The pins near the narrow water gap are underrated. Therefore, the following conclusion was drawn.

The absorption cross section of the blade is too high or high enough already. Any increase in absorption parameter of the blade, as in Case 3, will not improve the results. On the contrary, as Case 3 shows, it will worsen the criticality and the homogenized thermal absorption parameter without much, if any, improvement in power distribution. Yet one still would like to shift the flux to the higher enrichment pins boardering the narrow water gap. This could be done if one placed some absorber in the wide gap water. As was seen in Section 4.3.2.4, a small amount of boron in the water should shift the flux greatly, and improve both our power distribution and criticality. The theoretical justification for this rests in approximations 4.2.3 and 4.2.4

It is possible that the approximations that the diffusion equations hold for the water up to the blade boundary are overpredicting the flux shape in this corner of the subassembly.

Chapter 5

DESCRIPTION OF THE ACCIDENT

The accident to be analyzed is that of a control rod expulsion. For a BWR this means a rod drop accident. The accident is assumed to occur during reactor hot standby for Commonwealth Edison's reactor Dresden 3. Beginning of life fuel composition is assumed. The reactor subassemblies are of the type previously described. The reactor is assumed critical, and the temperature of the fuel clad and moderator is 547 °F. This is saturation temperature for the coolant whose pressure is 1025 psi. The coolant is not circulating and no-flow conditions are imposed.

A core layout of the subassemblies is presented in Appendix I. Also included there is a list of pertinent information on Dresden 3. The power of the reactor is 10^{-6} of rated, or 2.527 KW.

Hypothetically the accident could be caused by the disconnection of a control blade from its drive mechanism. The blade then remains in the fully inserted position until the drive mechanism has been fully withdrawn. This rod is assumed to be the first in-sequence control rod selected for withdrawal in Rod Worth Minimizer Sequence B Group 3. Groups 1 and 2 have already been removed, so our configuration is as outlined in figure 5.1 The rod drop velocity is 5 feet per

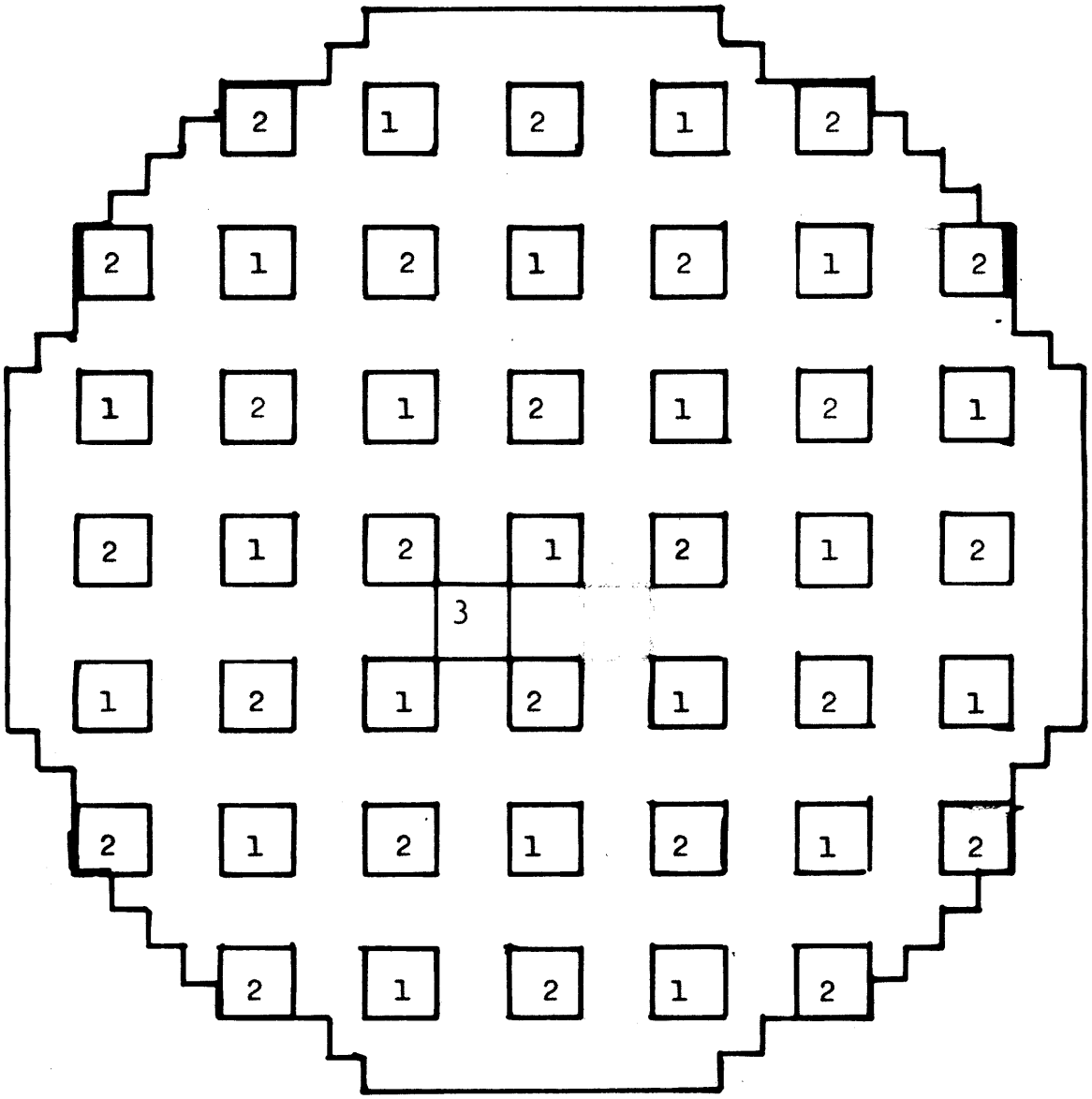

Control Rod Worth Minimizer Sequence B
Showing Rods Removed
At Initiation Of Accident
Fig. 5.1

second. Scram is assumed to be initiated at 120% rated power level or 3032.4 MW. A .2 sec delayed time from detection of this level to actual movement of the scram rods is used in agreement with Dresden's PSAR. Scram velocity is 2.16 ft. per second.

This accident is assumed to result in a Δ K of about 1%. This is not the most severe anticipated rod drop accident condition, however, they are the set of conditions requested by Commonwealth Edison.

In the remainder of this Chapter we investigate the criteria for rod failure in Sect 5.1. This is followed by a presentation of the method used by General Electric to analyze this accident in Sect 5.2. Finally, as a means of comparison, Westinghouse's method of analysis for this type of accident in their PWR's is presented in Sect 5.3.

5.1 Criteria for Failure

The ultimate limitation for the accident is that the off-site dose restrictions not be violated. In our accident it is assumed that no-flow conditions are in effect. This will conservatively estimate the maximum fuel enthalpies and clad temperatures. It is the fuel temperature which is linked to off-site dose. In this thesis we determine only whether fuel damage occurs.

The criteria for fuel damage as taken from the PSAR for Dresden III are in terms of peak fuel enthalpy.

1) At 170 cal/gm one gets eventual cladding perforation.
2) Fuel melting is estimated to occur between 220 to 280 cal/gm.
3) At least 425 cal/gm would be required to cause immediate fuel rod rupture due to UO_2 vapor pressures.

This data is based on the ANL-Treat tests[7] on zircaloy clad UO_2 pins.

From G.E. analysis of the accident we expect that peak fuel enthalpy will be below 100 cal/gm and hence not violate any of the above limits.

5.2 General Electric's Method of Analysis and Results[22]

In the past the vendor has used what is called the adiabatic model in which the flux is represented by

$$\phi(\underline{r},t) = \phi^t(\underline{r})\ F\ (t)$$

where F(t) is a function dependant upon time only and $\phi^t(\underline{r})$ is the fundamental mode spatial flux at selected points in time. After each time step the nuclear properties of the core are altered to suit the changing temperature by means of a nonlinear Doppler feedback for nodal points

throughout the core. Hence one obtains a power distribution in 2-D (radius and height) from $\phi^t(\underline{r})$ for one specific time step. Knowing the change in the eigenvalue of the diffusion equation due to the transient rod motion and change in nuclear properties, one can find the change in the multiplication factor k(t). This k(t) can then be directly fed into a point reactor model to get F(t). We use this F(t) to determine how much the flux has changed in the time step, and by multiplying it by the spatial flux we can find how the power has changed throughout the core. We then can break the core up into spatial nodes, and from knowing the spatial power distribution for the time step determine the temperature change in reactor properties for each of the chosen nodes. We then use this to get new diffusion group parameters and determine the new eigenvalues and functions for the next time step. After this we repeat the above procedure. No moderator feedback is conservatively assumed.

To assure that the method is conservative it is compared to results using the 1-D finite difference code, WIGLE[8] for a number of test cases.

For this accident, the vendor predicts that maximum fuel enthalpy will not exceed 100 calories/gm.

5.3 Westinghouse Analysis of Their Rod Expulsion Accident

This vendor makes use of a 1-D neutron kinetics code with feedback but, with the following assumptions:

1) The worth of the withdrawn rod is determined from the different core k values with the rod in and out. The feedback effects due to redistribution of the power with rod removed are neglected in determining this Δk.
2) With the rod removed and feedback treated as above, a conservative hot channel factor is determined and used throughout the transient.
3) A 1-D nodal kinetics code with feedback is then used to represent the average core bundle during the transient. A conservative spatial weighting for the Doppler feedback is used for this channel to account for the missing dimensions. No weighting is used for the moderator feedback.

Results - This 1-D approximation gives conservative results when compared to 3-D nodal kinetics results[23] (for a number of test cases). This analysis is indeed different from the General Electric analysis which uses point kinetics, not 1-D nodal kinetics. Also, Westinghouse can indeed guarantee that its 1-D analysis is conservative by amending it until it does give conservative results. Westinghouse uses the code TWINKLE[24] for both its less expensive 1-D and 3-D calculations.

Chapter 6

SIMPLISTIC ANALYSIS OF THE ACCIDENT

There are two very important items that it would be good to have prior knowledge of before the accident is analyzed using MEKIN.

The first of these involves some idea of the time-table for the accident. Most importantly, just what does the reactivity and power histogram look like. Should the power rise start out slow or fast? At what point is prompt critical reached if it ever is? When do feedback effects become significant? Some of these questions can be approximately answered by using point reactor kinetics. In particular the Fuchs Ramp Input Model[25,26] with feedback is used in section 6.1.

Another important question concerns the thermal-hydraulics part of this problem. In a transient that is expected to increase the reactor power by many orders of magnitude within a time period of seconds, how much of this power is liberated to the coolant? This gets into the determination of an effective RC constant for the fuel pins.

If the amount of heat liberated to the coolant is significant enough to cause coolant voiding, will this voiding fraction be the same in the gap water as it is in the lattice (area within the Zr can in a subassembly) water? For that matter, will the void fraction be uniform with the lattice water itself?

These questions of mixing, heat release to the coolant, and segregation effects between the gap and lattice water are investigated in section 6.2.

6.1 Neutronics

In the section that follows we shall use results based on point reactor kinetics with feedback theory. This is, of course, very simplistic. The equations used are those to be found in Hetrick[25] and Canosa's article[26].

Of particular concern is how to consider the core average temperature change that this analysis gives. Since one starts the transient from a flat core temperature distribution it seems inappropriate to use this distribution to obtain weighting factors to get peak transient region wise temperature changes. Going hand and hand with this is what functions should be used for the Doppler feedback. This was given spatial weight factors in the Westinghouse analysis of the accidents. It appears that some calibration is to be required with more

Fig. 6.1

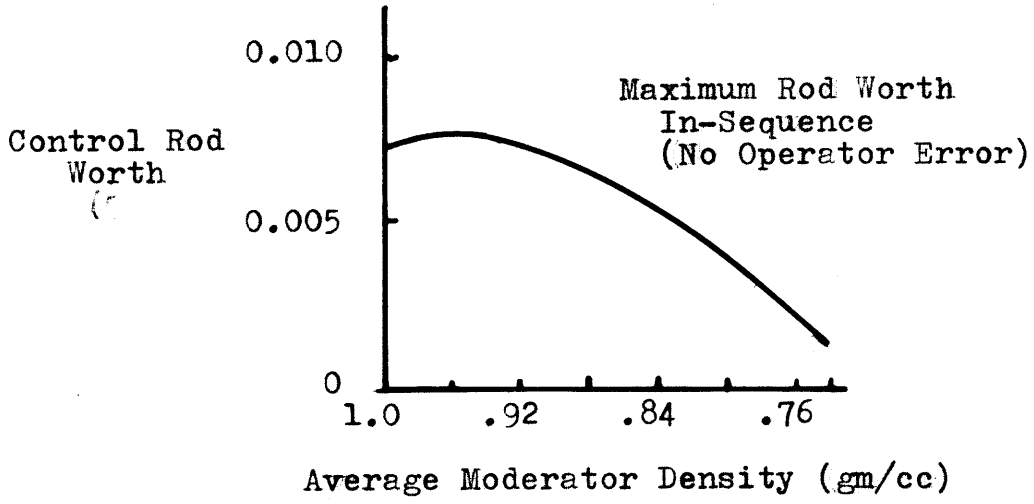

G.E. Plot Of Maximum Rod Worth
vs
Moderator Density For Hot Standby Conditions

exact methods like MEKIN, WIGLE or TWINKLE to see whether simple core averaging gives good results with the more exact methods, and what weights to use.

In what follows core averaged parameters are employed and so the results are believed to be the averaged core results. The major assumption is that $\Delta K = .01$ is the worth of the expelled control rod. This is based on G.E. supplied data for the accident's circumstances[22] (figure 6.1).

6.1.1 Fuchs Ramp Input Model

The following are a list of the assumptions for this model:

1) Point kinetics
2) Adiabatic feedback approximation (no moderator feedback due to speed of transient)
3) Prompt approximation (delayed neutrons are neglected)
4) Reactivity input ramp is never ended.

These assumptions are assumed in both Hetrick's and Canosa's analysis. In addition, in Canosa's development ρ denotes net prompt reactivity ($\rho_{total}-\beta$) and n_o is the power at prompt critical. This is assumed not to be appreciably larger than the initial low steady state value. Canosa's analysis initializes time at the point prompt critical is reached. Hetrick sets time equal to zero when

reactivity changes. Both of them use assumption 4. However, this is modified in the final timetable analysis to be presented to account for no additional ramp of reactivity once the rod has fallen completely out. It also appears that since the drive out velocity is so large, and the control rod worth is only $\Delta K = .01$, there will be no new increase in reactivity once the first decrease in ρ due to Doppler feedback occurs. This, of course, assumes that scram occurs more quickly than it takes to get positive reactivity feedback from any cooling of the fuel.

The governing equations are:

$$\frac{dn}{dt} = \frac{\rho}{\ell} n \tag{6.1}$$

$$\frac{dT}{dt} = \gamma n \tag{6.2}$$

$$\rho = at - bT \tag{6.3}$$

$$\rho(o) = 0 \tag{6.4}$$

where:

n = power

$\hat{n}$ = peak power

n_o = power at prompt critical

ρ = net prompt reactivity

ℓ = prompt neutron lifetime

a = rate of reactivity insertion

b = constant temperature reactivity coefficient

$1/\gamma$ = reactor heat capacity

t_{tp} = time to prompt critical

$\varepsilon = a \cdot \ell$

$\rho_{total} = \rho + \beta$

β = total delayed neutron fraction. = .00725

For our accident if $\Delta K = .01$

$$a = \frac{.01}{2.4 \text{ sec to drive out}} = .004167 \text{ sec}^{-1}$$

$\ell = 10^{-4}$ sec

b is obtained from correlation data (see section 7.1.4)

$b = 6.042 \times 10^{-6}$ / °F

$n_o = 2.5 \times 10^{-3}$ MW = 2.5 KW

$1/\gamma$ = (heat capacity of one foot of fuel pin) x (total feet of fuel pins in core)

$1/\gamma = (6.984 \times 10^{-2} \ \frac{\text{KW - sec}}{\text{°F ft}})$ (425712 ft) =

$2.9732 \times 10^{4} \ \frac{\text{KW - sec}}{\text{°F}}$

$\gamma = .3363 \times 10^{-4}$ °F / KW - sec

$\gamma n_o = .841 \times 10^{-4}$ °F / sec

$\varepsilon = 4.167 \times 10^{-7}$

$t_{tp} = \beta/a = 1.740$ sec

The maximum prompt reactivity reached can then be determined using the following equation

$$\rho_{max} = \sqrt{2a\ell \left[\ell n \left(\frac{a}{b\ell n_o} \right) - 1 + \frac{b\gamma n_o}{a} \right]} \qquad (6.5)$$

This yields that $\rho_{max} = .003526$ or a total maximum reactivity $\rho_{total\ max} = \rho_{max} + \beta \simeq .0108$. This is just slightly greater than the assumed rod worth of $\rho_{total} = .01$, which would be reached when the rod drive out was complete. This signifies that feedback effects become important about the time that the rod has been completely expelled.

The $\rho_{total\ max} = .0108$ was obtained using Canosa's equation which assumes we have an infinite rod whose ρ insertion is at a rate of "a" = .004167 sec^{-1}. We therefore conclude that ρ_{max} occurs at time of completed drive out, 2.4 seconds.

We now wish to calculate the total change in temperature, ΔT. One can be conservative if one assumes the power burst to be symmetric with a total time equal to twice the rise time. This is because:

1) In reality we don't have any further ramp insertion of reactivity as is assumed in the symmetrical pulse results of Canosa.

2) We will have scram at 0.2 seconds after we reach 120% of full core rated power. This is also not accounted for in Canosa's solution.

Hence being conservative:

$$\Delta T = \frac{\tau_{cycle}}{b} = \frac{at_{cycle}}{b}$$

since $\tau = (a)\ (t)$, where τ cycle is the time dimensionless cycle parameter (See figure 6.2).

$$\tau_{cycle} = 2(S + F)$$

S = time elapsed from zero time to time of ρ_{max}

F = power burst half width

$$S = \rho_{max} + \frac{\varepsilon}{\rho_{max}}$$

S = .0036 (in τ units)

or since $t = \tau/a$, S = 0.87113 seconds

$$F = \frac{\varepsilon}{\sqrt{\rho_{max}^2 + 2\varepsilon}} \ln \frac{\sqrt{\rho_{max}^2 + 2\varepsilon} + \rho_{max}}{\sqrt{\rho_{max}^2 + 2\varepsilon} - \rho_{max}}$$

F = 0.153 seconds

ΔT = 1,362 °F

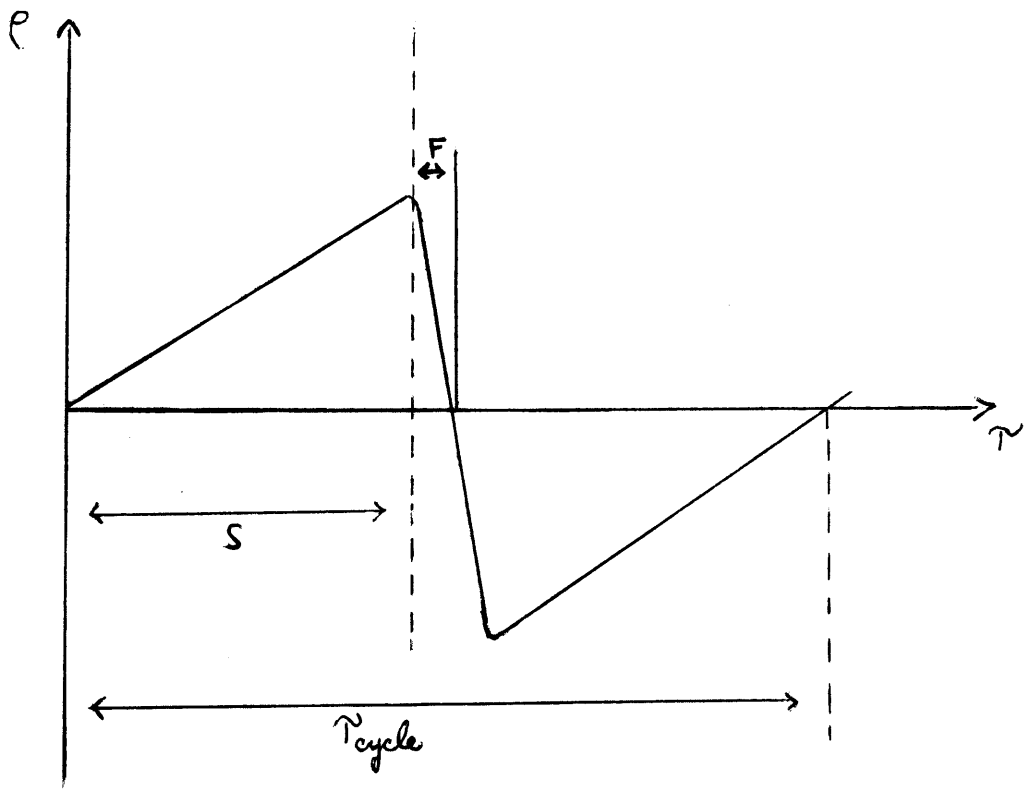

Figure 6.2

Reactivity vs. Cycle Parameter

This gives a temperature for pins of 547 + 1,362 °F or $T_{final} \tilde{=}$ 1910 °F, which is below the temperature corresponding to enthalpy of 100 calories/gm in agreeemnt with G.E.'s report.

Let us now find the peak power, $\hat{n}$

$$\hat{n} \cong \frac{\ell w_m^2}{2\alpha K}$$

where

$\alpha = b$

$K = \gamma$

$w_m = \rho_{max}/\ell$

This yields:

$$\hat{n} = 305.9 \times 10^3 \text{ MW}$$

This conservatively high estimate is about one-hundred times greater than needed for scram, and would be peak power if one had a continuous ramp input. We therefore believe that this value is higher than we will attain, but feel assured that scram will certainly occur.

Since the power burst has a half width of F = .153 seconds in which almost all power rise occurs, we conservatively assume that scram is tripped at $\hat{n}$, which is at

$$t_{scram} = 0.2 + t_{tp} + S + F = 2.75 \text{ seconds.}$$

The 0.2 term is due to mechanical and electrical delay time of scram equipment.

With the above analysis the following time table will be compiled. From the assumption of continual ramp input the time of ρ_{max} is

$$S + t_{tp} = .8711 + 1.740 = 2.611 \text{ seconds.}$$

This is a time greater than it takes the rod to drop out. So for our case:

1) ρ_{max} is reached at t = 2.4 seconds and not 2.611 seconds.
2) F will be a smaller time step since we have no ramp insertion during F as in the Canosa and Hetrick assumptions. Hence ρ will go to zero more rapidly.

Based on (1) and (2) above we therefore say that $\hat{n}$ will occur at

$$t_{\hat{n}} \tilde{} 2.4 + .15 = 2.55 \text{ seconds}$$
(end of drive out + F)

This value of 2.55 seconds for $t_{\hat{n}}$ is ≈.21 seconds less than the 2.761 seconds predicted by direct application of the continuous ramp input model which was used to obtain ΔT, ρ_{max} and $\hat{n}$. All of which should be smaller for our case if the point kinetics assumption is believed.

3) Time of scram will then be

$$t_{scram} = 2.55 + .2 = 2.75 \text{ seconds}$$

Since scram velocity is 2.16' / second, it will take 5.56 seconds to complete; and thus end at t = 8.31 seconds.

4) Fission power will continue to increase in our accident as long as $\rho_{total} > 0$. However, it appears that the additional energy added is negligible after the completion of the power burst. Conservatively the power burst will last for a period of 2F. Therefore, the burst will end at t = 2.71 seconds having gone on from t = 2.4 to 2.71 seconds.

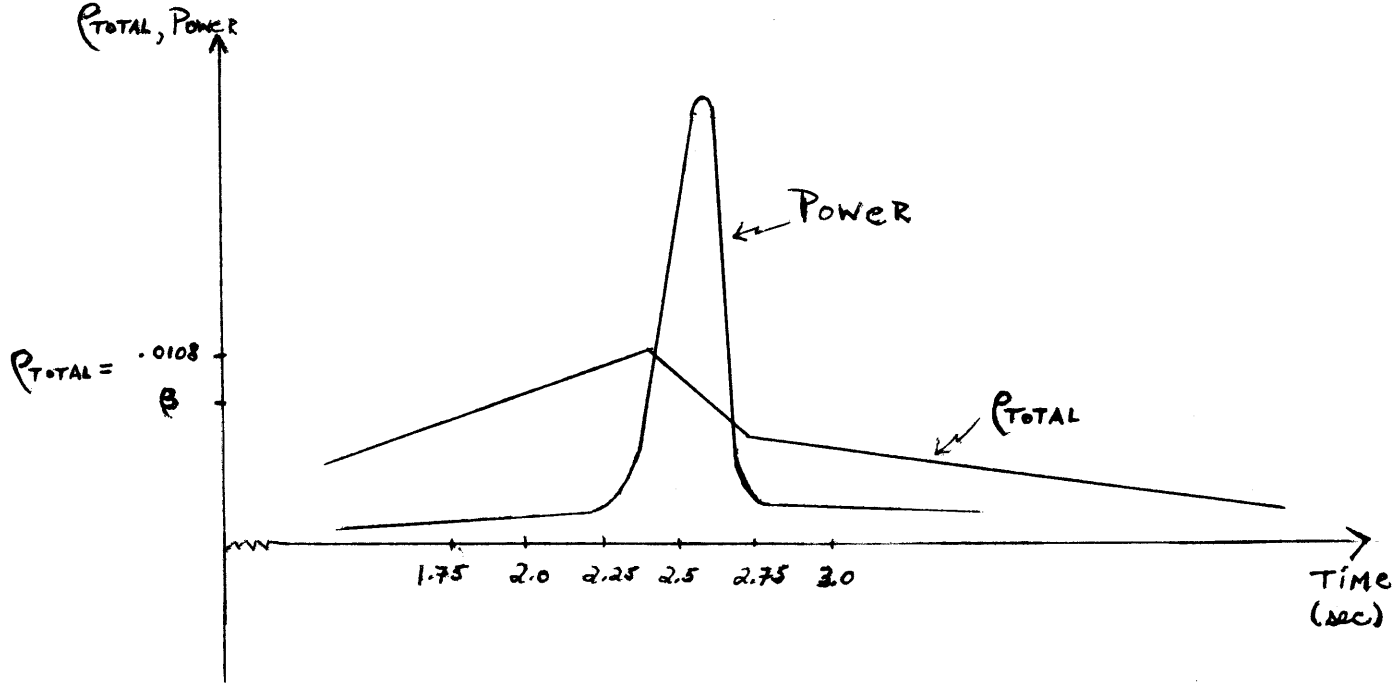

Figure 6.3

Power vs. Time

Table 6.1
Neutronic Time Table Prediction for Transient

t of accident (sec)	Condition
0.0to 2.4	control rod drives out
1.74	$\rho_{total} = \beta$
2.4	ρ_{max} reached
2.4 - 2.55	first half of power burst
2.55	$\hat{n}$ reached
2.55 - 2.71	power burst still substantial but decreasing
2.71	end of power burst
2.71 - 2.75	a constant (approximately) ρ_{total} maintained, it is below prompt critical but positive
2.75	time of physical scram starting
2.611 + .306 = 2.92	would be the end of burst if Canosa's ramp, and no scram conditions were the case. Should be end of any substantial energy increase to fuel.
8.31	all rods fully inserted

$\hat{n}$ $\leq$ 306. x 10^3 MW occuring at t = 2.55 seconds

ΔT = 1362 °F

F = .153 seconds

t_{tp} = 1.740 seconds

6.2 Thermal-Hydraulics

The feedback effects on the nuclear two group parameters of fuel temperature and coolant void fraction are necessary for a correct analysis of the accident. One could vary one of the state properties at a time and observe its independent effect on the neutronic parameters. A far less expensive and time consuming way would be to vary both static properties at the same time, and then use regression analysis to obtain the neutronic-state property correlations. Because the number of combinations of coolant density and fuel temperature pins would be limited, it was hoped to use pairs which would be representative of the accident. The idea of using COBRA [27] would accomplish this aim. However, only a small data base which didn't require regression analysis was used (see section 7.1.4).

A number of other important studies were done using the COBRA IIIC code. Among these studies are an investigation of the coolant mixing within a subassembly during a transient. In section 6.2.4 we investigated the important resistance - capacitance, RC, parameter and its related "f" factor (fraction of power generated in fuel pin that is released as heat flux). An outgrowth of this latter study was the effect the time step size has on these parameters when COBRA is used. The experience gained with COBRA IIIC was valuable in later work with MEKIN since the thermal-hydraulics part of MEKIN is a revised and improved COBRA.

The mixing study was later used in section 7.1.1 to determine the effect that the power distribution within a subassembly had on the MEKIN model parameters.

6.2.1 COBRA Studies

The subassembly lattice was divided into eighths. This division afforded the user boundaries across which there would be a minimum of mixing and still keep the computer core requirements below 250K. By placing the boundary through the middle of fuel pins the approximation that there would be equal heat conduction out from both halves of the pin was employed. This should result in near equal void fraction on both sides of the boundary near the dividing line, and hence little mixing. With this assumption, then, one-eighth segments of the subassembly were run in separate COBRA runs. This was required for only one-half of the subassembly, or four one-eighth segments, due to symmetry of the power distribution along the diagonal of the subassembly.

Each segment contains nine channels and parts of 10 fuel pins (see Fig. 6.4). The power distribution was close to that of control rod and curtain in case (see Fig. 6.5).

Most important for the mixing analysis are the empirically derived parameters. These include the turbulent mixing parameter (the A parameter), and the following diversion crossflow mixing factors: diversion crossflow resistance factor,K; turbulent momentum factor, f_T; and trans-

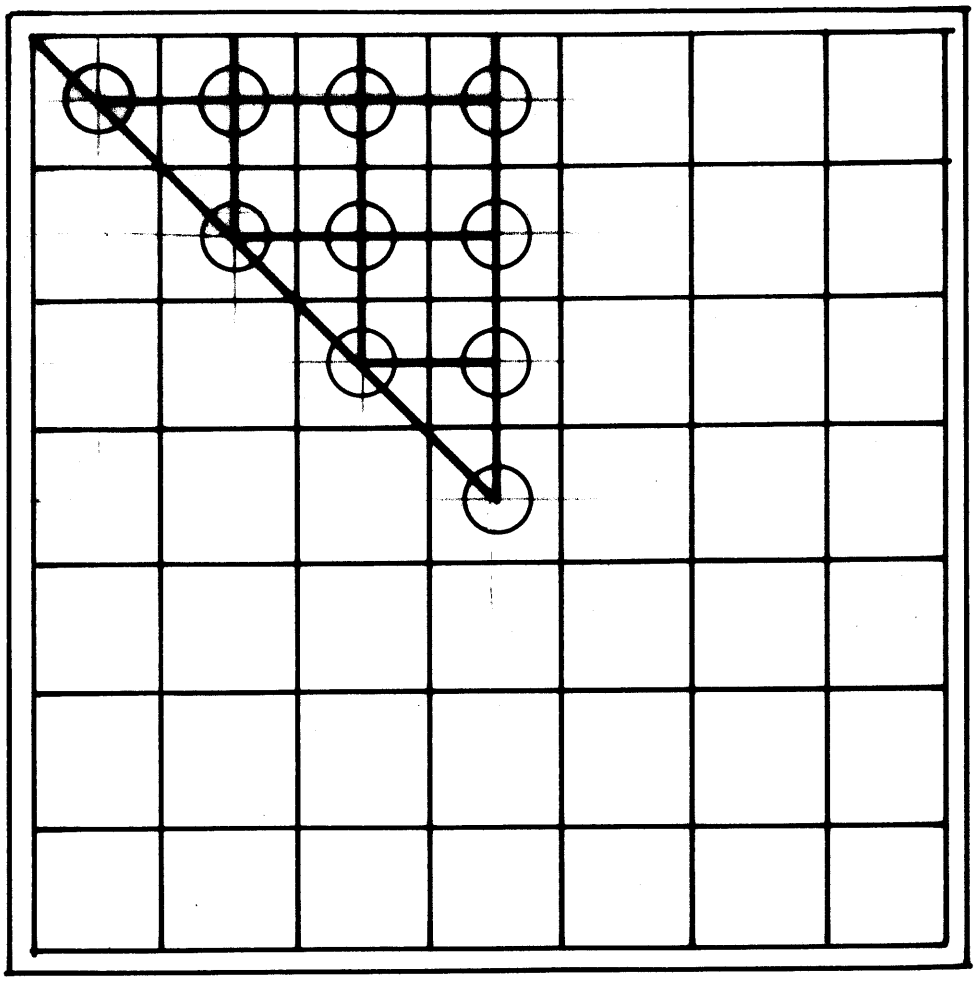

COBRA 10 Pin And 9 Channel Layout
For One-Eighth Subassembly Runs

Fig. 6.4

.32	.39	.56	.62	.68	.80	.90
	.60	.67	.93	1.00	1.12	.92
		.95	1.03	1.10	1.18	1.23
			1.11	1.18	1.25	1.30
				1.25	1.33	1.38
					1.44	1.53
						1.27

COBRA Run Power Distribution

Fig. 6.5

verse momentum parameter, S/L. Using the same values that Argonne used in a similar bundle:

$$K = .5$$
$$f_T = 0.0$$
$$S/L = .5$$
$$A = .02$$

Turbulent crossflow is calculated from the A parameter by the equation

$$w_{ij}' = A\ S_K \bar{G}$$

where

S_K = rod spacing

w_{ij}' = turbulent fluctuating crossflow between channels i and j

$\bar{G}$ = mass velocity

The fact that f_T is set equal to zero results in the turbulent fluctuating cross flow term in the axial momentum equation to be neglected. However, it is not neglected in the energy equation; and so enthalpy is exchanged due to the turbulent fluctuation as well as diversion crossflow.

6.2.2 Mixing Within the Subassembly

It is important to know whether the power distribution within a subassembly would have any effect on how the MEKIN nodal parameters are determined (see section 7.1). Since the void fraction is a very important parameter in determining the correct homogenized cross sections for our subassembly, the effect of mixing within the subassembly was investigated.

For this analysis the following conditions were used:

1) Inlet flow conditions were those at steady state full power (.9210 MLB/hr-ft^2) during the transient.
2) Initially the coolant and fuel are at 547 °F (hot standby conditions).
3) A heat flux forcing function raises the core power from .1656 BTU/hr-ft^2 to .2823 x 10^6 BTU/hr ft^2 in an exponential manner over a 3.3 second period.
4) Subassembly power distribution among pins is that of control rod in-curtain in case.

From these conditions we will pick a simple COBRA IIIC axial level and observe the void fractions in the various LEOPARD cells.

.415	.474	.542	.591	.621	.631	.612
	.546	.617	.661	.682	.693	.648
		.646	.707	.725	.734	.699
			.720	.745	.750	.737
				.754	.761	.751
					.768	.753
						.741

Void Fractions Found In Mixing Study

Fig. 6.6

From Fig. 6.6 it can be seen that the LEOPARD cell void fractions varied from .42 to .75. This was when the average heat flux for the axial plane was .3444 x 10^6 BTU/hr - ft^2. This being close to the .313 x 10^6 BTU/hr ft^2 maximum steady state full power heat flux of Dresden III. The average void fraction for the subassembly at this level was .67. This should be below the maximum exit void fraction of our reactor at full power steady state.

The major value of this study is that our peak to average void fraction is 1.12. This can be correlated with a neutronic figure of merit which compares the homogenized neutronic parameters obtained by discrete representation and flat representation of the power in our subassembly. This is done in section 7.1.

In making comparisons with this above result, and any other transient one should realize what variables effect mixing.

From section 6.2.1 it can be seen that the fluctuating turbulent mixing is a function of the variable, mass velocity. It should also be remembered that the amount of mixing any one particular packet of fluid undergoes is a function of time it spends in the core, and hence inversly proportional to fluid velocity. The other important mixing is diversion mixing. This depends on the transverse pressure difference between the channels. The equation governing this is

$$\Delta p_{ij} = K \frac{\rho v^2}{2}$$

where:

Δp_{ij} = pressure difference between channels i & j

ρ = two phase density

v = velocity in transverse direction

K = diversion cross flow resistance factor

6.2.3 Void Fraction In Gap Water vs. Lattice Water

The MEKIN code will not realistically allow the gap region to be represented specifically, rather that gap is homogenized into the neutronic node or neglected in the thermal-hydraulic node (see Chapter 7). Thus to perform an accurate neutronic homogenization the gap must be treated with care.

We propose to average the void fraction of the gap with that of the bundle, in proportion to their respective volumes, to find the nodal void fraction. We assume that the void fraction in the gap is proportional to the lattice water void fraction with the following first order relation:

$$(VF)_{gap} = (VF)_{LW} * \frac{(Q)_{gap}}{(Q)_{LW}} * \frac{(Vol)_{LW}}{(Vol)_{gap}} * \frac{(MF)_{LW}}{(MF)_{gap}} \quad (6.6)$$

where:

VF is the void fraction

Q the heat generation

Vol the region volume

MF the mass flux

The subscript "gap" is the gap and "LW" the lattice water. The equation states that the void fractions should be directly proportional to their respective heat generation rates; inversely proportional to the volume of the regions, and the mass flux.

The first expression to be investigated is the amount of heat received by the gap as opposed to the lattice water. The case to be considered is that of control rod out-curtain out. The gamma ray energy distribution is a function of the mass distribution of the subassembly materials. The neutron energy distribution due to slowing down collisions is essentially a function of water mass distribution. Both of these distributions require some estimate of the water density in the gap region and in the lattice. For the analysis we assume zero voids in either water region, and a water density compatible with hot standby conditions. If in the accident, significant void fractions occur, a new value of Q_{gap} / Q_{LW} must be determined based on new mass distributions, but using Eq. (6.6) to get an estimate on $(VF)_{gap}$ knowing $(VF)_{LW}$ up to that point. The frequency

with which we do this during the course of the accident depends on how quickly the void fraction of the lattice water changes and the accuracy in the terms of Eq. (6.6) we wish to keep.

Let us now determine Q_{gap} / Q_{LW} under the above assumptions. The relative mass distribution is then

72.44 gm in Zr-can
721.01 gm in pins
75.31 gm in L.W.
30.69 gm in G.W.

899.45 gm total

among which 7.5 Mev of prompt γ / fission are distributed by mass. Also 5 Mev / fission due to neutron slowing down must be distributed among the two water regions based on mass. The 168 Mev / fission due to the fission fragments is distributed in the fuel pins. This 168 Mev plus the pin's 6.015 Mev/ fission, which is its share of the gamma rays, are not all immediately released to the lattice water. The amount of this power generated in the pins released to the lattice water as heat flux is "f". Using this fact we obtain:

$$\frac{Q_{gap}}{Q_{LW}} = \frac{2.01}{4.48 + 174.015\ f}$$

This ratio may range from .449 to .0113 as f ranges from 0 to 1.

From the PSAR geometric data at hot conditions the

$$\frac{(\text{Vol})_{LW}}{(\text{Vol})_{gap}} = 2.45$$

In the determination of flux ratio the equivalent diameter of the gap water was found to be 1.93 cm and that for the lattice water 1.87 cm. Any effect of this parameter on the difference in the friction loss or MF between the two waters was therefore neglected.

However, due to the increase of such a great amount of heat in such a short period of time, the ratio of the MF from exit to entrance for a lattice channel in COBRA can be very high. It is a hard problem to determine whether the MF in the gap water will follow that in the lattice once the transient begins. For a problem with non-negligible mass fluxes one would attempt to solve the problem by bounding it.

Fortunately for the hot standby case, the mass fluxes are initially zero. We can obtain a more exact form of Eq. (6.6) for this case.

$$\frac{d(Vf)_{LW}}{dt} = \frac{\dot{Q}_{LW}}{h_v \rho (\text{Vol})_{LW} (1-Vf)_{LW}} \qquad (6.7)$$

where

$\dot{Q}_{LW}$ = heat generation rate in LW

ρ = saturated liquid density

h_v = heat of vaporization

Solving Eq. (6.7) one gets

$$(Vf - \frac{Vf^2}{2})_{LW} = \frac{\dot{Q}_{LW}\, T}{h_v\, \rho\, (Vol)_{LW}\, (1-Vf)_{LW}} \qquad (6.8)$$

A similar equation exists for the gap water, so one obtains

$$(Vf - \frac{Vf^2}{2})_{gap} = (Vf - \frac{Vf^2}{2})_{LW} \frac{(Q)_{gap}}{(Q)_{LW}} \frac{(Vol)_{LW}}{(Vol)_{gap}} \qquad (6.9)$$

Equations (6.9) is the exact form of Eq. (6.6) for the hot standby case. It is not limited by only flow up the channel but is independent of how the hot channel's water is removed once voiding begins. In it one must remember that the heat generation factors are implicit functions of void fraction, and the ratio should be recalculated if we start diverging very far from the assumed void fractions on which it is calculated.

6.2.4 RC Constant and "f" Factor

The usually quoted RC constant for a reactor fuel pin is between 7 to 10 seconds. In an attempt to become better acquainted with this and other important thermal-hydraulic parameters for the accident, an analytic lumped parameter circuit analogy was developed. This was compared to a number of COBRA IIIC runs.

6.2.4.1 analytic circuit analogy

Quoting from Tong's book on "Thermal Analysis of PWR's"[28] "The lumped parameter technique is basically equivalent to the use of an electric analog. The conditions at the nodal points of the electric network represent the average conditions of a particular region. To use such an analog, we note the correspondence between voltage and temperature, between current and flow, and between the product of electrical resistance and capacity of the electrical system and thermal diffusity. Thus, Fourier's law of $q = \Delta T/R_t$ is represented by Ohm's law for current flow $i = \Delta E/R$"

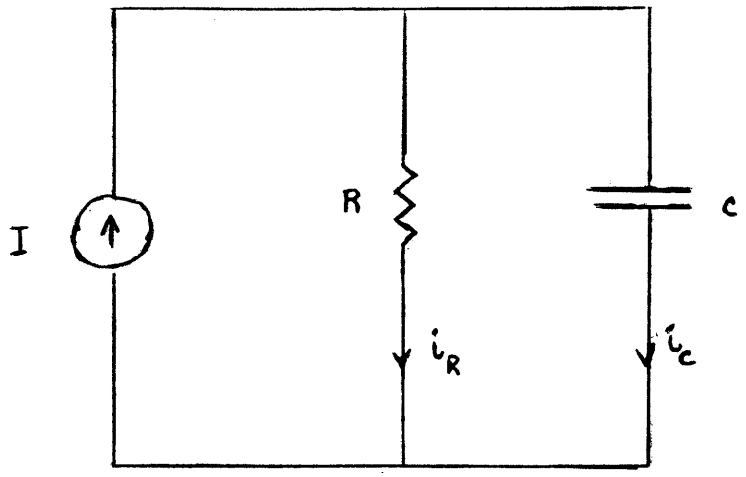

Figure 6.7

RC Circuit Analogy

The standard analog circuit can be seen in figure 6.7 where we have lumped the total capacitance and resistance into single parameters and represented the power as a time varying current source. The governing equations are:

$$I = i_R + i_C \tag{6.10}$$

$$I = e^{at} - We^{a(t-3.3)}\alpha(t-3.3) + We^{-\beta(t-3.3)}\alpha(t-3.3) \tag{6.11}$$

where we have assumed maximum power is reached at 3.3 seconds after beginning of rod drop. Then

$a \equiv$ that value which when used in e^{at} will give maximum power at time 3.3 seconds.

$W \equiv$ constant equal to e^{at} at $t = 3.3$ seconds

$\beta \equiv$ parameter for the decaying power.

$\alpha(t-3.3) \equiv$ the alpha function whose property is that

$$\alpha(t-3.3) = 0 \text{ for } t < 3.3$$

$$\alpha(t-3.3) = 1 \text{ for } t \geq 3.3$$

The final equation then must express the fact that since the resistance and capacity are in parallel the voltage drops across them must be equal.

$$Ri_R = \frac{\int_o^t i_c \, dt}{C} \tag{6.12}$$

Combining Eq. (6.10, 6.12) yields

$$RI = Ri_C + \frac{1}{C} \int_o^t i_C \, dt \tag{6.13}$$

Then Laplace transforming Eq. (6.13) and using the notation that

$\bar{I}_C \equiv$ the Laplace transform of i_C

$L\{I\}$ = the Laplace transform of I

we get

$$RL\{I\} = \{R + \frac{1}{sc}\} \bar{I}_c \tag{6.14}$$

which becomes for $t \geq 3.3$

$$\frac{R}{(R + \frac{1}{sc})} \left(\frac{1}{s-a} - \frac{We^{-3.3s}}{s - a} + \frac{We^{-3.3s}}{s + \beta}\right) = \bar{I}_c \tag{6.15}$$

Since

$$L\{F(t-c)\alpha(t-c)\} = e^{-cs} \bar{F}(s)$$

for $t \geq 3.3$ seconds and

$$\bar{I}_c = \frac{R}{(R + \frac{1}{sc})(s - a)} \tag{6.16}$$

for $t \leq 3.3$ seconds, the inverse Laplace transform leads to for Eq. (6.15)

$$i_c = Ae^{-t/RC} + Be^{at} + \alpha(t-3.3)Y$$

where

$$Y = \left[-C'e^{-\frac{t-3.3}{RC}} - D'e^{a(t-3.3)} + E'e^{-\frac{(t-3.3)}{RC}} + F'e^{-\beta(t-3.3)} \right] \tag{6.17}$$

and

$$A = \frac{1}{1 + aRC}$$

$$B = \frac{aRC}{aRC + 1}$$

$$C' = \frac{W}{1 + aRC}$$

$$D' = \frac{aRCW}{aRC + 1}$$

$$E' = \frac{W}{1 + RC\beta}$$

$$F' = \frac{\beta RCW}{RC\beta - 1}$$

The inverse transform of Eq. (6.16) is Eq. (6.17) without its Y term.

We can get some idea of what fraction of the power appears as heat flux, i_R, and what part as latent heat of the fuel pin, i_C. For t = 3.3 seconds, assumed maximum power time when $I = I_{max}$

$$i_c = \frac{e^{-t/RC}}{1 + aRC} + \frac{aRC}{aRC + 1} e^{at} \qquad (6.15)$$

where if 1/RC is on the order of "a"

$$i_c(t=3.3) \simeq \frac{aRC}{aRC + 1} \; I_{max} \qquad (6.16)$$

and that fraction of the power liberated in fuel appearing as heat flux is

$$\frac{i_R\ (t=3.3)}{I_{max}} = \frac{1}{aRC + 1} \qquad (6.17)$$

For RC = 10 seconds and a = 4.2 seconds we get that about 2.3% of power appears as conductive heat flux at t = 3.3 seconds.

6.2.4.2 effect of temperature distribution in pin on parameters

Using a constant connective heat transfer coefficient for out pins of 5000 BTU/hr ft^2 °F, for different power forcing functions of the form e^{at} where only "a" was varied we obtain:

Table 6.2

Power Forcing Function vs. "f" Parameter

RUN	HEAT FLUX AT 3.3 SEC.	f
M0606	.1684 MBTU / hr ft^2	18.0%
M0624	.6015	18.0%
M0171	5.1850	17.4%

The dependence of the "f" factor on "a" can be examined. From Eq. (6.17) and Table 6.2 it appears that this "f" parameter is quite insensitive to "a" This would be possible if "RC" was small. There is a big difference between these results and the 2.3% value obtained in the previous section.

Another very interesting result from the COBRA runs was that the radial temperature distribution was almost flat. In run M0624 the results are given in Table 6.3.

Table 6.3

Pin Temperature Distribution

Radial Pin Node	Transient Pin Temp.	Pin Temperature at Steady State
1(pin ctr)	2767.4 °F	3234.4 °F
2	2751.8	3104.2
3	2682.2	2713.2
4	2443.4	2062.7
5	1619.7	1151.4
6 (clad)	667.9	618.5
$\sum_{i=1}^{5} \frac{T_i}{5}$	2044.0	2044.0

A steady state temperature distribution which was obtained from a previous COBRA run when capacitance of fuel and clad were equal to zero is shown for comparison.

In this table as well as in table 6.2, a dependence on the time step size taken in the COBRA runs is manifested. This will be discussed in the next section. What we will attempt to show now is that the effective RC constant is a function of the temperature distribution within the pin.

Let us neglect the clad's capacitance, then the pellet's capacitance "C" is

$$C = C_p \rho V = 0.0664 \text{ BTU/°F}$$

where

C_p = specific heat of fuel

ρ = fuel density

V = fuel volume

We then compare four cases:

1) Node at Fuel Center - To obtain resistance, R, we simply add the resistances of the materials in series between node and water. C used is that of the total pellet.

2) COBRA run with Steady State Temperature Distribution- Here used a COBRA run where although we inputed a forcing function for the power with time; the specific heat of fuel and clad in the COBRA input had been set to zero. So, for this run we get the effective steady state temperature distribution and heat flux for the pin at each time step. The C is again chosen as that of the total pellet = .0664 BTU/°F, and R is found from the equation

$$\frac{1}{R} = \frac{q''}{\Delta T} = \frac{\text{Heat Flux}}{\text{Temp. difference between pin center and coolant}}$$

Both q" and ΔT are part of the COBRA output.

3) Transient COBRA Run - Here "R" is found as in above Case 2. In this COBRA run our a = 4.35 seconds for the pin considered. The specific heat of fuel and clad (not C), were set to their appropriate non-zero values in the code.

4) Single Node at Fuel Pellet Surface - The resistance will then only be equal to that for flow across gap, clad and film. The capacitance will be that of the fuel pellet lying within the first one-eight of the radial distance from the pellet surface. This is based on the practice that two adjacent equally spaced nodes will share the radial distance between them equally. The "C" for this case is then 0.01556 BTU/°F.

The RC and f parameters for our cases are then given in Table 6.4

Table 6.4

Circuit Analog RC and "f" Parameters For Different Cases

Case	RC	a	f	f From COBRA Output
1	22.33 sec	4.35	1.0%	--
2	12.32	--	--	100%
3	5.66	4.35	3.9%	18%
4	.753	3.91	25.3%	--

In Table 6.4 the RC and first f value are those used in Eq. (6.17) for the circuit analog. The RC values used for each case were explained for each case above. The f from the two COBRA runs were taken from the COBRA edit.

The 18% value for "f" is assumed to be the standard, that is we shall compare our other results to this. It was calculated by COBRA under accident conditions.

In Case 1 the very large RC value results in such a low "f" value. Clearly one would need a point power source in the center of fuel to consider placing a single electrical analog node at the center. The 18% standard value lies between this and Case 4, where we have placed the node at the surface of the fuel pellet. The standard effective node for the electrical analog to this problem then lies between Case 1 and Case 4 but, as can be seen, very close to the surface. This could be predicted from the shape of the temperature distribution in the pellet as shown in Table 6.3.

One can obtain such a flat power distribution for at least two reasons. One, a good conductor (such as a metal ingot) would exhibit such a potential difference within it of near zero. Two, a very strong resistor would show very little flow and hence maintain a flat temperature profile. The material properties of UO_2 are such that the latter situation is the one to be considered. Effectively the

power transient is occuring too fast for the heat from the interior nodes to leak out in any appreciable quantity. This results in almost a flat temperature profile for the first four nodes. However, the last fuel node, (node 5), is affected by the clad temperature which is kept low due to the coolant. A potential driving force is therefore created between node 5 and clad node 6 before any of the other nodes. Hence, it seems that for times and powers on the order of this transient only node 5 contributes much heat to the fuel pin heat flux. That is the reason we only included its effective capacitance and resistance in case four above. The "a" value was reduced to reflect the fact that only 23.4% of fuel pellet volume is in this node so only 23.4% of pellet power is produced in this node.

The steady state RC value in Table 6.4 is higher than the usual quoted value of 7 - 10 seconds. This is because the convective heat transfer coefficient used in the COBRA runs, and for the purpose of single node calculations, is also much lower than the actual steady state value.

The "f" value of Case 3 when we use Eq. (6.17) and the method of obtaining "C" for that case shows poor comparison with the COBRA value for "f". There is certainly an approximation in the method used to obtain the value for "C". We neglect the clad capacitance and also reduce the 5 fuel nodes that were used in the COBRA modeling of the pellet to 1 node.

The capacitance of this one node being the sum of the capacitance for the five node case. Even so, the large differences in "f" are too great to be solely due to these causes.

After an investigation of another COBRA run which used a smaller time step, and looking more closely at the equations that COBRA uses; it was decided that for COBRA "f" is a function of the time step size. We shall look at this in the next section. The important point of this section is that there is a real dependence of "f" and "RC" on the temperature distribution of the pellet.

6.2.4.3 the effect of time step size on COBRA

From Table 6.5 it is seen that the fraction of power appearing as heat flux actually increases as one increases the maximum heat flux or parameter "a". This is in contradiction to Eq. (6.17).

Table 6.5
Time Step Size vs. "f"

Run	Heat Flux at 3.3 Sec	Δt	f(%)
L 1397	.0823 MBTU/hr-ft^2	.8250 sec	15.2
M0606	.1684 MBTU/hr-ft^2	1.100 sec	18.0

The answer lies in how COBRA IIIC, and also MEKIN, determines "f". They both solve the heat conduction equation

$$\rho c \frac{\partial T}{\partial t} = K\left(\frac{d^2 T}{\partial r^2} + \frac{1}{r}\frac{\partial T}{\partial r}\right) q'''$$

in finite time and space differencing form. The equations are forward time differenced, so one obtains for the center node, i = 1.

$$\rho c \frac{T_1 - \bar{T}_1}{\Delta t} = 4K \left(\frac{T_2 - T_1}{\Delta r^2}\right) + q_1'''$$

The overscore bar denotes previous time. All other terms are at present time.

In obtaining the left hand member of the last equation the time derivative was replaced by Taylor series expansion terms.

$$T_1 = \bar{T}_1 + \Delta t \frac{\partial T}{\partial t} + \ldots$$

So we can get

$$\frac{\partial T}{\partial t} = \frac{T_1 - \bar{T}_1}{\Delta t}$$

If one more term was carried we would have

$$\frac{\partial T}{\partial t} = \frac{T_1 - \bar{T}_1}{\Delta t} - \Delta t \frac{\partial^2 T}{\partial t^2}$$

For a fast transient as we will have in a rod drop accident, high order derivatives may be positive and significant. If this is the case then

$$\frac{T_1 - \bar{T}_1}{\Delta t} > \frac{\partial T}{\partial t}$$

Of course if Δt is significantly small than the $T(t)$ function may be approximated linearly quite well, and high order derivatives terms become insignificant. There appears, however, to be a connection between the speed and severity of the temperature increase, and the time step chosen to obtain good results. This same reasoning carries itself into the affect the time step size has on the parameter "f".

Taking once again only the heat balance equation for the center fuel pin node we have that

$$\rho c \frac{T_1 - \bar{T}_1}{\Delta t} = 4K \left(\frac{T_2 - T_1}{\Delta r^2}\right) + q_1'''$$

For a particular time t_o and time step Δt we have

$$\rho c \frac{T_1^{t_o} - T_1^{t_o - \Delta t}}{\Delta t} = 4K \left(\frac{T_2^{t_o} - T_1^{t_o}}{\Delta r^2}\right) + q_1^{t_o'''}$$

$q_1^{t_o'''}$ is the known or forcing function for the heat generation density at time t_o for node 1. If Δt is too large then we get that

$$\frac{T_1^{t_o} - T_1^{t_o-\Delta t}}{\Delta t} > \frac{\partial T}{\partial t}$$

Then

$$\left| \rho c \frac{T_1^{t_o} - T_1^{t_o-\Delta t}}{\Delta t} - q_1^{t_o'''} \right| < \text{differential formulation}$$

because

$$\rho c \frac{(T_1^{t_o} - T_1^{t_o-\Delta t})}{\Delta t} < q_1^{t_o'''}$$

So,

$$\left| T_2^{t_o} - T_1^{t_o} \right| < \text{exact differential solution.}$$

This says that if too large a Δt is chosen for our transient time step one would overestimate the flatness of the temperature distribution in our pin. Further, since the heat flux is determined by the temperature difference and heat conductance for the clad and water nodes, this too will be overestimated along with "f". This is because the temperature of the clad node is overestimated and that of the water is a constant. Since the

power produced is the forcing function ($\sum_{\text{all nodes}} q_i'''$), "f" is also, therefore overestimated.

It therefore appears that one can not predict to a good degree what will be the typical void fractions during the rod drop accident without doing a time sensitivity on COBRA IIIC. Instead it will be more useful to understand the problem of the time step size, and that the RC constant for a fuel pin is very much a function of the temperature distribution within that pin.

This section has not invalidated the previous section's results, but does indicate that the temperature distribution that the fuel pins actually acquire during the accident will probably not be as flat as the transient run used for explanatory purposes in the previous sections.

To guarantee good results with MEKIN, the thermal-hydraulic time steps will be taken as small as five milli-seconds.

Chapter 7

MEKIN INPUT MODELING

All the work up to now has been to develop input data for the MEKIN code. It is believed that the accident can be correctly modeled by judiscous choice of input parameters. Since MEKIN was developed as an accident analysis code it is also hoped that if the input is chosen correctly, that the results from MEKIN will be the most accurate results attainable through analysis. However, the analysis is only as good as the modeling of the accident.

It is the intention of this chapter to explain the choices taken in some of the more important MEKIN input parameters. In section 7.1 we deal with the neutronic input modeling. This is kept separate as much as possible from the thermal-hydraulic modeling. However, as will be seen choices in some neutronic input parameters have an effect on the possible choices in the thermal-hydraulic data and vice-versa. Some of this trouble will be explained in section 7.1.

Most of the thermal-hydraulic choices have been relegated to section 7.2. Most important here is the choice of what constitutes a thermal-hydraulic channel.

For a code the size of MEKIN one must get involved with the area of computer data management. The optimization of physical record lengths used to store data on dishpack, and how to restart the problem at different times by use of Define File is explained in Appendix II.

Finally, the last section deals with suggestions for improvement to the MEKIN code based on experience gained through modeling and running this accident.

7.1 Neutronic Input

The neutronic input parameters are supplied on type N cards of the input deck. Most fundamental concern here is the choice and assumptions governing the neutronic node. Underlying this choice is the effect the pin power distribution within the subassembly has on the homogenized cross sections for our nodes. This will be covered in some detail in section 7.1.1.

As mentioned previously the neutronic and thermal-hydraulic input are not always independent. Section 7.1.2 represents a case in point. Explained in that section is the fact that due to the computer core limitation; one is forced to choose a specific geometry for a thermal-hydraulic channel and this effects just how one chooses a neutronic node.

The accident is driven by a drop in a control rod. One models this in MEKIN by changes in neutronic parameters due to the presence of the control rod. These important parameters are given in section 7.1.3.

Similarly the Doppler feedback mechanism is to turn around the power once the accident has occured. The change in the neutronic parameters due to increase in fuel temperature are presented in section 7.1.4.

MEKIN uses what is called albedo boundary conditions to represent the reflector. An investigation of how these albedos are found and their relationship to the more familiar reflector savings terms is made in section 7.1.5.

Finally, the last section, 7.1.6, deals with the choice of neutronic time step size.

7.1.1 Homozenized Parameters vs. Pins Power Distribution

Initial attempts of choosing a neutronic node involved dividing the core into 10 axial segments of 14.4". Each of these ten planes was divided into its 724 subassemblies, and a node was placed in its center. The core was therefore represented by a total of 7240 neutronic nodes. Within the plane, the subassembly traced out a square 6" on a side.

Each node is requested to have the same neutronic properties throughout its region. We have already generated

neutronic parameters for just such types of nodes. This was done for the hot standby condition where all fuel pins are at the same temperature, and the power distribution of the subassembly among its 49 pins was not a factor. This, however, may not hold true through the course of the transient. Then a non-flat power distribution will result in pins having fuel at different temperatures. If sufficient power is produced, the regions surrounding each pin may have unique void fractions (see figure 6.6). All of this requires consideration when we attempt to give MEKIN the correct homogenized parameters throughout the course of the accident for each of its nodes.

In the following the homogenized two group parameters for a subassembly are investigated under two conditions. The first involves a pin power and coolant void distribution as presented in the mixing study of Chapter 6. This is compared to the same subassembly but with subassembly (or nodal) averaged temperature for its pins and averaged void fraction for its coolant.

Both situations involve the use of results from section 6.2.4 to calculate the void fraction in the gap once the average void fraction in the lattice water is known.

Finally, the assumption that the transient will occur so rapidly that no significant void fractions will be produced was used to determine whether discrete representation of the power distribution was necessary to obtain good homogenized cross sections.

7.1.1.1 Mathematical Proof of the Problem

In this section we will attempt to show the conditions under which discrete power and average nodal power agree in giving the same homogenized cross sections. For this let us consider one parameter, the macroscopic thermal absorption cross section. Assume a functional dependence of a constant times the temperature to a power

$$\Sigma (T) = CT^{a}$$

Using the simpler method of flat or node average power distribution

$$T_{avg} = \left[\frac{\sum_{i=1}^{49} (T_{fi})^{x}}{49} \right]^{1/x}$$

In the discrete power representation we find Σ_{node}

$$\Sigma_{node} = \frac{\sum_{i=1}^{49} \Sigma_i}{49}$$

We want to know under what conditions

$$\Sigma\,(T_{avg}) \stackrel{?}{=} \Sigma_{node}$$

$$\Sigma\left[\left[\frac{\sum_{i=1}^{49}(T_{fi})^{x}}{49}\right]^{1/x}\right] \stackrel{?}{=} \frac{\sum_{i=1}^{49} CT_i^a}{49}$$

$$\Sigma\left[\frac{\sum_{i=1}^{49}(T_{fi})^{x}}{49}\right]^{1/x} \stackrel{?}{=} \frac{\sum_{i=1}^{49} CT_i^a}{49}$$

$$C\left[\left[\frac{\sum_{i=1}^{49}(T_{fi})^{x}}{49}\right]^{1/x}\right]C \stackrel{?}{=} \frac{\sum_{i=1}^{49} T_i^a}{49}$$

will hold when x = a. Since one uses x = 1 in the definition of T_{avg}, this means that the macroscopic cross section must depend linearly on the fuel temperature for the two methods to be equal.

7.1.1.2 computed results with significant void fraction

Comparison of the effect of power distribution on the homogenized two group parameters was carried out using the power and void fraction distribution of the mixing study in section 6.2.2. The compared cases are labeled DP (discrete power) and FP (flat power).

FP - Use bundle average temperature for all pins and $(V\bar{F})_{LW}$ in LEOPARD calculations.

DP - Use discrete pin temperature and void fractions in LEOPARD calculations.

The following average parameters were used for the FP case.

$\bar{T}_F = 2129.59°F$

$(\overline{Vf})_{LW} = .6741$

$(\overline{Vf})_{gap} = .0428$

$(\overline{Vf})_{node} = .525$

$\bar{T}_{clad} = 670.66$

$\bar{T}_{coolant} = 547.6\ °F$

The zone arrangement for the FP CITATION run can be seen in Fig. 7.1. Fig. 7.2 shows the zone arrangement for the discrete power case. The control in-curtain in case with its higher peak to average pin power value than the control

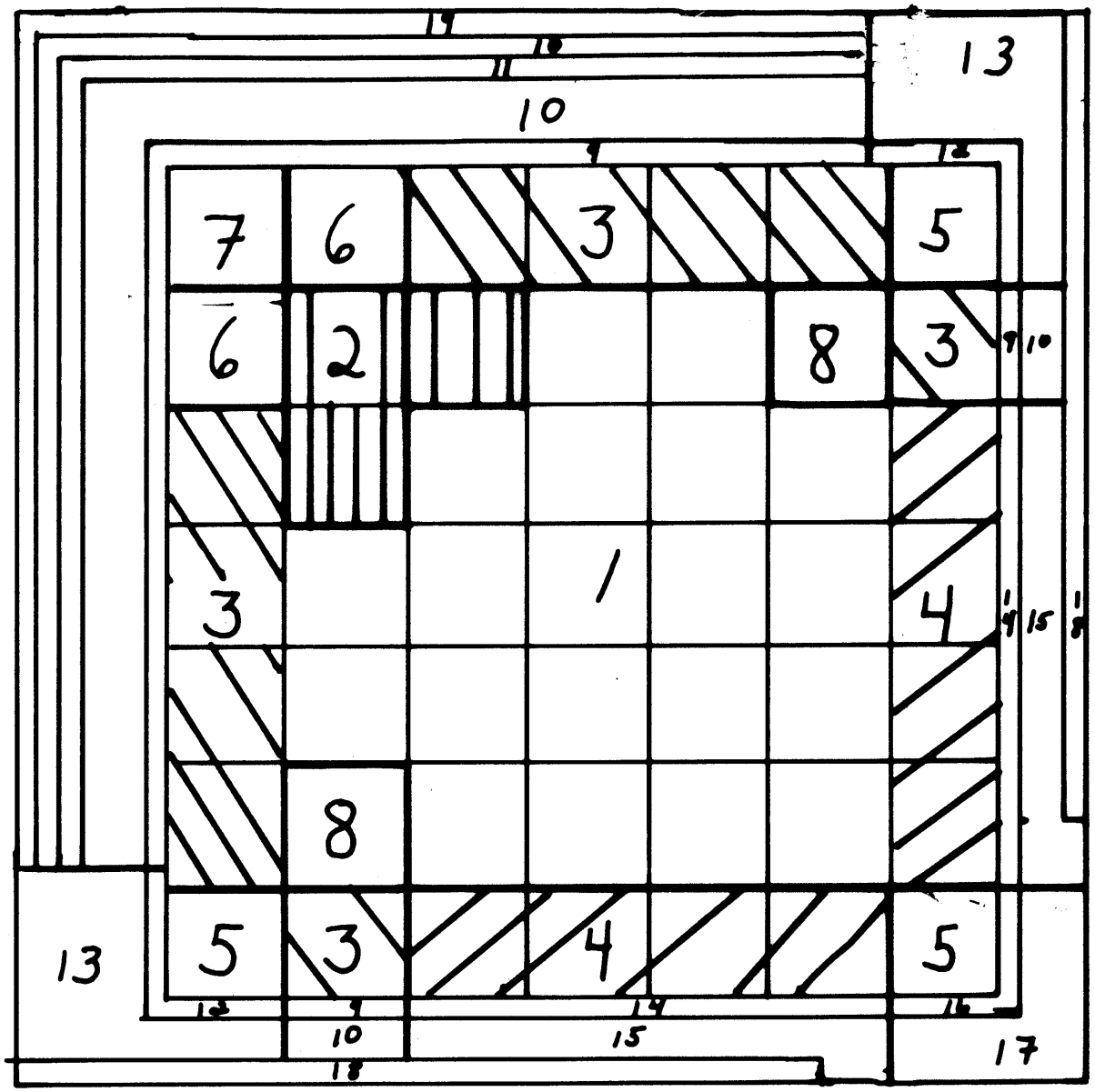

CITATION Zone Arrangement
For Flat Subassembly Pin Power Distribution

Fig. 7.1

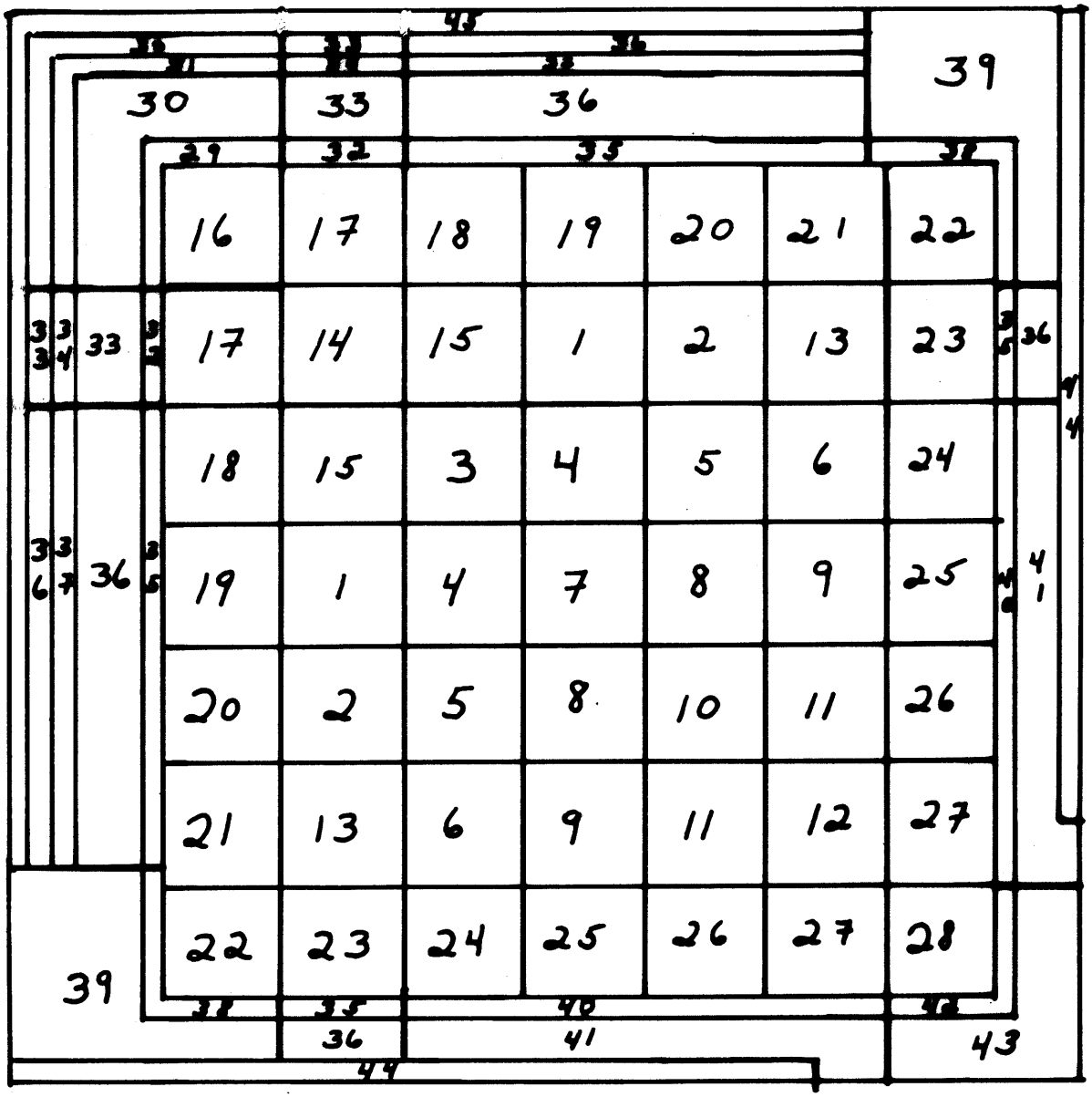

CITATION Zone Arrangement
For Discrete Subassembly Pin Power Distribution

Fig. 7.2

rod out - curtain in case was used. For this DP case zone 12 had the highest void fraction, .76825; zone 27 had the highest pin average fuel temperature, 2962 °F; and zone 16 had the lowest fuel temperature, 1058 °F, and void fraction, .41525.

The results of the comparison are given in Table 7.1. Homogenization Model II was used to obtain the results.

Table 7.1

Homogenized Two Group Parameters For FP vs. DP

	DP	FP	$\left\lvert \frac{DP - FP}{FP} \right\rvert$
D_1	2.1668	2.1660	.04%
Σ_1	1.2302 E-02	1.2335 E-02	.26%
$\nu\Sigma_{f1}$	3.0755 E-03	3.0756 E-03	.003%
Σ_r	5.1928 E-03	5.1927 E-03	.002%
D_2	7.9198 E-01	7.6729 E-01	3.2%
Σ_2	6.5476 E-02	6.0308 E-02	8.6%
$\nu\Sigma_{f2}$	7.0952 E-02	7.2871 E-02	2.6%

As can be seen there is as much as 8.6% difference for the thermal macroscopic absorption. This while the peak to average void fraction in the lattice water was

$$\frac{.76825}{.6741} = 1.14$$

and peak to average pin fuel temperature was

$$\frac{2962}{2130} = 1.39$$

From table 7.1 one can see that it is the thermal parameters that are effected significantly. It will be shown in the next section that this is because it is the variance in the void fraction that is the dominant parameter in determining the difference between the FP and DP results. This, of course, is very dependent on the f factor of section 6.2.4 and the mixing effects.

7.1.1.3 computed results when void fraction is not significant

Here we compare the same two bundles investigated in the previous section as concerns temperatures, however, the void fraction is taken to be zero for both power distributions. This could occur in our transient if our RC constant was large and "f" was small. Hence, the peak to average pin

fuel temperatures was still 1.39. The peak to average void fraction is now 1.0 and we are interested in the possible derivation in the two power distributions' homogenized cross sections.

It was found that one could avoid running an entire bundle homogenization for this no void case. The zone in the previous section's DP case that had the greatest void fraction was zone 12 (see fig. 7.2). The fuel temperature of the pin in that zone was 2821 °F. It was noticed in comparing DP to FP results in the previous section that the macroscopic thermal absorption cross section for this particular pin's zone, for the DP and FP case differed in absolute relative value by about the same amount as the subassembly cross section for the DP and FP cases did.

Therefore one should run the two cases for this pin again, but now with the void fraction equal to zero in both cases yet retaining the temperature effects. If the difference in the thermal absorption cross section is small, one can reasonably assume that it will be small also for the subassembly homogenized cross sections under the DP and FP conditions with no void. The results for such a run are presented in Table 7.2.

Table 7.2

Effect of Power Distribution on
Cross Sections When Have No Voids

Case	Bundle Homo Σ_2	Zone 12 Σ_2 (void fraction $\neq$ 0)	Zone 12 Σ_2 (void fraction = 0)
FP	.60308 E-01	.62615 E-01	.76912 E-01
% diff	8.6%	7.8%	0.67%
DP	.65476 E-01	.58086 E-01	.76400 E-01

As can be seen in the last column of results the difference when void fraction is zero is about an order of magnitude smaller then when void fraction is significant. It was then reasoned that the subassembly homogenized absorption cross section difference for the two power distributions, when voids are insignificant, will also be less than 1%.

For our accident it was now assumed that due to the expected low "f" factor and speed of the transient, we will have low void fractions. Therefore, the nodal cross section that will be inputed into MEKIN will be found using the flat power distribution assumption. If, in the course of the accident, we find that the voids are significant further iterations would have to be carried out on MEKIN with the newly determined nodal parameters if greater accuracy was desired. For our accident this was not done.

7.1.2 Homogenization of Four Subassemblies

After much work trying to run MEKIN with 724 thermal-hydraulic channels, it became apparent that due to computer space requirements (we had access to a computer core of around 912K) that the channel size would have to be increased resulting in fewer channels and a reduced computer core requirement. This was done by grouping four subassemblies into a single channel, which lead to complications concerning the neutronics. We need not decrease the number of neutronic mesh points, however, MEKIN requires that the neutronic properties within the region traced out by a single thermal-hydraulic (T-H) channel be homogeneous.

Since we now have four subassemblies, with possible different neutronic properties, making up a T-H channel, we are forced to further homogenize our neutronic data. We do lose something by doing this. The fine neutronic detail which possibly four different types of subassemblies might exhibit in a full core calculation is now lost by the homogenization of that particular region into a single set of neutronic parameters.

We had very little alternative to this choice. To decrease the number of axial nodes would have lowered the computer code requirements only slightly. Further, we couldn't use anything but full core geometry. Assembly

homogenization seemed the only way to go, and with it we need not lower the number of neutronic nodes, though we still have weakened to some extent the fine detail of the flux. There exists one major problem in carrying this homogenization out.

Let us call a planar cross section of one of our new homogenized assemblies a box or channel. MEKIN requires that all boxes be the same size and square. This is fine for the interior of the reactor core, but not so for its reflector boundary. In an attempt to group the subassemblies in fours, some boundary subassemblies remained by themselves. A box formed with one of these subassemblies also included some of the reflector and possibly some of the core shroud.

Our intention was to homogenize the assembly nuclear parameters by flux weighting. This was accomplished with any assembly containing four subassemblies by using CITATION with a mesh of 30 points by 30 points. Reflective boundary conditions surrounded the assembly on all sides. The previously homogenized subassembly parameters were used to represent each subassembly region in the assembly homogenization scheme.

For the boxes that included some of the reflector, the reflector was taken to be 4 inches in length. This was based on correspondence with Commonwealth Edison. They

stated that the thermal flux went to zero after four to 4.8 inches of reflector. Hence, a typical reflector containing box would have a six inch by six inch subassembly in its lower left hand corner. To the right would be placed four inches of water of equal (6 inch) height. Then on top of the subassembly and this already added water would be placed four inches of water. This traced out a geometry that was ten inches by ten inches. A 25 x 25 mesh using CITATION was then employed. Reflective boundary conditions were placed on the two sides of our described sample reflector containing box which faced another box. The two outside surfaces were given extrapolated boundary conditions. The previously homogenized subassembly parameters were used for the subassembly region of this assembly, and Wigner Wilkens spectrum averaged parameters were used for the reflector water. These latter parameters were obtained from a LEOPARD run with nothing but water in its regions. The resulting homogenized parameters were used for a 12 x 12 inch MEKIN box which partially lies outside the physical reactor core boundary.

No investigation of the accuracy of handling the reflector containing boxes was carried out. This in itself could constitute another thesis. However, a few things are recognized. First, the reflective boundary conditions holds less true for boundaries where the neutron current

starts to deviate much from zero. At the boundaries of a reactor core the slope of the flux tends to increase in magnitude, therefore, increasing current between assemblies. It should be remembered here also that the initial configuration of "hot standby" for our reactor will yield anything but a nice cosine flux shape, hence even for the core interior there will be much neutron mixing between assemblies. Still, for the reflector containing boxes the reflector boundary approximation holds less true.

Further, because of the equal box size requirement of MEKIN we have in effect added on a small amount of reflector-subassembly homogenized material to our core in those places where we have a reflector containing box.

These approximations for our reflector containing boxes were not seen to effect our transient accident analysis in any significant way. This is because our control blade will be expelled from almost dead center in the core, and it is in this region which we will be primarily interested.

Yet, if further time had permitted a deeper investigation of the core flux shape changes due to the above homogenization procedures, as compared to the 724 channel case, should have been carried out.

Finally we then have 12 different box compositions and 193 boxes with 4 points per box. In addition, there are 10 levels of these boxes.

The new and old box, control rod gang and composition core map are shown on figures 7.3 to 7.6. The composition for the old map can be defined in terms of the 8 different types of subassemblies we have. The compositions for the new map are then defined in terms of the old.

The old compositions are:

Composition	Description
1	Dished - control rod in - curtain full
2	Undished - control rod in - curtain full
3	Dished - control rod in - half curtain
4	Dished - control rod in - no curtain
5	Dished - control rod always out - curtain full
6	Dished - control rod always out - no curtain
7	Dished - control rod out - curtain full
8	Undished - control rod out - curtain full
9	Dished - control rod out - half curtain

If a control rod is in initially for an assembly whose rod is going to drive out one must input the control rod out composition. From the above definitions we can now define the new composition assignments.

New Composition for 193 Box Setup	Old Compositions for 724 Box Setup
1	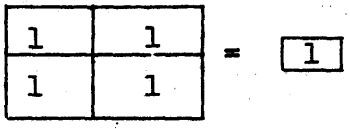 = 1
2	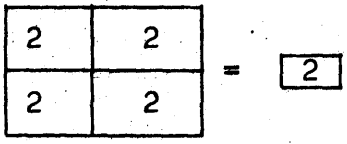 = 2
3	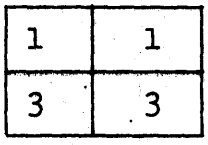
4	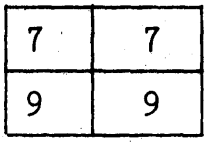
5	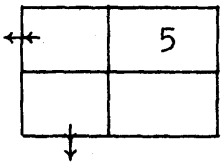 box includes some reflector.
6	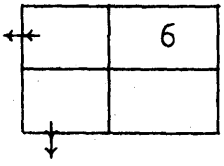 box includes some reflector
7	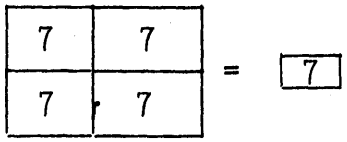 = 7
8	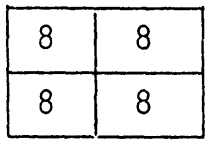 8
9	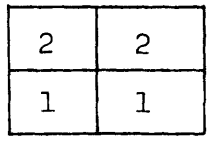

(continued)

New Composition for 193 Box Setup	Old Compositions for 724 Box Setup
10	7 8 7 7
11	1 2 1 1
12	3 1 4 3

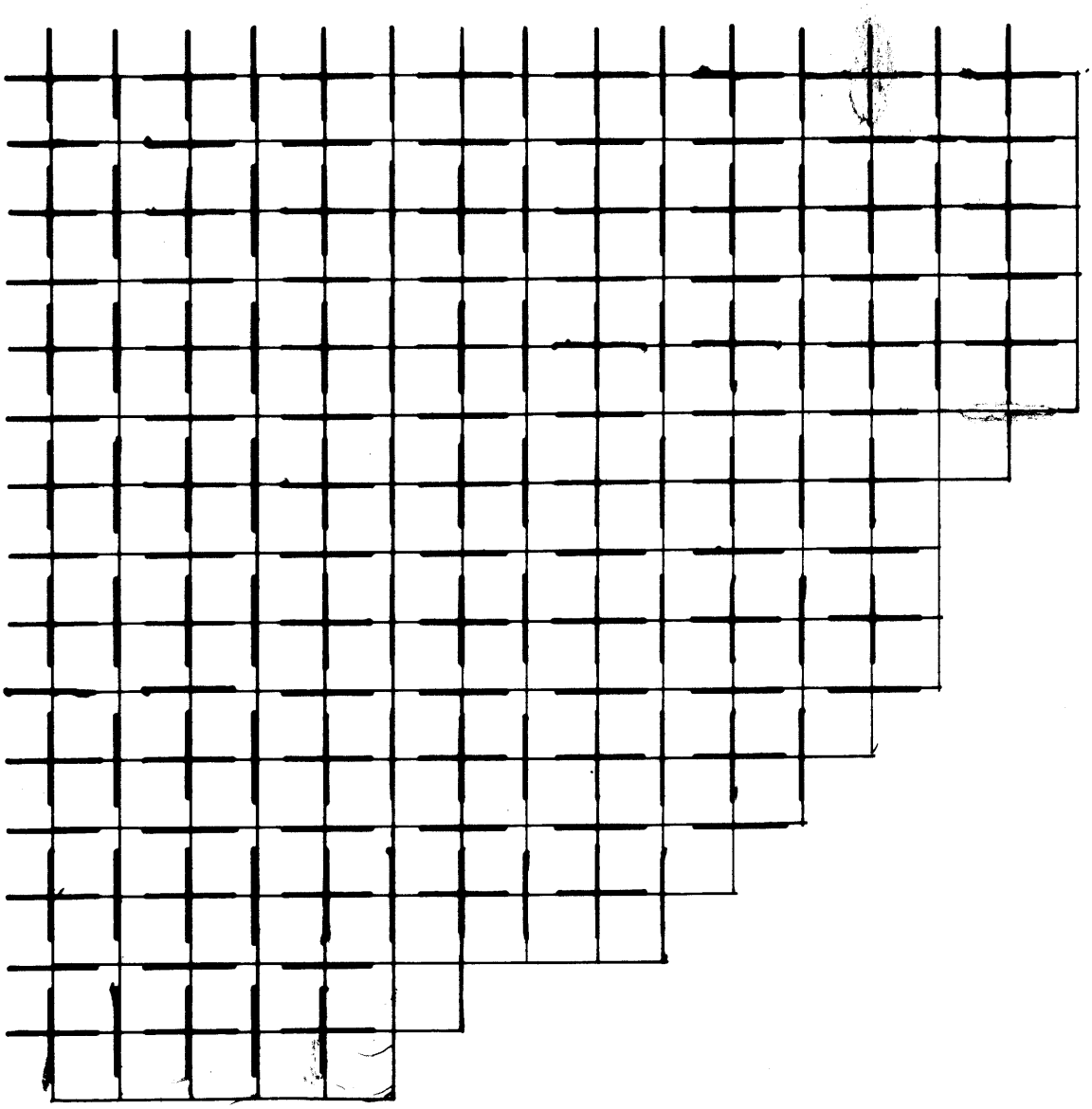

Control Rod And Curtain Locations

Fig. 7.3

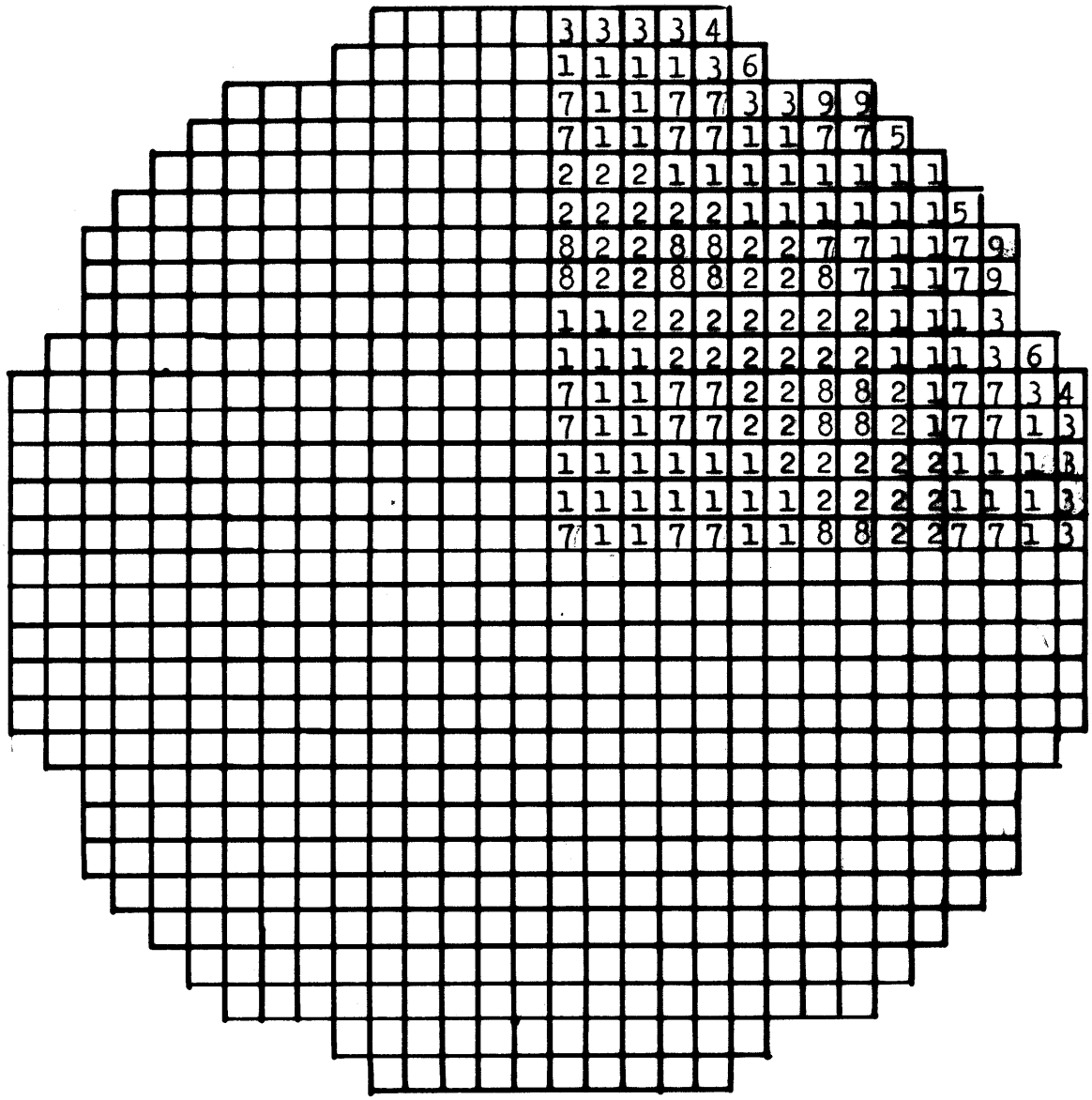

Subassembly Composition Map

Fig. 7.4

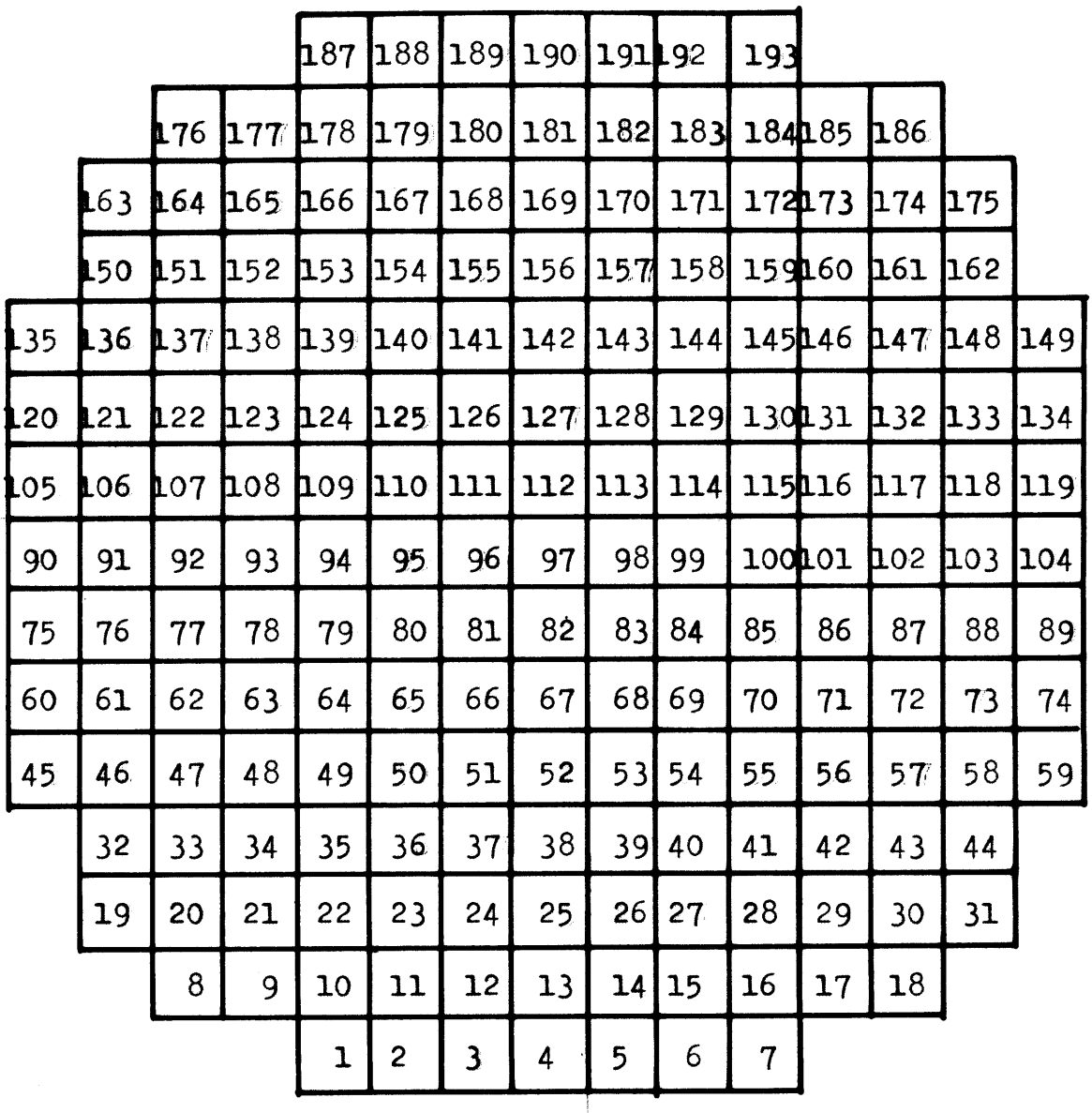

MEKIN Box Map

Fig. 7.5

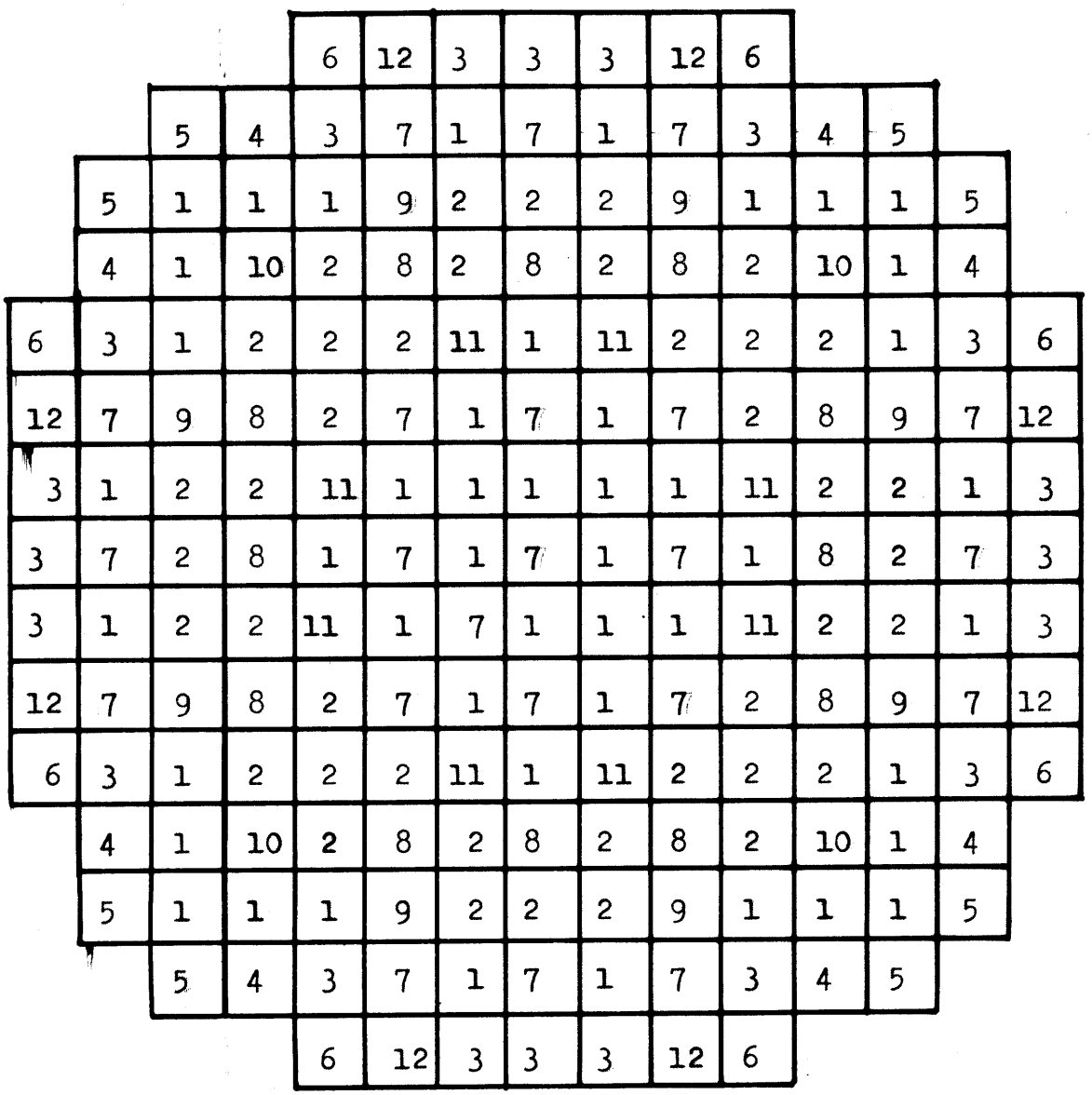

MEKIN Box Composition Map

Fig. 7.6

Table 7.3
Composition Input For MEKIN

Comp	6	5	3	4	9
D_1	1.52894	1.52155	1.37536	1.41774	1.36888
Σ_1	5.09585E-03	5.13833E-03	1.12701E-02	6.84745E-03	1.13514E-02
$\nu\Sigma_{f1}$	3.16943E-03	3.16850E-03	4.48544E-03	4.37245E-03	4.52730E-03
Σ_r	2.31994E-02	2.30477E-02	1.76940E-02	1.81155E-02	1.75749E-02
D_2	3.02756E-01	3.00517E-01	3.60804E-01	3.57065E-01	3.59896E-01
Σ_2	2.61889E-02	2.67738E-02	6.73606E-02	5.04150E-02	6.89712E-02
$\nu\Sigma_{f2}$	2.94573E-02	2.86013E-02	8.17623E-02	7.11916E-02	8.25719E-02
K_∞	.7801684	.7441043	.8963687	1.1999283	.8839017
Comp	10	11	12	7	8
D_1	1.41246	1.37133	1.37694	1.41393	1.40806
Σ_1	6.89115E-03	1.13251E-02	1.12421E-02	6.86399E-03	6.97241E-03
$\nu\Sigma_{f1}$	4.39375E-03	4.50634E-03	4.48550E-03	4.37317E-03	4.45534E-03
Σ_r	1.80497E-02	1.75976E-02	1.77676E-02	1.80632E-02	1.80100E-02
D_2	3.55681E-01	3.60292E-01	3.60954E-01	3.55324E-01	3.56765E-01
Σ_2	5.11026E-02	6.87508E-02	6.62446E-02	5.08966E-02	5.17287E-02
$\nu\Sigma_{f2}$	7.11796E-02	8.21724E-02	8.17822E-02	7.08294E-02	7.22440E-02
K_∞	1.1842003	.8830256	.9107544	1.184	1.185

Table 7.3

Composition Input for MEKIN

Comp	1	2
D_1	1.37379	1.36400
Σ_1	1.12987 E-02	1.14038E-02
$\nu\Sigma_{f1}$	4.48533 E-03	4.56898E-03
Σ_r	1.76204 E-02	1.75298E-02
D_2	3.60686 E-01	3.59099 E-01
Σ_2	6.85316 E-02	6.94146 E-02
$\nu\Sigma_{f2}$	8.17748E-02	8.3376 E-02
K	.88215	.88505

7.1.3 Change in Neutronic Two Group Parameters Due to Control Blade Presence

A closer investigation of just how much the control blade effects the neutronic parameters is presented in table 7.4. This is for the important case of dished full curtained assembly.

Table 7.4

Control Blade vs. Neutronic Parameters

Parameter	No Control Blade	Control Blade	$\frac{NCB-CB}{CB}$
D_1	1.4139	1.3738	2.92%
Σ_1	6.8640E-03	1.1299E-02	39.25%
$\nu\Sigma_{f1}$	4.3732E-03	4.4853E-03	2.50%
Σ_r	1.8063E-02	1.7620E-02	2.51%
D_2	3.5532E-01	3.6069E-01	1.49%
Σ_2	5.0897E-02	6.8532E-02	25.73%
$\nu\Sigma_{f2}$	7.0829E-02	8.1775E-02	13.39%
K	1.184	.882	34.24%

The worth of the rod as determined by ΔK with rod in and out shows it to be quite high for the assembly. Since MEKIN in the 3-D option one will drive the transient by the change in nuclear parameters, the changes in Σ_1, Σ_2 and $\nu\Sigma_{f2}$ are the most significant. The effects of control rod for other compositions can be found using table 7.3.

7.1.4 Effect of Fuel Temperature Feedback on Nuclear Parameters

Subassembly homogenization Model III was used to generate points for variable changes in the fuel temperature, but keeping the coolant conditions to be saturated water at 547 °F. The clad temperatures that went along with those fuel temperatures up to 3000 °F are given in table 7.5.

Table 7.5

Clad Temperatures Used With Fuel Temperature

Clad Temperature	Fuel Temperature
547 °F	547 °F
585	1000
662	2000
662	3000

The clad expansion has an effect on the amount of water in each subassembly and hence is an important property. From General Electric's analysis of the accident it is believed that the fuel temperatures will not exceed 3000 °F for the accident and so a straight line approximation was made to the data to obtain a slope. The results are presented in table 7.6.

Table 7.6
Temperature Change Correlation Data

	Dished-Control Rod In-Curtain Full	Dished-Control Rod Out-Curtain Full
$\frac{\partial D_1^{-1}}{\partial T}$	-9.3×10^{-6} / °C	-8.8×10^{-6} / °C
$\frac{\partial \Sigma_{c1}}{\partial T}$	$+1.53 \times 10^{-7}$ / °C	$+1.43 \times 10^{-7}$ / °C
$\frac{\partial \Sigma_{f1}}{\partial T}$	-2.30×10^{-8} / °C	-2.30×10^{-8} / °C
$\frac{\partial \Sigma_{1\to 2}}{\partial T}$	-8.3×10^{-8} / °C	-1.3×10^{-7} / °C
$\frac{\partial D_2^{-1}}{\partial T}$	-1.15×10^{-5} / °C	-1.53×10^{-5} / °C
$\frac{\partial \Sigma_{c2}}{\partial T}$	-1.67×10^{-7} / °C	-1.31×10^{-7} / °C
$\frac{\partial \Sigma_{f2}}{\partial T}$	-3.57×10^{-7} / °C	-2.77×10^{-7} / °C

The correlation data is caused by the following:

1) Doppler Effect
2) Volume expansion cause number density of fuel to decrease and amount of water in subassembly to decrease.
3) Possible shifting of flux within the subassembly due to the above.

7.1.5 The ALBEDO Data

There appears to be some similarity between the albedo, α_1, formula[29] and the concept of reflector savings, δ, as presented by Lamarsh[30].

$$\delta = \frac{D^c}{\sqrt{D^r \Sigma_a^r}} \tanh \left(\frac{\Delta}{D^r} \sqrt{\Sigma_a^r \; D^r} \right) \qquad (7.1)$$

Where superscript

r = reflector

c = core

The albedo from energy group g to g is

$$\alpha_{gg} = \frac{\tanh\left[\frac{\Delta}{D_g}\sqrt{D_g\Sigma_g}\right]}{\sqrt{D_g\Sigma_g}} \tag{7.2}$$

Now the purpose of the albedo is to correctly allow us to represent the flux in the core by using the correct boundary condition at the core reflector interface. So we want $\phi(x_1)$, the flux at the boundary, to correctly represent the flux due to the presence of a reflector of thickness Δ.

The two equations for the reflector flux are:

$$\phi_1(x_1) = \alpha_{11} J_1(x_1) \tag{7.3}$$

$$\phi_2(x_1) = \alpha_{21} J_1(x_1) + \alpha_{22} J_2(x_1) \tag{7.4}$$

The reflector savings concept says the critical size of a core of a given composition can be reduced by its reflector saving for each boundary reflector that is present. The point is that since at the boundary x_1

$$\phi_i^r(x_1) = \phi_i^c(x_1) \tag{7.5}$$

and

$$J_i^r(x_1) = J_i^c(x_1) = -D_i^r \left.\frac{d\phi_i^r(x)}{dx}\right|_{x=x_1} =$$

$$= -D_1^c \left.\frac{d\phi_i^c(x)}{dx}\right|_{x=x_1} \qquad (7.6)$$

Eq. (7.3)could be written:

$$\phi_1^{r=c}(x_1) = -\alpha_{11} D_1^c \left.\frac{d\phi_1^c}{dx}\right|_{x=x_1} \qquad (7.7)$$

so using Eq. (7.7 , 7.2) one gets that

$$\phi_1^{r=c}(x_1) = \frac{-D_1^c \tanh\left[\overline{\Delta}\sqrt{D_1^r \Sigma_1^r}\right]}{\sqrt{D_1^r \Sigma_1^r}} \left.\frac{d\phi_1^c}{dx}\right|_{x=x_1} \qquad (7.8)$$

Comparing Eq. (7.8) to Eq. (7.1) we get

$$\phi_1^{r=c}(x_1) = -\delta_1 \left.\frac{d\phi_1^c}{dx}\right|_{x=x_1} \qquad (7.9)$$

Hence, if $\left.\frac{d\phi_1^c}{dx}\right|_{x=x_1}$ has a value of $\frac{-10 \text{ neutrons}}{\text{cm}^2\text{-sec-cm}}$

and if $\delta_1 = 5$ cm, then Eq. (7.9) states

$$\phi_1^{c=r}(x_1) = 5 \text{ cm} \cdot 10 \frac{n}{\text{cm}^2 \text{ sec cm}} = \frac{5n}{\text{cm}^2 - \text{sec}}$$

Or, knowing the gradient of the flux in the core at the core-reflector interface one can find the appropriate flux at this interface by saying the flux will linearly decrease to zero (with a slope of the gradient of the flux in the core at the interface) at a distance of a reflector saving from the core. This, of course, doesn't correctly model the flux in the reflector, but we are not interested directly in that. The use of the albedo is to correctly predict $\phi_1(x_1)$, and from MEK-33 results[29], it seems to accomplish that quite well.

Figure 7.7

The Albedo Effect on Flux

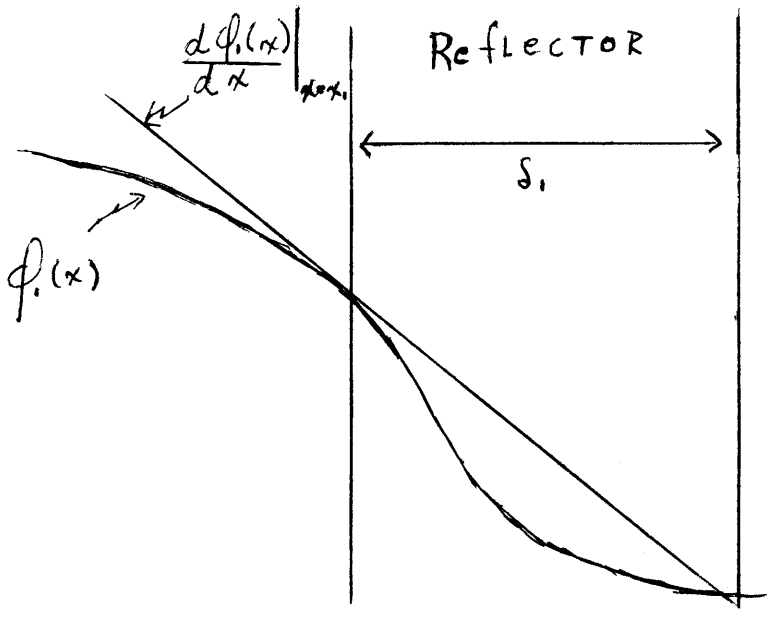

Equation (7.4) is the thermal flux in a two group representation. Neglecting the first term on the RHS one has a similar equation to Eq. (7.3). The first term on RHS is to account for the production of thermal neutrons in the reflector which are produced by the fast flux source $J_1(x_1)$. The α_{21} albedo term is effectively represented for a large reactor problem by

$$\alpha_{21} = \frac{\Sigma_{21}^r \left[D_1^r \alpha_{11} - D_2^r \alpha_{22} \right]}{D_1^r \Sigma_2^r - D_2^r \Sigma_1^r} \qquad (7.10)$$

This bears no resemblance to the reflector savings terms of one group theory.

For the top and bottom reflectors in this accident analyses one assumes infinite reflectors. Then, using the spectrum generated by a LEOPARD where all regions had only water in them one obtains

$$\alpha_{11} = 30.40$$

$$\alpha_{22} = 18.88$$

$$\alpha_{21} = 96.60$$

For those boxes in the MEKIN arrangement which contained some reflector water, one uses the same thermal spectrum above, but an average subassembly fast spectrum for the fast spectrum since the reflector was assumed to be only 4.0 inches thick. For this one obtains:

$$\alpha_{11} = 7.8638$$

$$\alpha_{22} = 18.88$$

$$\alpha_{21} = 13.71$$

Those boxes that were composed of some reflector water were not given albedo but extrapolated boundary conditions.

7.1.6 Choice of Neutronic Time Step Size

As shown in volume one of the MEKIN manual, it solves the kinetics equation

$$\frac{\partial \psi}{\partial t} = \underline{A}\ \psi \qquad (7.11)$$

by means of the NSADE (non-symmetric alternating direction explicit) method. It is not the intention to go into that method here except to show how the choice of the neutronic time step size is effected by this particular NSADE method. The following is based on Ferguson's article[31]. To solve Eq. (7.10) numerically one gets

$$\psi^N = e^{\underline{A}\Delta t}\ \psi^{N-1} \tag{7.12}$$

where ψ^N is the flux at time step N. To solve Eq. (7.12) it is assumed that $\underline{A}$ is constant over Δt. This is of course not true during a transient. Since $\underline{A}$ contains all of the Diffusion theory parameters, as well as the precursor concentrations, its elements vary greatly in magnitude causing $\underline{A}$ to be a stiff matrix. Thus to solve Eq. (7.10) as it stands would involve the inversion of matrix A, which would be too time consuming. Since, during the accident, one will have the rod falling and significant feedback effects, so the elements in matrix A will always be changing.

To help alleviate these two problems the following is done. Let

$$\psi = e^{\Omega t}\ \phi \tag{7.13}$$

then Eq. (7.11) becomes

$$\frac{d\phi}{dt} = e^{-\Omega t}\ (A-\Omega)e^{\Omega t}\ \phi(t) \tag{7.14}$$

Let

$$W = e^{-\Omega t}\ (A-\Omega)e^{\Omega t} \tag{7.15}$$

Then

$$\frac{d\phi}{dt} = W\phi \tag{7.16}$$

and $$\phi^N = e^{W\Delta t}\ \phi^{N-1} \tag{7.17}$$

Now one states that it is W which one wishes to be constant over Δt to have a good numerical solution to the problem.

If one lets Ω for time step N to N + 1 to be determined by

$$\Omega \equiv \frac{1}{\Delta t}\ \ell n\ \left(\frac{\psi^N}{\psi^{N-1}}\right) \tag{7.18}$$

$$\Omega = \frac{1}{\Delta t}\ \ell n\ \left\{\ \frac{e^{A^N \Delta t}\psi^{N-1}}{\psi^{N-1}}\ \right\} \tag{7.19}$$

$$\Omega = A^N \tag{7.20}$$

then

$$W = e^{-\Omega t}(A - A^N)e^{\Omega t} \tag{7.21}$$

So it becomes the difference in the A matrix over the time step Δt which we now desire to be a constant. If during the time step from N to N + 1 we choose

$$W = e^{-\Omega t} (A^{N+1} - A^{N}) e^{\Omega t} \tag{7.22}$$

then this Ω transform allows us to assume that the rate of change of A over step Δt is a constant instead of assuming A is a constant as was done in the untransformed Eq. (7.12).

The matrix W is also broken up so that one need not invert such a large matrix. It is then represented as an advancement matrix where even if the terms in A over Δt changed at a constant rate one would still get temporal truncation error. For the NSADE method employed here, the error starts to appear (when one expands the advancement matrix in a Talyor series) for terms of order h^2 where h is a half time step ($\Delta t/2$).

So it is that one has two major approximations in solving numerically for the flux. From a time step sensitivity analysis carried out for a 2-D nodal kinetics code using NSADE it was found that to guarantee a solution to 1% accuracy one should have 100 time steps for a doubling of the flux.

In our accident a Δt = 1 millesec was used up to the time of prompt critical. At that time, the time step size was only halved due to computer time availability.

7.2 The Thermal-Hydraulic Model

There is a basic difference in the geometrical set up of fuel pins and channels in the BWR option of MEKIN and the COBRA IIIC code as outlined in section 6.2.1. In the MEKIN case, the pin must be placed in the center of the channel. For the initial attempts of setting up MEKIN with 724 channels, this means one pin per subassembly. This one pin then in effect represents all 49 pins in the subassembly. The power produced, and temperature distribution within the pin would be that of an average pin in the subassembly. That is, one forty-ninth of the power produced in the subassembly, as calculated by the neutronics, is attributed to our representative pin.

The equivalent thermal hydraulic diameter and the effective heat capacitance of the water calculations forbid one to include the water outside that zircaloy can.

The thermal hydraulic diameter is calculated by MEKIN by feeding in the total wetted perameter and total flow area in our channel. Then the familiar formula

$$\text{Thermal Hydraulic Diameter} = \frac{4 \times \text{Flow Area}}{\text{Wetted Perimeter}}$$

is used. Since the gap water is kept separate from the lattice water by the subassembly can, it should not be included in this calculation. Further, in the transient it is important to determine the correct heat capacity of the water. The lattice water is effected by both direct heating due to photon and neutron heating, and conductive heat flux from the fuel pins themselves. Only the former of these affect the heat of the gap water. Hence, to include the gap water would be to overestimate the water's heat capacitance for our primary flow within the lattice. This could result in less lattice void fraction, and possibly a lower convective heat transfer coeffient for our pins. To neglect the gap water puts one in error in the opposite direction.

Since one is primarily interested in correctly modeling the lattice water, the gap water was excluded from the total flow input parameter; and the power of the reactor was derated. Also from sec. 6.2.3 one could obtain a reasonable idea of what the conditions in the gap water were if the conditions in the lattice water were known.

To correctly represent the amount of heat produced by the reactor within the subassembly cans one has three input parameters. They are the steady state power, the energy produced in the metal and in the coolant per fission.

In a manner analogous to sec. 6.2.3, and assuming the average void fraction for our core will be very close to zero for our accident; the following table is repeated from sec. 6.2.3. This table assumes prompt fission energy distribution only, and control rod out case.

Table 7.7

Fast Fission Power Distribution
for No Voids Situation

174.015	Mev/fission	in pins
.6	"	in Zr - can
4.18	"	in lattice water
1.71	"	in gap water

so for control rod out case (no voids)

$$\frac{1.71 + .3}{180.5} = 1.11\%$$

of power is distributed in the gap water. For the control rod in case 1.4663% of power is produced in the gap water.

Now at the time of the accident three-quarters of the core has its control rods in, and about one quarter have them out. These factors were used as weight in determining that the derated power of the reactor at steady state is

$$(.75)(1-.014663)(2527 \times 10^{-6}\text{MW}) = 1867.460$$
$$+ \quad (.25)(1 - .0111)(2527 \times 10^{-6}\text{MW}) = \quad 624.738$$
$$2493 \times 10^{-6}\ \text{MW}$$

To determine the amount of energy deposited in fuel per fission one again uses table 7.7 to derive

$$180.5 - (1.71 + .3) - (4.18 + .3) = 174.01\ \frac{\text{Mev}}{\text{fission}}$$

Similarly for the amount of energy directly deposited in the coolant, one considers only the lattice water to get

$$4.18 + .3 = 4.48\ \text{Mev/fission.}$$

These numbers are for the control rod out case. This case was considered the most appropriate since it will result in more of the core heat being released (in the region) within the zircaloy can of the subassemblies. In terms of MW - sec / fission one then gets

2.789×10^{-17} MW - sec / fission in metal

and

7.181×10^{-19} MW - sec / fission in coolant

With these values one hopes to correctly simulate the conditions in the lattice of our subassemblies.

As was mentioned in section 7.1.2 one had to decrease the number of thermal-hydraulic channels. This change affected the thermal hydraulic conditions in the sense that the flux which determines the power in the new 4 subassembly channels may not be as accurate as before. But probably most importantly, now one will have in effect complete mixing of the coolant of 4 subassemblies that would normally be separated. Fortunately the expelled blade will affect the four subassemblies it controlled in almost exactly the same way so that the thermal - hydraulic conditions in each of these subassemblies should almost be identical. This means that allowing mixing here should not have too great of an affect on the resultant coolant conditions than if one had the true case of no mixing.

Some mention should be made concerning the mixing and two phase flow parameters that the user of MEKIN has an

option in choosing. For a BWR with segregated channels there is no mixing of coolant between channels. Therefore the random turbulent mixing parameters of ABETA and BBETA on card type T9 of the MEKIN User's Manual are set equal to zero. Similarly the diversion mixing parameters: KIJ(the cross flow resistance coefficient), FTM (the turbulent momentum factor) and SL (the transverse momentum factor) of card type T17 are all set equal to zero.

The homogeneous two phase friction model was chosen over that of Baroczy[9]. This is because for the rod drop accident involving a ΔK of only 1% is not believed to cause a large amount of voiding in our hottest channels. However, if void fractions of 35% or higher were anticipated then the Baroczy model would be perferred provided signifiant flow also occured.

Since our accident starts with saturated coolant, no subcooled void will be permitted.

Also, because of low flow and void expectations, a slip ratio of vapor velocity to liquid velocity was taken as one.

The low power and flow conditions of our accident caused a number of changes to be made in MEKIN. These are reported in Appendix III.

It is possible to determine the "f" factor for each time step and channel from the MEKIN output edit. The heat flux for each of the axial nodes of the channel are printed out. The corresponding power produced at that time for the correct node of a channel can be determined by the edit channel power and the corresponding thermal axial flux distribution. This method shall be used in Chapter 8.

Finally, the time step length of the thermal hydraulics was varied throughout the transient but normally was on the order of 20 millisec. The relative size was decreased when the power was increasing rapidly to as low as 5 milliseconds.

7.3 Suggestions for Improvement of MEKIN

As MEKIN stands now, it is quite expensive to run. Some work should be done to improve the run time. It might be possible that for a large core problem, such as was investigated here, the finite element method would be a worthwhile time saving option over the present finite difference scheme.

For BWR problems, the gap and control blade region between subassemblies should be able to be better handled than the neglection technique used in section 7.2. Some way of allowing it to be a separate channel, with its heat

source dependent on the gamma radiation sources surrounding it and its neutron moderator ability should be incorporated into the code. This will, however, lead to the requirement of more channels. But, the flow conditions in the gap may be substantially different than that within the cans so there may be no way of getting around the added channel requirement.

The requirement that the boxes must all be of the same size is a limitation that one would like to change. As is shown in section 7.1.2 the required neutronic homogination at the core-reflector boundary to satisfy this limitation resulted in yet another approximation. To have had the option to neglect the flow condition (and hence the requirement for a thermal-hydraulic channel in this non-important region); and yet maintain neutronic nodes in the single protruding subassembly which cannot be grouped into a set of four would help to alleviate this problem. Another solution would be to be able to vary the box size, however, it is feared that this may increase the computer core requirement. Of course this whole problem resulted from not having enough computer core to execute the problem when each subassembly was a box. Hence, the ideal solution would have been a bigger computer or a smaller problem.

Presently MEKIN cannot handle reversed flow conditons. This is because of the upward channel stepping flow routine used to solve the hydraulics. The accident analyzed in this thesis most likely would have coolant flowing out of the core in both the up and down direction as the coolant begins to void causing mass displacement.

A more general symmetry requirement would have allowed us to represent this accident in 1/2 core symmetry along the diagonal.

The time step sizes are at times limited to round off error. Therefore a selected conversion of some variable to double percision is suggested.

Condition of prompt critical with a $\Delta K = 1.0\%$ will require neutronic time steps of the order of .0001 seconds to preserve the 1.% accuracy of the neutronics. This is very expensive and hence one should think before running MEKIN for prompt critical excursions.

Chapter 8

MEKIN RESULTS OF THE ACCIDENT

In this chapter we present the results of the MEKIN modelling of the "Rod Drop Accident". In reviewing these results it should be noted that insufficient error analysis was done (see Chapter 9) to state an error band for the contents of this chapter.

We show the steady state solution in section 8.1. This is followed by the histogram of the total reactor power. In section 8.3 we will investigate the prompt neutron and gamma heating of the coolant. As will be shown this severely affects the thermal-hydraulic modelling of the MEKIN code. A detailed examination of just this last comment is made in section 8.4.

Having looked at the total reactor response in the first few sections of this chapter, we then observe how the flux is being shaped through the course of the transient by means of axial and radial form factors. These are presented in section 8.5.

Once we have tied the total reactor picture and power form factors together we then investigate channel eighty-one's response. This is the channel from which the control blade has been expelled.

In section 8.7 the timetable for the accident is presented based on MEKIN's results.

A time sensitivity analysis was carried out and the results are presented in the following section. This is followed by the closing section of the chapter which deals with the peak fuel temperatures obtained as a result of the accident.

8.1 Steady State

Before the accident begins, it is assumed that the reactor has attained a steady state power distribution. Since the reactor should not have yet become critical upon the removal of just groups one and two of sequence B (see chapter 5), it is artifically made critical. This is accomplished by multiplying the production cross-section ($\nu\Sigma_f$) by the inverse of the effective multiplication constant. It should be understood that this is not a trick, but something that is usually done to analyze the RDA from the hot standby case. Essentially it allows one to obtain the flux shape that the reactor would maintain for this geometry if it was critical. In our case k was .9745 before the production cross sections were altered to attain criticality. The resulting power distribution is presented in figure 8.1.

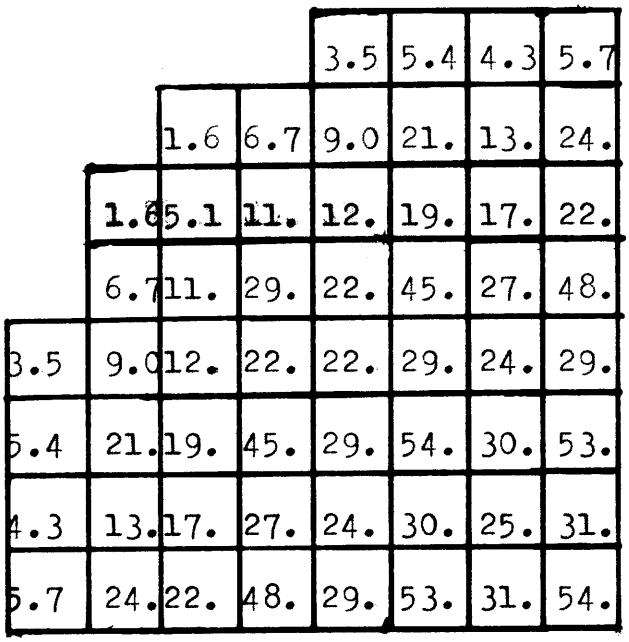

Power In 10^{-7} MW

Start Of Accident
Assembly Power Map

Fig. 8.1

As can be seen, quarter core symmetry exists before the asymmetric rod drop. Note also that the peak power for any node is 54.4×10^{-7} MW_t, and occurs at the center of the core.

8.2 Total Reactor Power vs. Time

These results are presented in table 8.1 and figure 8.2. From these two illustrations one can see that the power rises very slowly for the first second or so. The total reactor power approximately doubles over the first full second of the accident. One can get a good idea of how it behaves after that by examining table 8.2. Here is listed the "e - folding time" over selected regions of accident time. The shortest period is .016778 seconds and occurs at the time between 1.55 and 1.60 seconds into the accident.

Using the simple formula given in Lamarsh[33] for e-folding time or period when a reactor is prompt critical one obtains

$$T = \frac{\ell p}{k-1}$$

where ℓp is the prompt neutron lifetime. Since the delayed neutron factor for our reactor is .00725, let us set $k = 1.00725$ to obtain when $\ell p = 10^{-4}$ seconds.

$$T = .0138 \text{ seconds.}$$

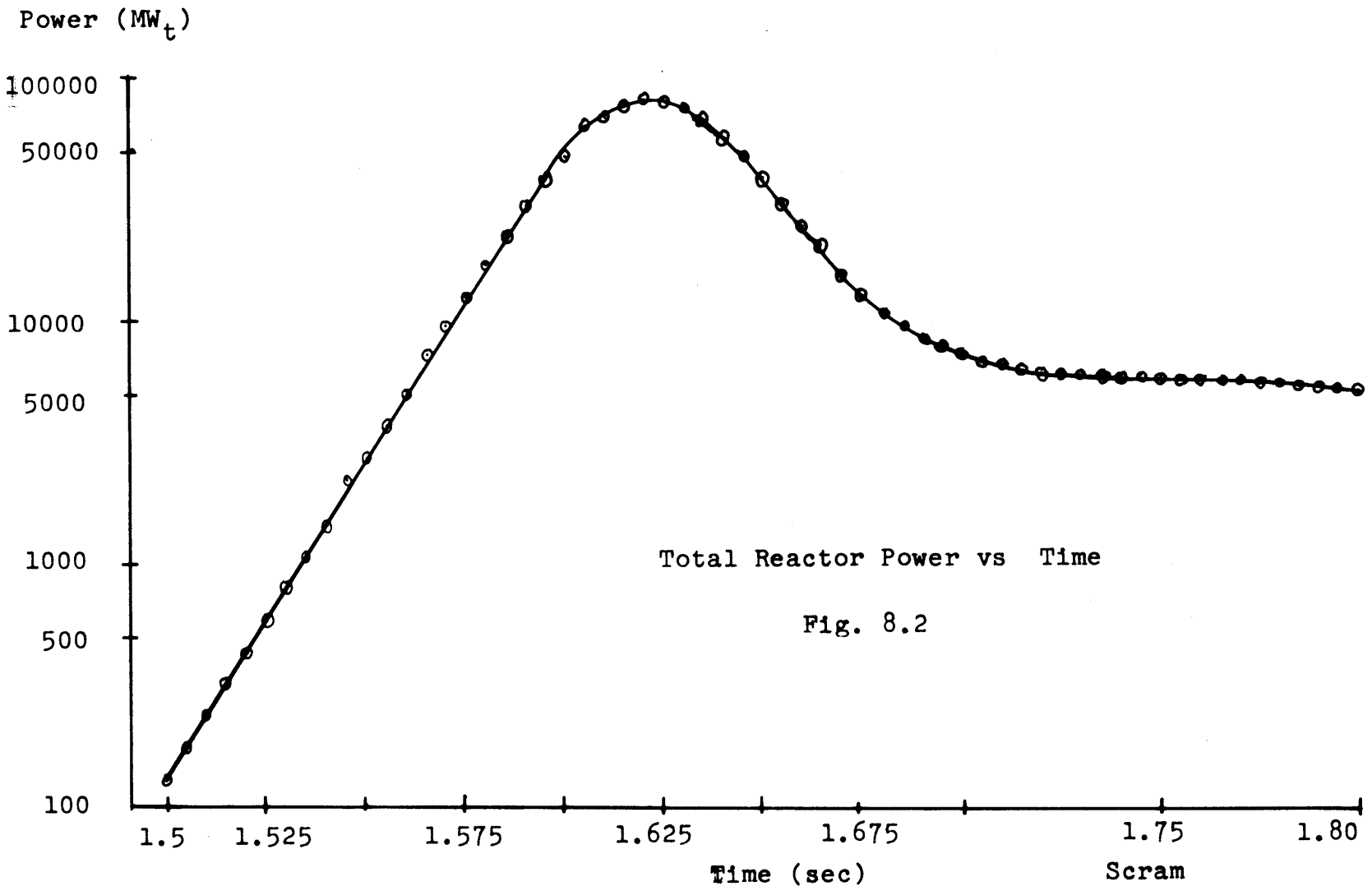

Total Reactor Power vs Time

Fig. 8.2

Table 8.1

Total Reactor Power vs. Time

Time	Power (MW)	Time	Power
0.000	2.493 E-03	1.460	12.78
.100	2.493 E-03	1.465	17.02
.200	2.496 E-03	1.470	22.72
.300	2.506 E-03	1.475	30.35
.400	2.532 E-03	1.480	40.57
.500	2.606 E-03	1.485	54.33
.600	2.672 E-03	1.490	72.85
.700	2.88 E-03	1.495	97.81
.800	3.17 E-03	1.500	131.6
.900	3.605 E-03	1.505	177.2
1.000	5.379 E-03	1.510	239.0
1.100	6.824 E-03	1.515	323.0
1.200	1.578 E-02	1.520	437.1
1.300	8.705 E-02	1.525	592.5
1.400	.8452	1.530	804.6
1.410	1.19	1.535	1094.0
1.420	1.74	1.540	1490.0
1.430	2.66	1.545	2031.0
1.440	4.26	1.550	2771.0
1.450	7.25	1.555	3783.0
1.455	9.61	1.560	5163.0

(continued)

Table 8.1

Total Reactor Power vs. Time
(continued)

Time	Power (MW)	Time	Power
1.565	7039.0	1.640	60,610.0
1.570	9574.0	1.645	50,051.0
1.575	12,968.0	1.650	40,186.0
1.580	17,456.0	1.655	31,328.0
1.585	23,268.0	1.660	25,314.0
1.590	30,600.0	1.665	20,152.0
1.595	39,496.0	1.670	16,288.0
1.600	49,713.0	1.675	13,462.0
1.650	60,584.0	1.680	11,443.0
1.610	70,925.0	1.685	10,020.0
1.615	79,168.0	1.690	8,992.0
1.620	83,758.0	1.695	8,227.0
1.625	83,716.0	1.700	7,662.0
1.630	79,067.0	1.705	7,248.0
1.635	70,808.0	1.710	6,945.0

(continued)

Table 8.1

Total Reactor Power vs. Time
(continued)

Time	Power	Time	Power
1.715	6,724.0		
1.720	6,561.0	1.790	5,708.0
1.725	6,439.0	1.795	5,652.0
1.730	6,347.0	1.800	5,596.0
1.735	6,276.0	1.85	5,118.0
1.740	6,219.0	1.90	4,777.0
1.745	6,172.0	1.95	4,514.0
1.750	6,133.0	2.00	4,140.0
1.755	6,094.0	2.05	3,607.0
1.765	5,998.0	2.10	3,171.0
1.770	5,942.0	2.15	2,965.0
1.775	5,883.0	2.20	2,952.0
1.780	5,825.0	2.25	2,993.0
1.785	5,766.0	2.30	2,923.0

Table 8.2

"e-Folding Time" At Different Points In Time

Time	Period
0.0 - .10	$\approx \infty$
1.3 - 1.4	.044 seconds
1.45 - 1.50	.0173
1.50 - 1.55	.0170
1.55 - 1.60	.016778
1.60 - 1.625	.0480
1.625 →	negative period corresponding to decreasing power.

From the edit of LEOPARD runs made previously it appears the ℓp is actually less than 10^{-4} seconds. Yet, the smallest T which is shown in table 8.2 is greater than .0138 seconds. This would then indicate that over no significant time does the reactor become prompt critical everywhere.

Let us try to interpret these results physically. In the area of the rod drop one is reasonably assured that the reactor is prompt critical. Disregarding temperature feedback, the nuclear parameters of the surrounding region have not changed. However, one has essentially introduced a large source in the rod drop area. This source now drives our transient. Production becomes greater than loss for the region near the rod drop, and hence for the reactor on a whole. When production exceeds loses to the extent that the region is critical on prompt neutrons alone, the region is now prompt critical. This is believed to happen. Yet the neutron balance equation for regions far removed from the rod drop area have yet to receive sufficient external source neutrons to attain prompt criticality. What happends then is that there is a finite delay time from when the subassemblies controlled by the rod which has dropped makes their effect on adjacent subassemblies as a form of an external source. One can then envision a prompt critical region growing radially outward from

the rod drop in time. Before this region encompasses the entire reactor, feedback effects take over. To be remembered, however, is that precursor concentrations have been increasing all during this time representative of the increasing power.

Neither of the above two effects could be observed in a point reactor kinetics formulation which neglects delayed neutrons as Canosa's formulation presented in chapter 6. By his formulation, one would truly expect a symmetric power brust. Even if one included delayed neutrons in one's formulation,the time delay effect of the expanding prompt critical region and its subsequent Doppler feedback expanding region (if one now included feedback) would not be observed in point kinetics. Hence the importance of a correct weighting function for Doppler feedback in a point kinetics formulation.

From a multidimensional analysis, such as that modelled by MEKIN, all these results can be seen. The asymmetric power burst is particularly interesting. It is most probably due to a combination of the above two mentioned conditions.

The total energy release during the transient is also of interest. The accident was carried out in time until the power was below 120% of rated. By that time the peak clad temperature had already been reached. Approximate

total energy release over this time span is about 10,000 MW-seconds with about 4650 MW-seconds being released during the rise in power.

8.3 Newtron and Gamma Heating of Water

The percentage of energy released directly into the pin lattice coolant due to neutron slowing down and prompt gamma decay is approximately 2.51%. This is if there is no void fraction. If one just considered the power rise energy deposition into the hotter channels due to this direct heating one can get some idea of the void fraction generated. From the previous section one has 4650 MW-second generated in the entire core during the power rise to peak. There are 193 channels but the hotter channels have more than eight times the average power production over much of the important power rise. Hence for the hotter channels during the energy rise one has

$$8 \cdot 948 \frac{\text{BTU}}{\text{MWS}} \cdot 4650 \text{ MWS} \cdot .0251 \cdot \frac{1}{193 \text{ channels}} = 4586 \text{ BTU}$$

That is 4586 BTU's delivered to the approximately 4.167 cubic feet of water in a channel or 192 lbs of water. At 1025 psia saturated water one needs 645 BTU/lb as energy of vaporization. This results in a .037 average void fraction in one of our hotter channels. Nearly all of this energy is released in a period of .073 seconds.

The difference in specific volume of saturated liquid and vapor at this state is v_{fg} = .42431 ft^3 / lb. So the change in volume of the water in the channel is

$$.42431 \frac{ft^3}{lb} \cdot .037 \cdot 192 \text{ lbs} = 3.0168 \text{ } ft^3.$$

The resulting velocity change in the channel water is then

$$\Delta \text{ velocity} = \frac{3.0168 \text{ } ft^3}{.347 \text{ } ft^2 \text{ } (.073 \text{ sec})} = 119. \text{ ft / sec.}$$

Since one had no flow conditions at the start of the transient, and because the resulting volumetric expansion will result in flows both up and down the channel; one gets flows of about 60 ft/sec in both directions.

8.4 Breakdown of the MEKIN Thermal-Hydraulic Model

From the previous section it appears that a water hammer or steam hammer has been created. A pressure wave travels at a sonic velocity of about 4800 ft/sec. if rigid wall conditions are assumed. With a change in velocity across the wave of 60 ft/sec one can calculate the pressure difference across the wave to be using[34]

$$\frac{\Delta \text{Pressure}}{\Delta \text{Velocity}} = \text{density} \times \text{sonic velocity} \qquad (1)$$

Eq. (1), 2875 psi. This is what the Δ pressure in the channel would be if all the volumetric change in the channel due to expansion was not released as it was created during the power rise.

Indeed, this whole question of just how quickly the pressure in the channel is relieved by expansion throughout the total coolant loop is an important and difficult question. Oscillations are most likely set up in some of the channels because the pressure wave generated will be partially reflected by the upper and lower plenums.

Presently MEKIN cannot handle steam hammers or reversed flow. Neither is it coupled to the total coolant loop. Instead it forces all the flow out in one direction. Further, it gives the pressure drop across the core based on the instantaneous velocity generated by volumetric expansion. Since it doesn't increase the total pressure of our water due to the volumetric expansion between two semi-rigid plenums, one obtains the mistaken edit that the total water pressure is negative at core exit.

It is clear that the coolant model has broken down, but how does this affect the fuel temperature. This is the

parameter of prime interest. The answer lies in two areas. The first deals with the convective heat transfer coefficient, and the second with the direct neutron and gamma heating of the water.

The convective heat transfer coefficient is a function of heat flux and the water pressure. It is determined by the Jens-Lottes equation. So

$$h_c \alpha \sqrt{q'' e^{P/1260}}$$

where

h_c = convective heat transfer coefficient

q'' = heat flux

P = pressure

First off, MEKIN doesn't use the correct heat flux in determining h_c. The heat flux is a function of h_c and h_c is a function of q''. An iterative scheme therefore comes to mind. MEKIN, however, uses the heat flux of the axial node below it to determine h_c for the new node as it marches axially up the channel in its solution scheme. This results in edits where the heat flux is greater for one node though the fuel temperature and linear heat generation rate are greater for the node immediately below it.

As also can be seen the pressure is an important term in the heat transfer coefficient. MEKIN always underestimates this as can be discerned from the method it uses to calculate the pressure as outlined previously in this section. At the time the accident was 1.6 seconds old the flows were artificially set equal to near zero so that the pressure didn't deviate from 1025 psia in the rod drop channel by more than 100 psi, for the hottest axial node positions.

For these reasons it is likely that for our hottest nodes our heat transfer coefficient is underpredicted for nucleate boiling. However, it is possible that some film boiling occurs. This is based on the following.

The peak heat flux is 1.4810 million BTU/hr ft^2. Using Redfield's correlation for critical heat flux during a transient[35] one obtains

$$q''_{crit} = 1.66 \text{ MBTU/hr } ft^2$$

This doesn't include the effect of oscillations due to the steam hammer in our flow which might drop the q''_{crit} below our peak heat flux. However, even if this happend the oscillating flow would continually cool the spot which may exceed q''_{crit} provided wetability is maintained.

Based on this above discussion it is difficult to say if the heat transfer coefficient was kept below actual conditions everywhere and for all times throughout the accident. If it was, our fuel temperature results will be conservative.

Concerning the neutron and gamma heating of the coolant. It should and appears to be a function of the void fraction. The void fraction in turn is a function of both the convective heat transfer coefficient as well as the flow rates, both of which have been shown not to be correctly modelled by MEKIN for such a severe accident.

The fact that the pressure of the coolant is also not correct results in wrong void fractions for a given coolant enthalpy rise.

8.5 The Power Form Factors

There are three basic form factors which will be investigated in this section. They point out in an explicit way the coupling between the space and time coordinates.

The maximum radial form factor (MRFF) tells one the axial level at which the flux has its largest amplitude in a radial direction. It then gives one the normalized size of this amplitude. The maximum axial form factor (MAFF) gives one the channel in which the maximum axial amplitude

can be found and also its value. Finally, the maximum channel factor (MCF) gives one the position of the hottest channel and how much greater in power it is than an average channel power rating at that time.

Since the rod drops from the upper core, the MRFF is always located at axial position 10 or the top axial plane.

The MAFF also tends to become,almost immediately after the start of transient (t = .450),uniquely located in channel 81. Up to t = .450 seconds there appears to be no single channel in which MAFF is supreme.

MCF is a different story. This factor is initially located in the center channel of the core, channel 97. It then moves to channel 65 on the opposite side of channel 81. Finally it settles down in the channel which has its control rod being expelled, channel 81.

Table 8.3 and Figure 8.3 show the results. The MRFF is the smoothest curve as it should be. Once the control blade has dropped through the first axial node (t = .24 sec) the nuclear properties of this plane remain constant until Doppler feedback occurs.

The MAFF clearly shows how the control rod motion affects it. Rising steeply after t = .4 seconds, until channel 81's control rod out region has become enlarged. This has the affect of spreading out the axial peaking and MAFF turns around. At t = .9 the MAFF has peaked. This

Fig. 8.3

Form Factors
vs Time

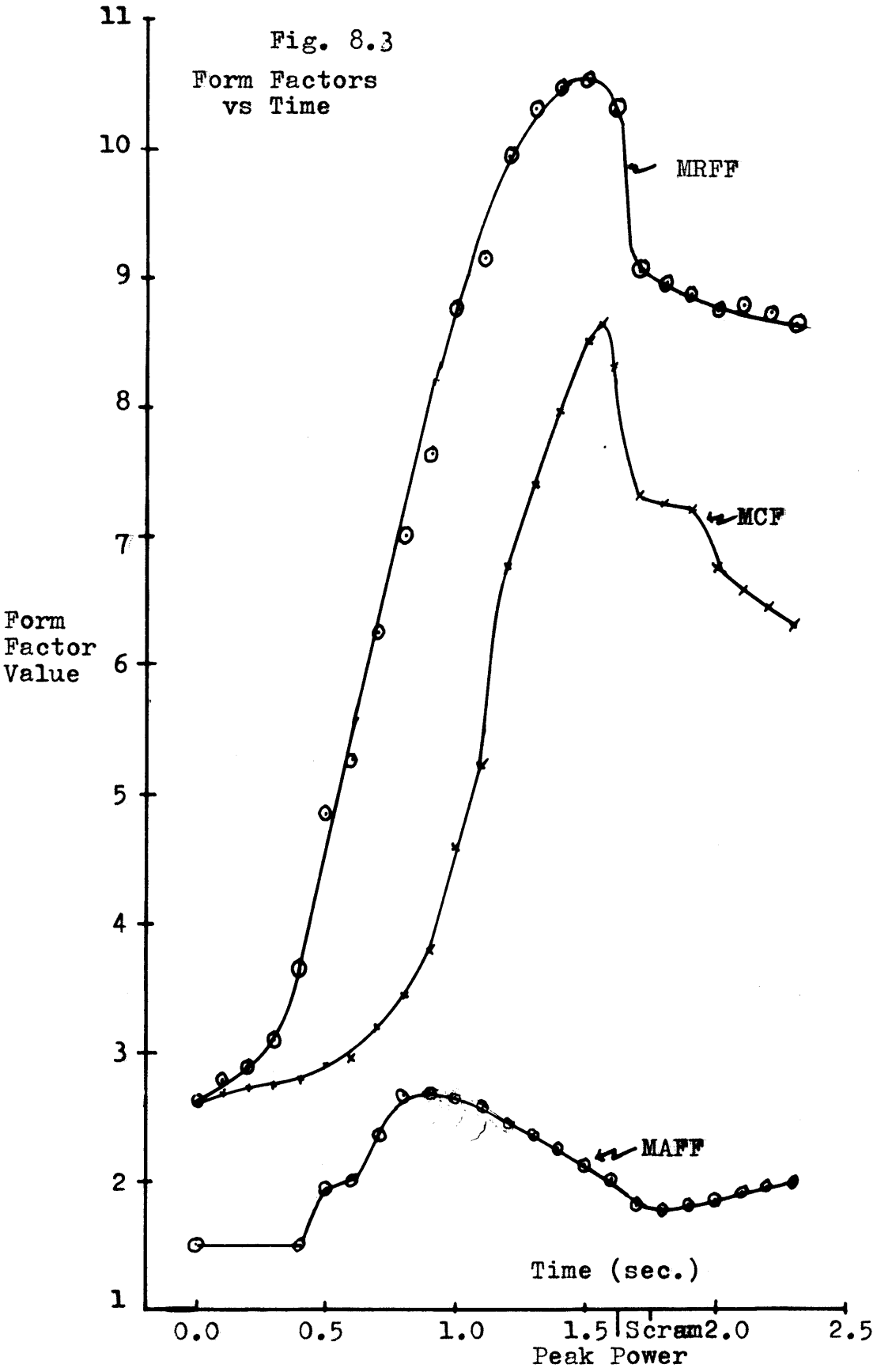

Table 8.3

Power Form Factors vs. Time

Time	MRFF	MAFF	MCF	Maximum Channel
0.0	2.600	1.515	2.5995	97
.1	2.790	1.515	2.7403	97
.2	2.891	1.515	2.7461	97
.3	3.106	1.515	2.7469	97
.4	3.662	1.515	2.7977	97
.5	4.851	1.957	2.8870	97
.6	5.256	2.036	2.9651	97
.7	6.261	2.358	3.2013	65
.8	7.008	2.662	3.4663	65
→ .9	7.624	→2.669	3.7984	65
1.00	8.787	2.660	4.6096	81
1.10	9.152	2.556	5.1942	81
1.20	9.964	2.436	6.7869	81
1.30	10.327	2.389	7.4117	81
1.40	10.470	2.262	7.9902	81
1.50	10.560	2.126	8.5365	81
→1.520	→10.561	2.113	8.5658	81
→1.560	10.543	2.079	→8.6166	81
1.60	10.290	2.013	8.32926	81
1.620	9.852	1.950	7.9053	81

(continued following page)

Table 8.3

Power Form Factors vs. Time
(continued)

Time	MRFF	MAFF	MCF	Maximum Channel
1.7	9.044	1.808	7.3335	81
→1.75	8.994	→1.787	7.3278	81
1.8	8.947	1.794	7.2689	81
1.9	8.896	1.806	7.2016	81
2.0	8.797	1.854	6.7789	81
2.1	8.802	1.913	6.6023	81
2.2	8.723	1.961	6.4661	81
2.3	8.656	1.992	6.3285	81

is also about one-half the time the dropping control rod spends falling.

It is the MCF which is of major concern. When it is rising it indicates that channel 81's power is increasing faster than that of the average core channel. It thus has a smaller e-folding time. From its plot and that of total core power one can observe a delay time in the expanding prompt critical region, as well as the Doppler feedback radius. As expected the peak in MCF occurs before that of the total core power. This indicates that channel 81 ceased to be the fastest growing in power before the transient turned around. MCF peaks at 1.560 seconds while the core power peaked at 1.623 seconds. A 63 millisecond delay time is therefore noted.

Also to be noted is the steep drop in MCF between 1.560 and approximately 1.7 as the Doppler feedback effects channel 81 before the other channels because its power and hence its temperature rose more quickly. This steep fall and leveling can also be observed in the power histogram, again with some delay time.

One has scram at 1.75 seconds. This scram effects the MCF curve more than the power curve because the worth of the channel 81 control rod is more than that of the other scraming rods for their initial motion. This is because channel 81's rod is scraming from axial node 3 while the

others are scraming from totally withdrawn positions. So one doesn't observe the same magnitude of increased decline seen in the MCF at about 1.9 seconds represented as strongly in the power plot. Instead an apparent slow decline is seen indicating that the large Doppler feedback effect, due to the major (in 10,000 to 100,000 MW power level) burst, has already caught up in almost all regions of the core, and the effect of the scram on the core worth level is slow and small.

The large precursor concentrations help prevent both the MCF and power from dropping too fast after this point. In this regard it can again be shown that the scram in channel 81 has a larger effect on the MCF than core scram has on power. There is, of course, a larger precursor concentration in channel 81 than the other channels, but the accident has reached a high enough power to guarantee a substantial delayed neutron source in other parts of the core. So the delayed neutrons emitted from channel 81 don't play as large a role as the major source term in driving the transient now, as did the prompt neutrons emitted from this initial prompt critical region during the early core power rise.

8.6 Channel Eighty-one

In this section the channel from which the rod drop occurs will be looked at more closely. In particular one will look at the shape of the power histogram for the channel as a whole and for two axial positions in the channel. The all important fuel and clad temperatures for this hottest of channels will also be examined. Finally, some investigation of the "f" and RC parameters will be made.

8.6.1 Power Histogram

Figure 8.4 shows the power history of channel 81 in arbitrary power units. Figure 8.5 shows the power history of two different axial nodes of this same channel. These nodes are at level 4 and level 7. Level 4 is the node into which the scram control blade is forced from 1.75 to 2.3 seconds into the transient. As can be seen its power plot reflects this by a greater degradation of power then level 7 over this time period.

Level 7 tended to be the hottest node in the channel during the transient. Thus its Doppler feedback effects should lead those of the level 4 node. This is explicitly shown by the fact that the power in level 7 peaks before that of level 4.

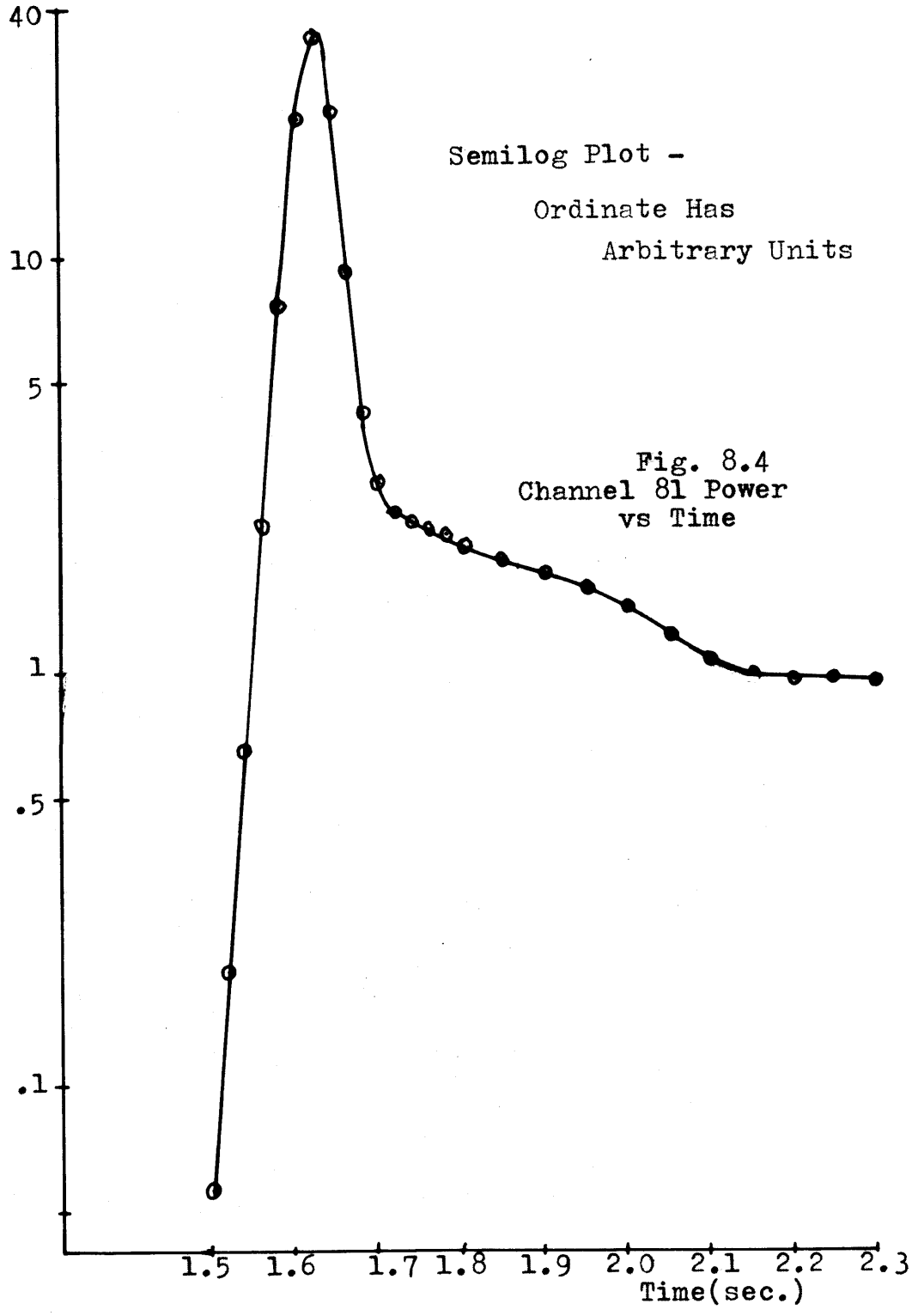

Fig. 8.4
Channel 81 Power
vs Time

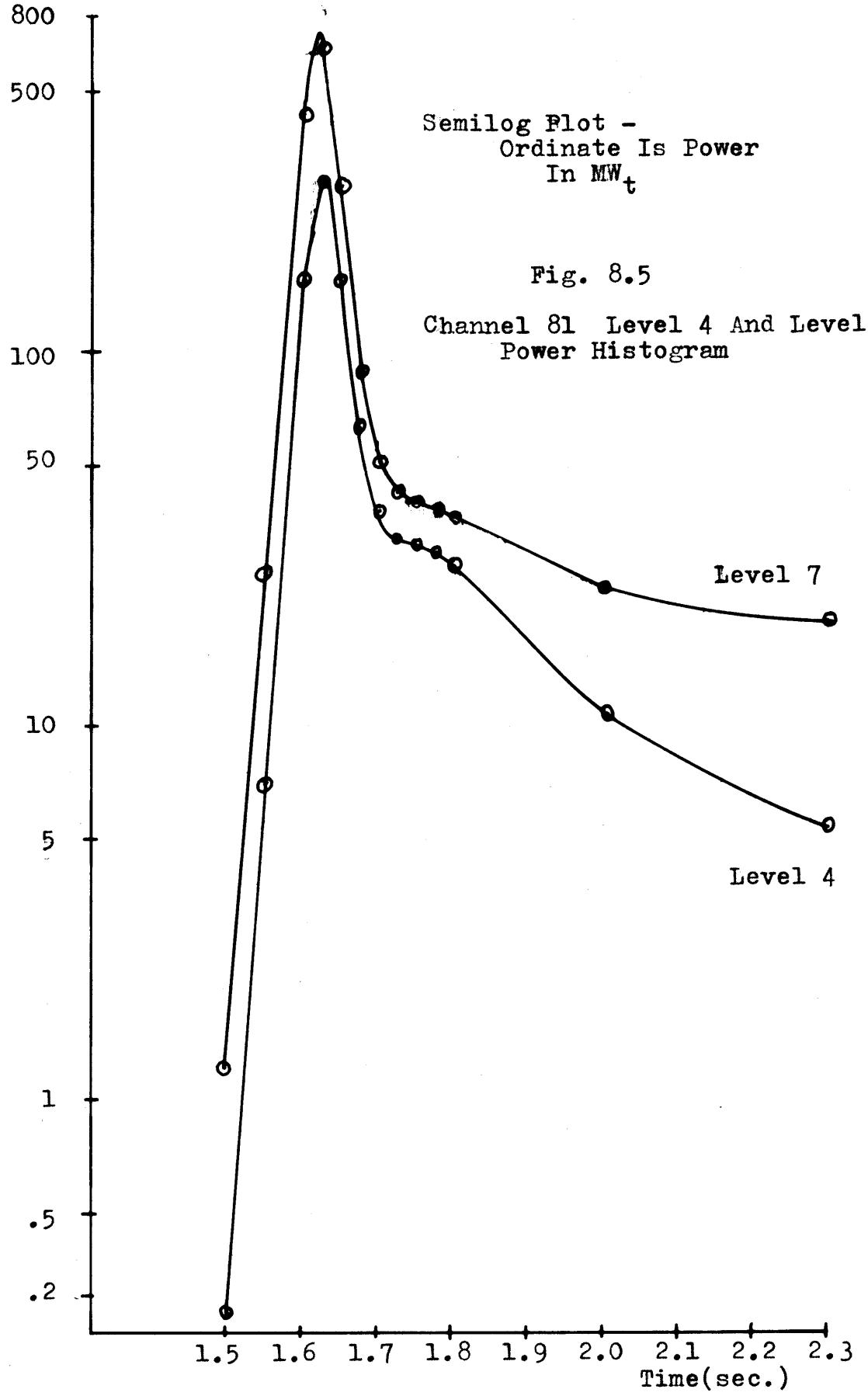

Semilog Plot -
Ordinate Is Power
In MW_t

Fig. 8.5

Channel 81 Level 4 And Level 7
Power Histogram

As expected, the power plot for the total channel 81 has a shape inbetween those exhibited by level 4 and level 7.

8.6.2 Temperature and its Distribution vs. Time.

Two points of importance are made in this section. The first is a table of how the peak temperature rises in channel 81 with time. The second deals with the radial temperature distribution within the fuel pellet and the clad temperature, and how these change with time.

Up to 1.450 there is no discernable increase in fuel temperature above the initial 547°F. The core power reaches the megawatt range after 1.40 seconds. Table 8.4 outlines the rise in the peak fuel temperature in the hottest channel, channel 81. The core power is also shown as a reference. As can be seen the temperature follows the core power fairly closely, especially for time up to 1.625 seconds. Up to that time there is almost no radial temperature gradient in the pellet. This is as was predicted in Chapter 6. However after that time of power rise the temperature throughout the pellet will take on a gradient. This is shown in Table 8.5. Note time intervals are <u>not</u> equal.

Table 8.4

Core Peak Full Temperature vs. Time

Time (sec)	Temperature Peak (°F)	Core Power (MW)
0.0	547	2.493 E-03
1.40	547	.8452
1.45	547.1	7.24
1.475	547.3	30.34
1.500	548.4	132
1.550	558.0	2771
1.575	680.5	12968
1.600	1102	49713
1.625	2015	83716
1.650	2670	40186
1.675	2889	13462
1.700	2978	7662
1.725	3045	6439
1.750	3106	6133
1.775	3165	5883
1.800	3221	5596
2.05	3660	3607
2.30	3946	2924

Table 8.5

Radial Temperature Gradient Vs. Time

Time	T_{avg}	$\hat{T}$	$T_{p.s.}$	T_{clad}
1.625	2002	2016	1979	578.2
1.650	2637	2646	2565	590.6
1.670	2834	2886	2749	585.5
1.700	2905	2978	2786	586.3
1.725	2951	3045	2798	586.6
1.750	2991	3106	2804	586.6
1.775	3029	3165	2808	586.6
1.800	3063	3221	2809	586.7
2.05	3290	3655	2725	585.7
2.30	3391	3946	2561	584.3

Here

T_{avg} = pellet average temperature

$\hat{T}$ = peak temperature of pellet

T_{ps} = temperature at pellet surface

T_{clad} = temperature at clad surface

From table 8.5 one can see that the temperature distribution is starting to take on more of a steady state form as time progresses. In the next section one will see that this is related to the heat flux and RC parameters.

Although the pellet centerline temperature is increasing over the total time span shown, it does it less rapidly as time progresses. Further, both T_{ps} and T_{clad} turn around at 1.8 seconds, and the average pellet temperature increase with time is less than that of the centerline temperature increase with time. This is, of course, as it must be.

8.6.3 The RC and "f" Factors for Level 7 of Channel 81

Let one consider a particular node in our core. The chosen node is axial node 7 of channel 81. Since from table 8.4 at time = 1.45 one obtains the first discernable increase in fuel temperature, for the purpose of determining the RC and f factors this will be our initiating time. Over the time span of 1.45 to 1.60 one can determine from figure 8.5 that the e-folding period is .01665 seconds. Also at 1.60 seconds the heat flux for our node is .1550 MBTU/hr ft^2 and the power produced is 435.24 MW. For our node .1550 MBTU/hr ft^2 = 1.5735 MW.

The formula for the "f" factor given in Chapter 6 didn't include the time dependence, which decays away quickly.

However, for completness it is

$$f = \frac{1}{aRC + 1} \left(1 - e^{-(\frac{1}{RC} + a)t} \right)$$

Using the present core average value of 2.38% for the power produced appearing as neutron and gamma heating of the coolant one gets

$$f = \frac{1.5735}{(.9762)\ (435.24)} = .0037033$$

Now "a" in the previous equation is the reciprocal of the e-folding time, and so ≈ 60. This yields that RC = 4.48 seconds. This is not to say the RC constant is always this low, indeed at 1.575 it is as large as 20 seconds. However, at 1.575 the convective heat transfer coefficient is about 5 times smaller and so the resistance should be greater. Yet, it is the value of RC near the time of peak power that is important.

This value of 4.48 seconds at accident time 1.60 seconds is not exact. Still, if one recalls the inaccuracies in determining the convective heat transfer coefficient as outlined in section 8.4 it would appear to be an upper value. This is because both the heat flux and pressure are most likely underestimated by MEKIN in obtaining the convective heat transfer coefficient. Also, since not a

very large void fraction exists at this time, the value of 2.38% of power going directly into neutron heating should be close to actual. Remember that the Jens-Lottes equation is independent of flow rate.

Finally in this section, one would like to show that more and more of the power produced goes into heat flux as one would expect if our RC circuit analogy is to hold. Table 8.6 does demonstrate this. Again level 7 of channel 81 is used.

Table 8.6

Heat Flux vs. Power for the Hottest Core Node

Time	Power Heat Flux (MW)	Total Nodal Power (MW)	Percent Ratio
1.625	8.5417	649.82	1.315
1.650	13.1343	279.81	4.694
1.675	14.4581	89.8	16.10
1.700	14.8236	50.59	29.30
1.725	14.9546	42.2	35.44
1.750	15.0084	39.9	37.62
1.775	15.0348	38.3	39.26
1.800	14.9607	36.4	41.10
2.05	14.4876	23.64	61.29
2.30	13.3902	19.10	70.11

The percent ratio is the ratio of the power appearing as heat flux divided by the total nodal power in percent form.

8.7 The Accident Time Table

It should be obvious by now that the time table set up in Chapter 6 using Canosa's formulation was wide of the mark. The assumptions of 1% ΔK rod drop and a power at prompt critical of 2.5 KW were major flaws. When the worth of the dropping control rod is set to 1.2% ΔK and the power at prompt critical set equal to 7.25 MW Canosa's formulation predictions improve.

One arrives at a rod worth of about 1.2% from the following consideration. From table 4.2 of Chapter 4 the generated cross sections showed a rod worth of 1.19 times that of the Commonwealth supplied data for a single assembly. Since the rod worth of the dropped rod was predicted to be 1% ΔK with the supplied data, a linear correlation would then predict about a 1.2% ΔK core worth for this same rod when the generated cross sections were used.

The choice of 7.25 MW is based on the MEKIN results that show the "e-folding time" to have basically taken on that of a minimum at the time of this power level (see table 8.2).

With these two changes Canosa's formulation then gives a maximum total reactivity of .0097. If a linear ramp is assumed, this would occur at 1.94 seconds into the transient. To this one must add the F term. This turns out to be .123 seconds. So the corrected formulation

shows a peak power occuring at 2.063 seconds. This is off by almost one-half a second from MEKIN's results. It appears that the point reactor formulation of Canosa and the MEKIN results are far apart where a time table is concerned. However, Canosa's formulation now predicts a peak power of 147,704 MW. This is within an order of magnitude of MEKIN's results.

Finally, the predicted increase in temperature is 541 °F. From this and MEKIN's results, it is clear that this temperature increment would have to be weighed by some scheme to give reasonable results.

8.8 Time Sensitivity Analysis

As was pointed out in section 7.1.6 the time step size is important in maintaining accuracy. From accident time 1.45 to about 1.7 seconds the power is changing so rapidly that a tenth of a millisecond time step is really required to allow for no more than a 1% change in power per neutronic time step. Due to computer time limitation a half of a millisecond time step was employed. However, to check the accuracy of this the power rise was checked against that using the recommended time step size over a short time interval. The interval chosen was 1.45 to 1.50 seconds. This is when the e-folding time changed from the previous time and levels off. This is exactly where one can

check the inertia effect of the method of computation.

The results were satisfying, they showed a lag of less than 1% in the power at 1.5 seconds when the half millisecond time step was used.

Table 8.7

Time Sensitivity

Time	Power When Δt = .0001	Power When Δt = .0005
1.45	7.25	7.25
1.455	9.67	9.61
1.460	12.88	12.78
1.465	17.18	17.02
1.470	22.94	22.72
1.475	30.65	30.34
1.480	41.02	40.57
1.485	54.96	54.33
1.490	73.73	72.85
1.495	99.07	97.81
1.500	131.31	131.6

A list of the time step sizes used throughout the computation is presented in Table 8.8. All units are in seconds.

Table 8.8

Time Step Sizes

Accident Time	Neutronic Time Step Size	T - H Time Step Size
0.0 - .1	.001	.02
.1 - .7	.001	.025
.7 - 1.4	.001	.02
1.4 - 1.45	.001	.01
1.45 - 1.8	.0005	.005
1.8 - 2.3	.005	.05

8.9 Peak Fuel Temperature Attained

As was mentioned at the outset and again in Chapter 5, one hopes to determine the severity of this accident based on the peak fuel temperatures attained by the pins.

The accident is symmetric about the diagonal which passes through channel 81. One need therefore report on those pins which lie close to channel 81 and on one side of this diagonal. The results are presented in Table 8.9. Three times will be listed. At 1.625 one has a time edit nearest the peak core power. T_{avg} and $\hat{T}$ are the average and peak temperatures for each of the channels at a certain

Table 8.9

Peak Fuel Temperatures for Various Channels

Time→ Channel	1.625		1.800		2.300	
	T_{avg}	$\hat{T}$	T_{avg}	$\hat{T}$	T_{avg}	$\hat{T}$
65	1571	1581	2346	2457	2596	2992
79	886	889	1154	1191	1247	1379
80	1299	1306	1860	1941	2042	2330
81	2002	2016	3061	3217	3391	3945
95	1524	1533	2265	2371	2506	2884
96	1281	1288	1829	1908	2007	2288
97	1502	1511	2228	2331	2465	2835
111	861	864	1111	1145	1198	1321

axial level. The axial level chosen is that which tended to be the one where the hottest fuel temperatures were found. For the 1.625 edit is is level 7, that is the seventh node up from the bottom inlet plenum, for 1.8 and 2.3 it is level 6. Time 1.8 was also chosen to be represented in Table 8.9 because it represents the MEKIN predicted time of peak clad and fuel pellet surface temperature as shown in Table 8.5. The 2.3 second edit represents the time at which the core power has fallen below 120% of rated, and is the farthest the MEKIN calculation was taken.

Section 5.1 lists the criteria for pin facture. Note that 170 cal/gm is equal to a temperature of 3846 °F, and 220 cal/gm is equal to 4532 °F.

In Table 8.9 the temperatures are given in degrees Fahrenheit. Each MEKIN pin represents 196 physical fuel pins. Its properties are the average of these pins. The temperature distribution among the physical pins can be backed out of this single average pin by knowing the power distribution among the pins, as given in Chapter 3. From Commonwealth supplied data the peak to average pin power is as high as 1.23 for the control rod out, curtains in assembly; and 1.62 for control rod and curtains in assembly. Thus to get the temperature of any individual pin one would multiply the temperature increase for the

MEKIN average pin by the correct normalized power factor, and then added 547 °F to it.

The hottest pin temperature in Table 8.9 occurs at 2.3 seconds in channel 81. With a 1.23 power factor the temperature is 4727°F. This is above 220 cal/gm value. So it is possible that some of the fuel will melt, however, it is far below the 425 cal/gm enthalpy required for prompt failure of the pin. Yet, it is above the 3846 °F temperature required for clad performation. If one uses the 2.3 second time edit, there will therefore be 128 pins which will exceed the clad perforation threshold. They are all contained in channel 81. At 1.8 or 1.625 seconds no pins reach this threshold.

The question is this, which edit should be used to determine failure? If the MEKIN calculation was carried out still farther, the centerline temperature of the pins would increase slightly farther before turning around. Should those temperatures then have been used to determine failure? The failure criteria was based on tests done on small fuel capsules like the Treat Reactor tests, or other small mock ups in an experimental reactor.

It might be that for these tests peak clad and fuel temperature occur at the same time. Then, maybe one should use the 1.800 second edit which shows no pin failure. It might not be appropriate to use the 2.3 second edit since

by this time a steady state radial fuel temperature gradient is being set up, as mentioned in section 8.6.2.

One would think clad failure was a direct function of clad temperature since this helps determine the hydrid pick up. The experimental tests which resulted in the 170 cal/gm value tied failure to fuel temperature only. The fuel specimen might have exhibited film boiling which drove the clad temperature up beyond failure threshold, and this occured if the fuel temperature exceeded 3846 °F. To really know which accident time edit is appropriate one would really have to check the tests used to determine the 170 cal/gm threshold.

If it is the peak fuel temperature at the time of peak clad temperature or at the time of peak heat flux (see Table 8.6) that is the failure criteria, then it appears that the 1.8 second edit should be used. In which case one should recall the discussion in section 8.4 before accepting the results. The mode of failure for clad perforation should also be examined.

Chapter 9
CONCLUSIONS

More than anything else this work should indicate that the results are interesting enough to warrant further detailed investigation. In particular the thermal-hydraulic model used should be made more appropriate to the circumstances that were encountered, and a quantitative error analysis should be carried out. This work really stacks up to be a preliminary investigation. Its major benefits lie in giving one an idea of what may be physically happening and what modelling must be made to handle their phenomena.

These results indicate that a steam hammer capable of being driven solely on neutron and gamma heating occurs. Further the heat fluxes attained are in the area of critical heat flux. The RC constant appears to range from very high values, greater than 20 seconds, at the start of the nucleate boling when the convective heat transfer coefficient is low; to values as low as 4.5 seconds which occurs close to the peak power during the power rise. Closely related to the RC constant is the amount of heat appearing in the water as a result of heat flux from the pins. Although less than one percent of the instantaneous power appears as heat flux during the power rise, this value grows substantially during the fall in core power. If the power tails off as it is shown to do in the results, this can result in a very

sizable contribution to the heating of the water by this mechanism. Significant void fractions occur. Canosa's point kinetics formulation also appears to give results in large disagreement with the attained multidimensional results.

The above shows that not only should the thermal-hydraulic modelling be improved, but density feedback effects, capable of being employed by MEKIN, should be. A high order Doppler feedback correlation should also be included in MEKIN.

Any error analysis should include the sensitivity of the transient results to variations in the two group parameters. This includes both the steady state parameters used to determine the initial core flux shape and the transient correlation data used to account for control rod motion and feedback effects.

Although a time sensitivity was carried out, there remains a space or nodal representation sensitivity which is required. The suggestions and problems mentioned in section 7.3 on improvement of MEKIN should be looked into in this regard.

The criteria of failure is very important. An in depth study at just how to interpret the Treat, Spert and other tests to arrive at a failure criteria is essential. In particular one should note if those experimental tests resulted in a large asymmetric power burst as was observed

in the MEKIN results. Published comparisons with previously accepted means of evaluating this accident should be made after an error band for the results is known.

As was mentioned in section 7.3 further work should go into improving the speed of computation. On an IBM 370/168 computer for a problem of this size (193 thermal-hydraulic channels, and about 8,000 neutronic mesh points) 10 CPU seconds were needed for each neutronic time step. This does not include the time needed for input-output management to disk which varies on the data shuffle routine. This in turn depends on the available computer core. For unknown reasons MEKIN ran into trouble occasionally when virtual storage was employed.

Concerning the poor subassembly criticalities obtained for the control rod out-curtain in case when homogenization Model III was used. In an effort to get a better pin power distribution match, the criticality of the subassembly was raised too high. One should have realized that a good pin power matching is not attainable with the codes employed; and that artificial techniques, like the addition of boron to the water, are sometimes used if good pin power distribution and criticality is desired.

Finally, just how much of the power histogram shape is due to the multidimensional modelling needs to be further investigated. The delay time for neutronic communi-

cation between different regions of the core, as discussed throughout the previous chapter can only be observed in a multidimensional analysis. That the power shape is correct can be verified by examination of some of the Spert tests[36]. Just what part the delay time effects play on the power shape, at what power the declining power levels off, and how they will affect the results between a point formulization and the present modelling should be further investigated.

REFERENCES

1/ Paone, Stern and Woolley, "Rod Drop Accident Analysis For Large Boiling Water Reactors", NEDO-10527, 72NED18, Class 1, March 1972

2/ Bowring, Stewart, Shober and Sims, "MEKIN: MIT-EPRI Nuclear Reactor Core Kinetics Code", Sept. 1975

3/ Commonwealth Edison Co., "Dresden Nuclear Power Station Units 2 & 3 Safety Analysis Report"

4/ Barry, "LEOPARD-A Spectrum Dependent Non-Spatial Depletion Code For the IBM-7094", WCAP-3269-26, Westinghouse Electric Co. (1963)

5/ Glasstone and Sesonske, "Nuclear Reactor Engineering", Van Nostrand Reinhold Ltd., New York, 1967, p209

6/ Duffy and Fisher, "Effectiveness of Linear Arrays of Absorber Tubes as Control-Rod Blades", Trans. Am. Nuclear Soc., 8(2) p. 450-451, Nov., 1965

7/ Baker and Tavebaugh, "Chemical Engineering Division Report, Jan.-June 1964, Section V- Reactor Safety," ANL-6900

8/ Cadwell, A.F.Henry, and Vigilotti, "WIGLE-A Program For the Solution of the Two-Group, Space-Time Diffusion Equations in Slab Geometry", WAPD-TM-416, Bettis Atomic Power Lab. (1964)

9/ Tong and Weisman, "Thermal Analysis Of Pressurized Water Reactors", American Nuclear Society, 1970, p129

10/ Van Binnebeek, "Resonance Integral and Doppler Coefficients in Nonuniform Cylindrical Reactor Fuel Rods", Nucl. Sci. Eng. 36, 47-58 (1969)

11/ Dresner, "Some Remarks on the Effect of a Nonuniform Temperature Distribution on the Temperature Dependance of Resonance Absorption", Nucl. Sci. and Eng. 1, 39-42 (1961)

12/ A.F. Henry, "Nuclear-Reactor Analysis", MIT Press, Cambridge Mass., 1975

13/ A.F. Henry, "A Theoretical Method For Determining the Worth of Control Rods", WAPD-218, Bettis Atomic Power Lab. (1959)

14/ Same as Ref.6

15/ Michelini, "Neutron Transmission Probabilities Across Control Blades Filled with Round Tubes: Formulation and And Accuracy", Nucl. Sci. Eng. 42, 162-170 (1970)

16/ Bell and Glasstone, "Nuclear Reactor Theory", Van Nostrand Reinhold Co., New York (1970) p. 163

17/ "CITATION",ORNL-TM-2496 Rev.2

18/ Harris, "Recommended Method for Performing NULAS Neutron Spectrum Calculations for the BWR Fuel Assembly", Northeast Utilities, (1971)

19/ Same as Ref. 16

20/ Farrar, "A Comparison of Simple Calculated Methods for BWR Fuel Assembly Analysis", MITNE Thesis (1971)

21/ Breen, "A One-Group Model for Thermal Activation Calculations", Nucl. Sci. Eng., 9, 91-93 (1961)

22/ Same as Ref. 1

23/ Risher, " The Control Rod Ejection Transient in a PWR", Westinghouse Nuclear Energy Systems; see also WCAP-7588

24/ Barry and Risher, "TWINKLE-A Multi-dimensional Neutron Kinetics Computer Code", Westinghouse Electric Corp., WCAP-8028 (1972)

25/ Hetrick, "Dynamics of Nuclear Reactors", University of Chicago Press (1971), Section 5.8

26/ Canosa, "A New Method for Nonlinear Reactor Dynamics Problems", Nukleonik, 9.Bd., Heft 6, 1967

27/ Rowe, "COBRA IIIC: A Digital Computer Program For Steady State And Transient Thermal-Hydraulic Analysis of Rod Bundle Nuclear Fuel Elements", Battle Pacific Northwest Labs, BNWL-1695 (1973)

28/ Same as Ref. 9, p. 108

29/ Kalambakas and A.F.Henry, "Replacement of Reflectors by Albedo Type Boundary Conditions" MEKIN Program Development Notes, Vol. 2.2,p.592

30/ Lamarsh, "Introduction To Nuclear Reactor Theory", Addison-Wesley Publishing Co. Inc., Reading, Mass. (1966)

31/ D.R. Ferguson and K.F. Hansen, "Solution of the Space-Dependent Reactor Kinetics Equations in Three Dimensions", Nucl. Sci. Eng., 51, 189-205 (1973)

32/ Reed and K.F. Hansen, " Alternating Direction Methods for Reactor Kinetics Equations", Nucl. Sci. Eng., 41, 431 (1970)

33/ Same as Ref. 30

34/ Same as Ref. 9, p. 139

35/ Same as Ref.9, p. 209

36/ Grund, "Experimental Results of Potentially Destructive Reactivity Additions to an Oxide Core," IDO-17028, Jan. 1964

Appendix I

DRESDEN III DATA

Figure I.1 shows that not all subassemblies are fully curtained. Some on the core-reflector boundary have no curtain control and others only one half curtain control. Further, figure I.3 shows that the term assembly will apply to a group of 4 subassemblies as outlined in figure I.2.

Some of the subassemblies contain dished fuel pellets in some of their pins. Figure I.4 illustrates one such subassembly. Those pins with a loading of 4377 gms are dished; while those with a loading of 4566 gms are not. Figure I.5 illustrates a subassembly with no dishing.

In figure I.6 a full core layout showing the curtain control, and dishing condition of the core's subassemblies is presented.

Further information on Dresden III can be found in its PSAR[3] and in Appendix I.

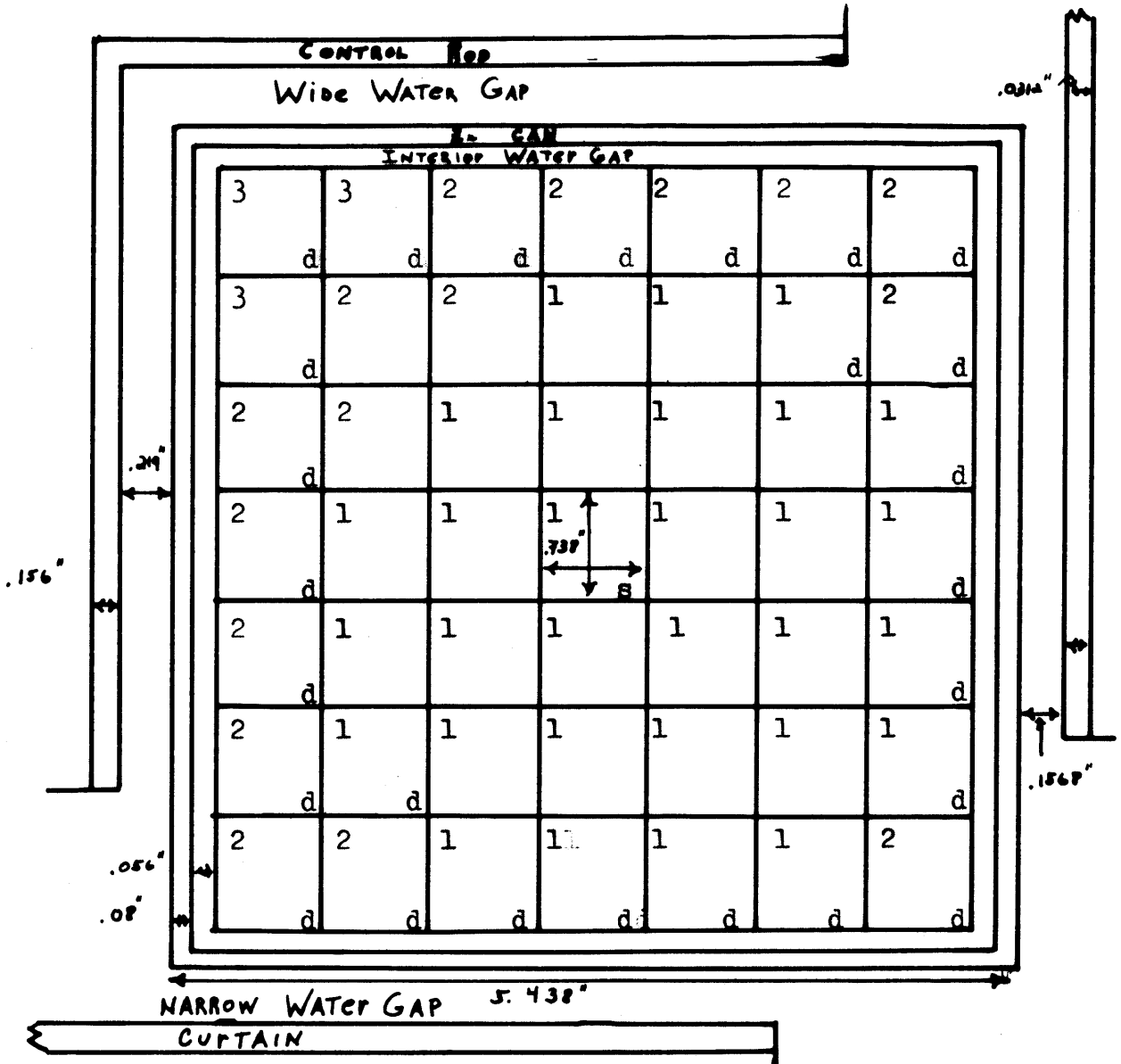

Rod Type	U-235 wt%	No. of Rods
1	2.44	30
2	1.69	16
3	1.20	3

s = Location of Spacer Rod (12" No Fuel In Center)
d = Location of Dished Rod In Dished Bundles

The Subassembly
Fig. I.1

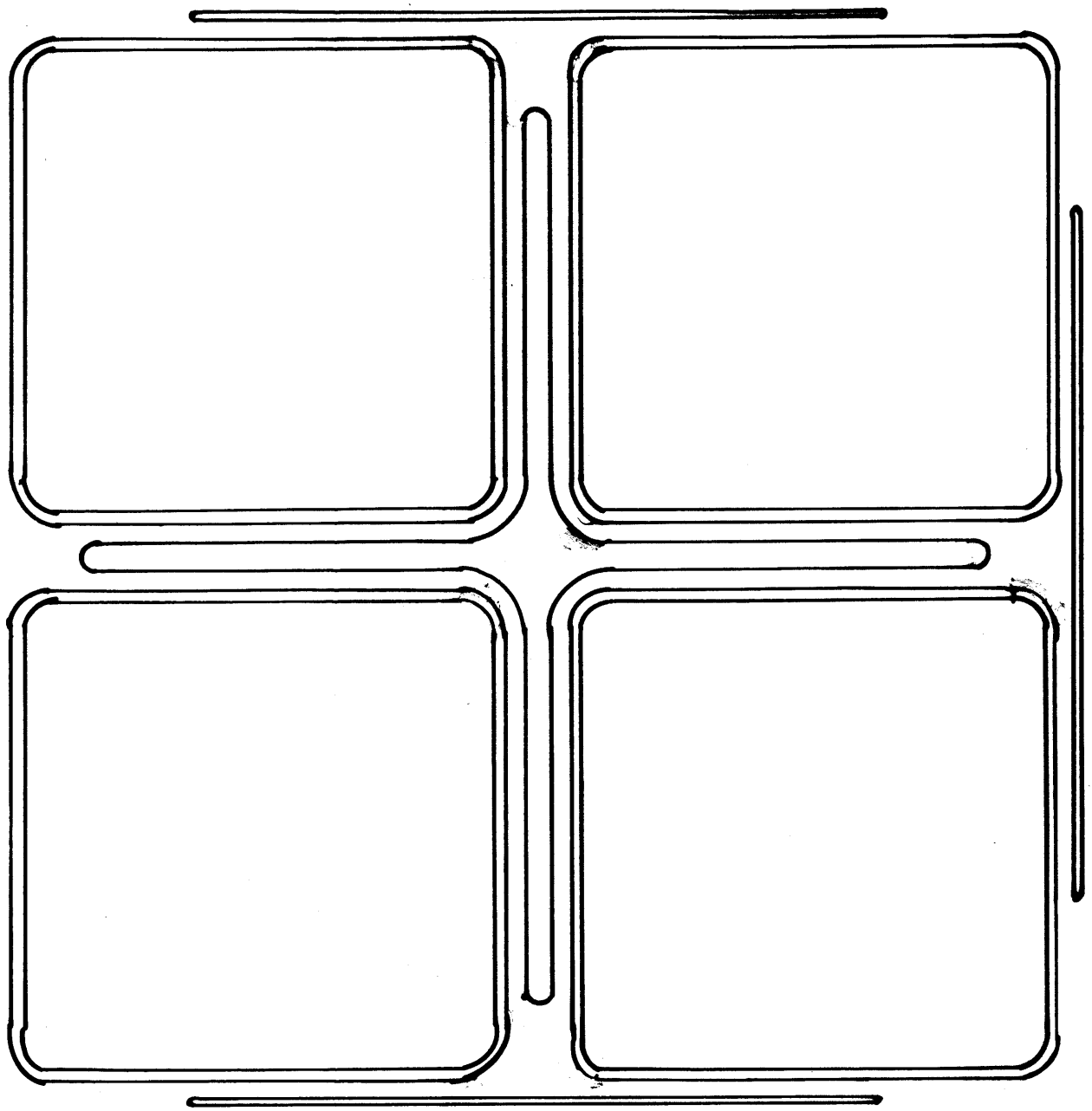

The Assembly

Fig. I.2

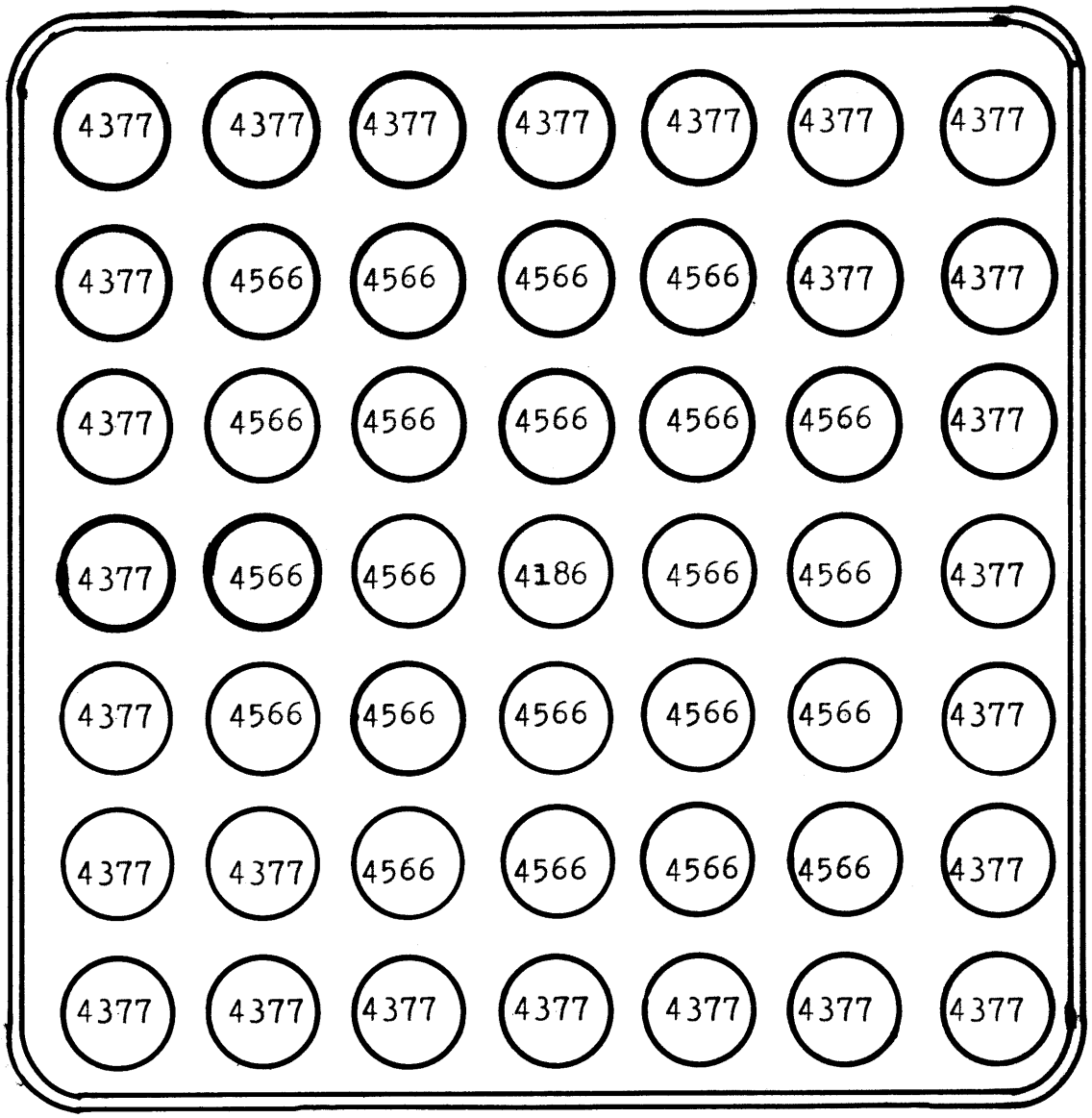

Fuel Rod UO_2 Loading In Grams
Low Weight Assembly

Fig. I.3

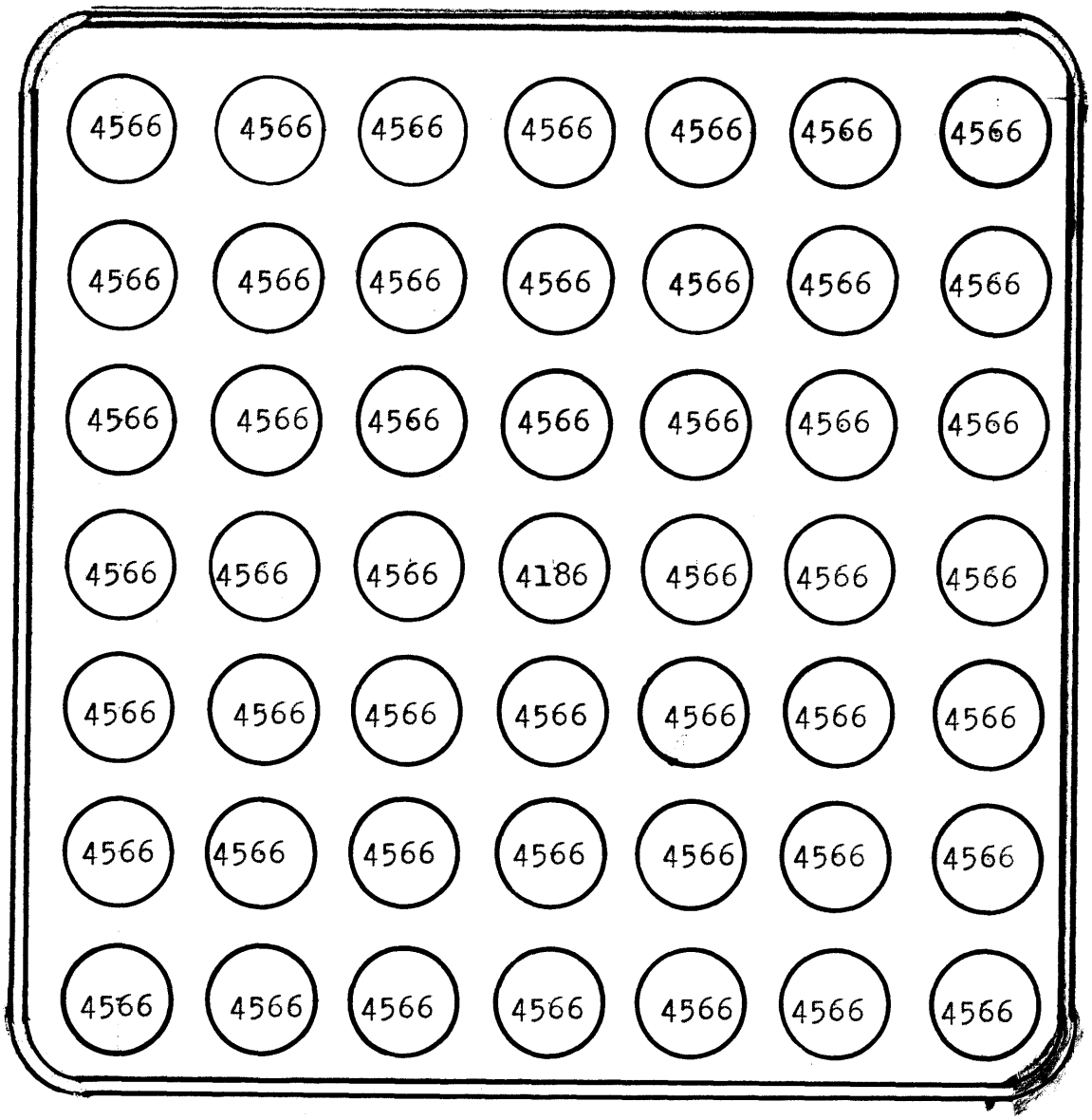

Fuel Rod UO_2 Loading In Grams

High Weight Assembly

Fig. I.4

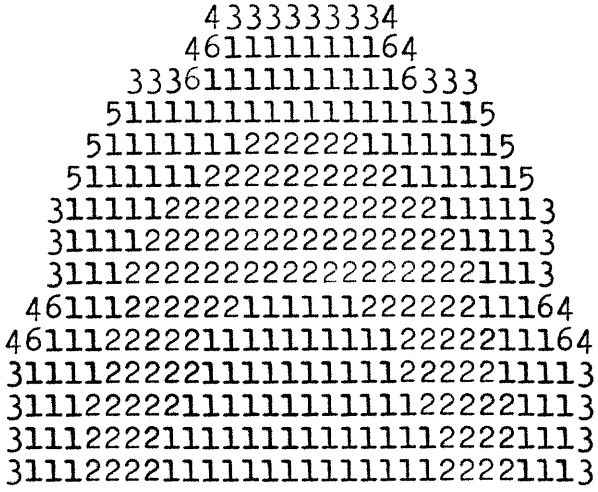

Type	Subassembly
1	Dished Full Curtained
2	Undished Full Curtained
3	Dished ½ Curtained
4	Dished No Curtains
5	Dished Full Curtained
6	Dished ½ Curtained

Subassembly Type Locations

Fig. I.5

Table I.1

Dresden III Characteristics

a.	Power (MWt)	2527
b.	Pressure	
	Steam Dome (psia)	1017
	Core (psia)	1032
c.	Flow	
	Total (10^6 lb/h)	98.0
	Bypass (10^6 lb/h)	7.5
d.	Core Inlet Water	
	Temperature (°F)	532.5
	Enthalpy (Btu/lb)	527.3
	Subcooling (Btu/lb)	20.2

FUEL DESCRIPTION

	Initial
Fuel Assembly	
Number of Fuel Assemblies/Batch	724
Fuel Rod Array	7 x 7
Fuel Rod Pitch (in.)	0.738
Bundle Average Enrichment (wt% U-235 in Total U)	2.13
Control Augmentation	
Type	Temporary Curtains SS(5400PPM B)
Number	340 in Core
Control Length (in.)	141.25
Control Material	Natural Boron
Locations	N-N Water Gap
Weight of U per Fuel Assembly (lb)	434.1 (undished) 424.6 (dished)
(kg)	196.9 (undished) 192.6 (dished)
Channel	
Thickness (in.)	0.080
Material	Zr-4
Water/UO_2 Volume Ratio	2.42 (undished)
(No controls rods or curtains - cold)	2.47 (dished)

	Initial
Fuel Rod, Cold	
Fuel Material	UO_2
Pellet Diameter (in.)	0.488
Cladding Thickness (in.)	0.032
Cladding Material	Zr-2
Cladding Outside Diameter (in.)	0.563
Active Fuel Length (in.)	144
Length of Gas Plenum (in.)	11.24
Reflector - H_2O	

Movable Control Rods

Number	177
Shape	Cruciform
Pitch (in.)	12
Stroke (in.)	144
Width (in.)	9.75
Control Length (in.)	141.25
Control Material	B_4C granules
Number of Control Material Tubes per Rod	84
Tube Dimensions, o.d. x i.d. (in.)	0.188 x 0.138

Appendix II

USE OF DEFINE FILE AND RESTART CAPABILITIES

As for most codes of its size MEKIN has a restart capability. Section D of Part II of the MEKIN manual defines the four datasets that are already built into the MEKIN code. Define File #12 is not presently in use and was not used at anytime during our runs. This leaves one with Define Files 10, 11 and 15. One will now define how one might go about setting up a problem and where along the way these Define Files come into play.

One should become familiar with Define File statements. They are a form of Fortran Direct Access Input / Output. At MIT information can be found from IPC release PP15.

In brief, a Define File for MEKIN would be a region set aside on a diskpack. This author made use of two types of diskpacks, a 3330 and a 2314. The 3330 is a much larger diskpack than the 2314 unit. Each unit is broken up into tracks. A track on a 3330 unit consists of 13030 bytes, or 3257.5 Real * 4 words (4 bytes to each Real * 4 word). A track on a 2314 unit is composed of 7294 bytes (or roughly half the size). When setting up a Define File one must satisfy two things. One, the space (that is the total number of bytes wanter) must be available, and two, the

skeleton records must be set up before one can write to a Define File. The skeleton records are how the information, in a form of physical records (groups of data) are stored on the diskpack to compose a meaningful dataset. One might request that his skeleton records be composed of 800 physical records each of 6400 bytes. For this one would require a Define File that has 5,120,000 bytes of space available. This is what was done in our problem.

The length of the physical records is then the basic building block of our Define File. It is this size which must be optimized to decrease running time and expense in our code. If one does that one will lower the number of Input-Output operations between desk and computer core. What is suggested is to choose the physical record length based on the array size of the block FLUX.1. The array size is equal to the number of flux points in a horizontal plane. THus, if one has 193 boxes or thermal-hydraulic channels and 4 points per box and two energy groups one has an array size of 1544 words or 6176 bytes. By choosing the physical records to be 6400 types in length one assures himself of fitting this array in 1 physical record. This will result in only one Input Output operation for that array and hence save time.

Note, one is limited to a record length of one track, that is 7294 bytes for a 2314 unit and 13,030 bytes for a 3330 unit.

Thus, if it turned out that the normalizing block, FLUX.1, was 7500 bytes in array size, the best thing to do would be to choose a physical record length such that one can fit the array in two physical records. So a physical record length of 3800 bytes would be a good choice. This is if one is using a 2314 unit.

If one had been forced due to expense of the runs to decrease the number of I/O's to alter or optimize the physical record lengths from those set up in the original version of MEKIN, one must also change the size of the buffers. To allow for double buffering, and the fact that one has four Define Files; the buffer region must be eight times the length of the newly chosen physical record size.

The final item that must be changed in the event one decided to alter the physical record length is the way MEKIN assigns the next block to the diskpack. If for example one has just entered the first array to the diskpack on Define File, and its size was enough for 3 physical records, the next block to be written would have to start in the fourth physical record space of the Define File. In subroutine Dinout under entry point DWRITE, MEKIN keeps track of this iterator (given the variable name LP in MEKIN). The iterator works by starting at zero or one for the first block to be written to disk and then determining the new entry point for the next block to be read in by calculating the number of physical record regions the previous block

occupied. It does this by dividing the previous block length by the length of a physical record. Hence, if one has changed the length of the physical records from the size used in the original version of MEKIN for the reasons discussed above, one must change its length here also.

The reader should hope he doesn't have to go through this optimization procedure, and that he can use the original version of MEKIN uncorrected for physical record length optimization. However, if he must, an example of the necessary changes (which this author had to go through) can be found in Appendix III.

Let us now assume that the reader has decided that a physical record length of 400 bytes, as set up for in the original version of MEKIN, suites his problem. Let us further assume that 3000 physical records of this length will fulfill his dataset requirements. He will know that he has asked for too small a number of physical records if he gets an IHN232I error message stating that the code was searching for the 3001 physical record and saw that this way out of the range of space alloted for.

Let us assume that the physical record length of 400 bytes and 3000 physical records are satisfactory for the problem, how do we set up the Define Files?

Preallocation of space on the diskpack by using the IEFBR14 program has <u>not</u> been found to work. Instead, the

space should be allocated and skeleton records set up in the first run of MEKIN. Since a scratch space must always be set up, a Define File 10 is mandatory. Hence, just before the go step job control card (//G SYSIN DD...) one should have, if he is using a public dataset, which is what one would use for scratch space:

```
 //G.FT10F001  DD  Unit = Scratch, Space = (400,(3000,300)),
// DCB = (RECFM=F,LRECL=400,BLKSIZE=1200)
 //G.FT11F001 DD DUMMY
 //G.FT12F001 DD DUMMY
 //G.FT15F001 DD DUMMY
```

Suppose one would like to be able to restart MEKIN from the steady state solution. One must then be sure to save the different block values on a diskpack. For safety one should use a private diskpack. After acquiring a diskpack with sufficient space the user's Define File statement for Define File will change to:

```
                                                  chosen chosen
                                Project Programmer's name   name
 //G.FT11F001 DD DSNAME=PV._Number_._Number_ _ _ . one . two ,
// DISP=(NEW,CATLG), SPACE=(400,(3000)),
// UNIT=2314,VOL=SER=234019
```

If a private 2314 diskpack is used one must be sure to have set it up. This requires using the following added job control card.

```
/*SETUP  UNIT=2314,ID=234019,A=RST,C='USINGM7514-10581'
```

The ID value of 234019 is the ID of the private diskpack the reader is using. This author used one whose ID was 234019. The C = 'USING M7514-10581' is a comment statement and need not be included.

This Define File setup along with the setting of the input variable IEDSSR on card type GO of the input data will write the steady state solution to the diskpack of the given two name identification. For the moment let us pick chosen name one to be Denise and chosen name two to be Lori.

Now, we should make it a point of never writting anything else to this diskpack, Denise.Lori, because a write to Denise.Lori issued in a later run of MEKIN will write over our previous stored steady state restart information. This can be an advantageous property of how MEKIN writes to its Define Files as illustrated by transient restart.

Suppose that we now want to start our MEKIN run from the already calculated solution and saved on Denise.Lori dataset. Let us further assume we wish to save a transient time step on a diskpack which is the same 2314 unit with

ID = 234019 but has a different region and hence name than Denise.Lori. Let us call it George.Eunice. Since we want to read the steady state dataset, it becomes Define File 15. Because we want to write a transient dataset to disk, it becomes Define File 11. So we have

```
                                Project   Programmer's
//G.FT11F001 DD DSNAME=PV.        #    .      #        . George. Eunice,
//  Disp=(NEW,CATLG), Space = (400,(3000)),
//  UNIT = 2314, Vol = Ser = 234019
 //G.FT12F001 DD DUMMY
                               Project   Programmer's
 //G.FT15F001 DD DSNAME=PV.      #    .      #       . Denise.Lori,
//.  Disp = OLD
```

The required diskpack set up card and Define File 10 cards would also be needed, but unchanged, for this run.

Finally, suppose one wanted to start MEKIN calculations from a previous disk stored transient time step. Further assume that once we carry out the calculation to a new transient time step, we no longer want to save the dataset from which we started this calculation. The Define Files 11 and 15 would then look like this:

```
                                  Project   Programmer
//G.FT11F001 . DD DSNAME = PV.      #    .      #      . Denise.Lori,
//  Disp = OLD
```

and

```
                                        Project   Programmer's
//G.FT15F001 DD DSNAME = PV.  #     .      #      . Denise.Lori,
// Disp = OLD
```

If one didn't want to lose the previous stored transient time step from which he started this calculation then a new dataset name would have to be used for Define File 11. Also, the disposition would be new and catalog and the space, unit member, and volume number would all have to be defined as was shown previously when we allocated space and set up the skeleton records for a new dataset.

Appendix III

CHANGES MADE IN MEKIN

The following are changes or noted mistakes in MEKIN which were found during this work. Table III-1 is a category list for these errors. Those noted as temporary were particular to this work, and should not be added to a permanent version of MEKIN.

To allow for a problem which has no coolant flow, a value of 1.0E-09 for variable GIN on card type T20 should be input.

Table III-1

Categorized Changes

Change #	Thermal Hydraulic Related	Data Management Related	Manual or Simple Fortran Error	Permanent Change	Temp. Change	Not Changed
1	X					X
2	X					X
3		X		X		
4		X		X		
5			X	X		
6		X		X		
7	X					X
8	X			X		
9	X			X		
10	X			X		
11	X			X		
12		X		X		
13		X		X		
14		X		X		
15		X		X		
16		X		X		
17			X	X		
18	X				X	
19			X			X
20	x				x	
21	X			X		
22	X			X		
23		X		X		

1) SUBROUTINE CHAN - Must input at least 2 types of T-H channels (they need not be different)

REASON - Do loop - Do 24 J = L,M will have L > M for only 1 type of T-H channel

2) SUBROUTINE CHAN - GP is dimensioned at 250 words. This will limit # of channels to 250 This was not altered after it was decided to use only 193 channels.

3) SUBROUTINE MANAGE

ENTRY ZIGET - To allow for possible double buffering, the buffer size was set to be twice the physical record length of the block sizes.

Since this was changed from 1600 to 6400 bytes in our case to minimize I/O to disk, we set aside a double buffer for each of our 4 Define File buffers. Hence

Double Buffer
↓
(2) (6400 bytes) (4 buffers) $(\frac{1}{4} \frac{\text{words}}{\text{byte}})$ 12800
↑
physical record length

used 13,000 words. So changed statement 130 in manage to

130 Call Ziget (Data (1), KMAX,4,KS,13000, & 905)

4) SUBROUTINE DINOUT

→ Entry DINIT — Sets up Define File. Have changed to 800 groups of 6400 bytes.

So Define Files 10, 15, 11 and 12 now become

```
Define File 10 (800, 6400, L, NPRSCX),
            15 (800, 6400, L, NPRRIX),
            11 (800, 6400, L, NPRROX),
            12 (800, 6400, L, NPREDX)
```

→ Entry DWRITE — Must take into account this new record length in assigning next record number. Since now have record lengths of 1600 words entry DWRITE should look like

```
      Entry DWRITE (BL, NBL, LX, DATA, *)
*     LP = LX / 1600
*     IF (LPA*1600 .LT.LX) LP = LP + 1

      s a m e
```

* denotes a changed card

→ Entry RREAD1 - Below comment card

```
C -   Determine Physical Record number of next block.
      Should now have

*     LP = (LX + 4) / 1600
*     IF (LP * 1600 .LT. (LX + 4) ) LP = LP + 1
      NPRRI = NPRRI + LP
```

where we have changed to 1600 words for same reason as in DWRITE. Also have added 4 words to block length (LX) to account for necessary space allotted to block name and associated variables.

5) USER'S MANUAL — Card type T19 format for variable NPROP is I5 not E5.0

6) SUBROUTINE SHUFO — Must add card defining LBXA(25) between statement 20 and comment card

C - can all blocks be core contained?
It must be added since we compute length of blocks here

```
      LBXA(20) = LBX(20) * NP3FX
*     LBXA(25) = LBX(25) * ND3X
      LBXA(27) = LBX(27) * NP3X
```

→ Also after comment card

C NEUTSS

There is a card out of place. Should read

```
      M4 = LDSRC + LDS RC1 + LDSRC2
      M5 = LDCOEF + LDFLUX + LDSRC
 NEUTSS = MAXO(M1, M2, M3, M4, M5)
X       + IFIVE * (NP1X - ITWO) * KORGD
   NEED = MAXO (NEED, NEUTSS)
```

7) SUBROUTINE TABLES — Seems to give error when read in more than 13 channels wanted for print out as denoted on card type T28

Mistake not corrected

8) SUBROUTINE HEAT

DATA($QPRIM) is the linear heat addition. If subroutine Temp calculates that the temperature of the fuel surface is below that of the coolant, the fuel will attempt to absorb heat from the coolant whose temperature is inputed. This results in a negative QPRIM - something MEKIN can't handle.

So do Loop - Do 65 should read

```
Do 65 I = 1, NCHANL
DATA($QPRIM+I) = DATA($PWRF+I)*DATA($FLUX+I+
                 MR*(J-1))*PI*DATA($D+I)
65 IF (DATA($QPRIM+I).LT.0.) DATA($QPRIM+I) = 0
```

9) SUBROUTINE DIFFER

For very low flow conditions at steady state (as have for Hot Standby) we don't want any enthalpy change.So between statement #185 and 190 we add card

```
If(DATA($F+I+MC*(J-1)).LE.1.0E-03.AND.
  DT.GE.1.0E0.9) DATA($DHDX+I)=0.0
```

10) SUBROUTINE SCHEME

Again because of low flow conditions it was necessary to set the time, DT of the steady state time interval from 1.0E 10 sec to 1.0 E20 sec. to assure the time derivative term in the enthalpy equation vanished for steady state

so should read

```
C     Calculate Enthalpy and estimate flow at x
      Do 425 I = 1, NCHANL
      IF (ITERAT.EQ.L..AND.JUMP.NE.3) DATA($F+I+
     1    MC*(J-1) + DATA($F+I+MC(JM1-1)
      SAVE 2 = DT
      IF (DT.GE.1.0E09) DT = 1.0E20
      DATA($H+I+MC*(J-1)) = (DATA ($H+I+MC*(JM1-1))
     1 + DX/DT/DATA($UH+I)*DATA($HOLD+I+MC+(J-1))
     2 + DX * DATA($DHDX+I)) / (1.0 + DX/DT/DATA($UH+I))
      DT = SAVE 2
  425 Continue
```

11) SUBROUTINE SEPRAT

To account for low flow conditions in steady state and possible round off error for real * 4 which may have a large relative effect at low flow conditions during transient we add following cards

```
      IF (IPART.EQ.2) Go to 10
      DO 2 I = 1, NCHANL
      DATA ($DFDX+I) = 0.0
      SAVE 4 = DT
      IF (DT.GE.1.0E09) DT = 1.0E20
      RHODIF = DATA($RHO+I+MC*(J-1))- DATA($RHOOL+I+MC*(J-1))
      IF(ABS(RHODIF).LE.1.E-04) RHODIF = 0.0
      DATA ($F+I+MC*(J-1)) = DATA($F+I+MC*(J-2))-DX/DT*
    1 RHODIF * DATA ($A+I)
    2 DT=SAVE4
      CALL DIFFER (3,J)
      RETURN
```

12) SUBROUTINE TDSKED — There was a mistake in the size of common blocks "LIMITS" and "FIXED"

So after

C write Limits Common Area to Disk
should read
LX = 43 not LX = 45

and after

C write Fixed Common Area to Disk
should read
LX = 190 not LX = 188

13) SUBROUTINES Power1, Power2, and Power T

→ A call to FIND must be issued after a call to PUSH was issued so that the new position of other data blocks in the core could be acknowledged. Hence after statement 300 of each of the 3 Power Subroutines we should have:

```
Call PUSH (WPWCO,O)
Call FIND (WGFAC,IZERO,KGFAC,IER)
Call FIND (WQFME, O, KQFME, IER)
Call FIND (WPWRT, O, KPWRT, IER)
KGFAC = KGFAC - IONE
KQFME = KQFME - 1
KPWRT = KPWRT - 1
```

14) SUBROUTINE TDSKED

Given the incorrect # of block qualifiers (like # of axial levels)
So IQUAL(62) = NGIX should be Placed after IQUAL(61) = NP3GX

15) SUBROUTINE STEADO

After statement #900 place

```
900 CALL DROP( WPOLD, IZCRO)
    CALL SHUFOB
    Return
```

Reason - to clear core to allow rolling to restart SS.

16) SUBROUTINE RSTART

Statement 210 should read:

```
   210 LL = 43
```

and #220 should read

```
   220 LL = 190
```

This is because the length of these blacks were changed in TDSKED (change 12)

17) SUBROUTINE RODS - Undefined Variable

Numbered Statement 101 should read

```
   101 IF(PWRT.GE.PSCRAM)  go to 200
```

18) SUBROUTINE SEPRAT

SEPRAT tries to adjust the inlet flow to the channels to account for equal pressure drops across the core. This requirement was lifted for our case of steam hammer and low inlet flows. So after statement 1001 change

```
      IF((1.0 - PMIN/PMAX).LT.FERROR) Return
```

to

```
      RETURN
```

19) SUBROUTINE QPR3

The format statement 3004 doesn't truly print out the heat flux but the power divided by the pin area. This is truly a difference in transient situations where we have the power increasing the fuel temperature as well as increasing the heat flux. This incorrect format statement is not changed however.

20) SUBROUTINE SEPRAT

After flow equation and before call to DIFFER (3,J) set flows to hot standby case

```
DATA($F+I+MC*(J-1)) = .12091E-06      ← added card
 2 DT = SAVE 4
CALL DIFFER (3,J)
Return
```

This is to account for steam hammer effect at ~ 1.5-1.7 seconds for our case

21) FUNCTION HCOOL

To allow for the case where one may get quality > 0 and still have $\leq$ 0 heat flux as get it water heated by γ and neutrons, must change statement 2.

```
OLD 2 IF (DATA($QUAL+I).GT.0.0) Go to 6
NOW 2 IF (DATA($QUAL+I).GT.0.0.AND. DATA ($QPRIM + I)
          GT.0.0) Go to 6
```

22) SUBROUTINE PROP

Again to allow for QPRIM = 0. one must not enter the Jens-Lottes equation of HCOOL, so in Prop when we check for Boiling, should read,

```
  C  Determine the START of Nucleat Boiling
     IF (IDAT($JBOIL + I).GT.0.0) Go to 110
Now→ IF (DATA($QPRIM+I).LE.0.0) Go to 110
```

23) SUBROUTINE INTRA 2

Because the low flow scram option doesn't really exist, and some variables were never defined the following changes are required:

Remove cards

```
IF (ISCRAM .EQ.IFOUR) WRITE(IOUT,2130)SCRMX
```

format statement 2120

Change If statement for ISCRAM = three to

```
IF(ISCRAM.EQ.ITHREE) WRITE(IOUT,2130) SCRMX
                                    ↑
                                  change
```

Add following cards after the above changed IF ISCRAM equal three statement:

```
                Go To  (701, 702, 703), SCRMX
                Go To  704

  701 PSCRAM = SCRMX
                Go To 704
  702 PRSCRM = SCRMX
                Go To 704
  703 TSCRM  = SCRMS
C
  704 IF(IDRIV.EQ.IZERO) WRITE (IOUT,2140)
   ↑
  add fortran statement number to card already present
```